BENJAMIN JOHN BROUGHTON

WOLFSON COLLEGE

UNIVERSITY OF CAMBRIDGE

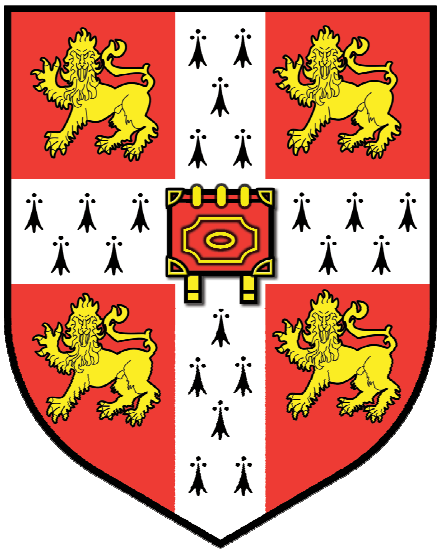

DEPARTMENT OF ENGINEERING

"THE FLEXOELECTRO-OPTIC EFFECT FOR PHOTONICS APPLICATIONS"

A Thesis Submitted for the Degree:

Doctor of Philosophy

December 2005

UNIVERSITY OF CAMBRIDGE
DEPARTMENT OF ENGINEERING

"THE FLEXOELECTRO-OPTIC EFFECT FOR PHOTONICS APPLICATIONS"

By Benjamin John Broughton

ABSTRACT

This thesis comprises an account of research carried out into the flexoelectro-optic effect, as observed in chiral nematic liquid crystals, and its potential for application in fibre optic communications components. The flexoelectro-optic effect provides a mechanism of fast, analogue rotation of the optic axis in chiral nematic materials via the application of an electric field to the sample. In particular, bimesogenic liquid crystal materials exhibit very large flexoelectro-optic tilt angles, and a large tilt angle per unit field in comparison to other mesogenic materials.

In this work a new geometry for the flexoelectro-optic effect is developed in which the chiral nematic liquid crystal is aligned with its helical axis along the normal to the cell walls and the electric field is applied in the plane of the cell. It is shown that polymer stabilization of this device by the addition of a small percentage of reactive mesogen to mixture increases greatly the ability of the device to withstand high amplitude a.c. electric fields. Applied fields of up to 6.8 V/μm are shown to induce a maximum birefringence of $\Delta n=0.037$, due to both flexoelectric and dielectric coupling, and $\Delta n=0.012$ due to flexoelectric coupling only in a sample based on symmetric difluorinated bimesogens. This induced birefringence is shown to consistently respond to field application and removal on the sub millisecond timescale.

Polymer stabilization of the same mixtures in the uniform lying helix texture is shown to effect the electro-optic response of the samples in a manner which is dependent on the concentration of reactive mesogen used, and the temperature at which the reactive mesogen is cured. A concentration of approximately 3% weight/weight, however, has little detrimental impact on the device characteristics, and curing of the sample at the lower end of the chiral nematic temperature range is shown to allow optimization of both tilt angle and response time of the samples.

The effect is also employed to demonstrate a new method of fast electrical tuning of the output wavelength from chiral nematic photonic band edge lasers. An 8nm shift was induced in these devices by a 3.5 V/μm applied field.

TABLE OF CONTENTS

Declaration

This thesis is the result of work done by the author whilst in registered postgraduate candidature at the University of Cambridge. The work is entirely original except where due reference is made and contains nothing which is the outcome of work done in collaboration with others, except as specified in the text and Acknowledgements. No portion of the work referred to in this thesis has been submitted in support of an application for another degree or qualification at this or any other university or institute of learning. This thesis comprises 41,408 words and 93 figures, thereby conforming to the Degree Committee specifications.

Benjamin John Broughton

ACKNOWLEDGEMENTS

I would like to express my gratitude to several people, without whom this work would not have been possible.

Firstly, my supervisor, Professor Harry Coles, for extending to me the invite to join his group in the adventure north to Cambridge, providing me with a project I have thoroughly enjoyed, and for managing such a friendly, productive research group, with whom it has been a pleasure to work with. Thanks very much for such an excellent opportunity and for an extremely enjoyable three years.

Thanks also to Harry for securing my CASE sponsorship for the project from Pi Photonics. A very special thank you to Ralph Betts and Terry Bricheno at Pi Photonics for all the guidance, encouragement, equipment, lab space, cartwheel cells and workshop know-how. Not to mention the extra cash. This work would have produced an entirely different and inferior result without their invaluable input.

For day-to-day supervision and guidance I have to thank Steve Morris and Oliver Hadeler. Having such an ever-ready source of answers, suggestions and practical knowledge at least halved the time these results would otherwise have taken to produce. Thanks also to Oliver for undergoing the onerous task of reading these Chapters, and improving them tremendously with his comments.

I would also like to thank all the CMMPE research group members during my time there for making the labs a very entertaining place to spend three years. Special mentions in this area must go to Damian Gardiner, Andrew Blatch, Matt Clarke and Ali Ford. Their example of how to produce quality work whilst always having fun is something I hope to find throughout my career.

I am grateful to the EPSRC for their financial support and to the COMIT Faraday partnership for arranging my CASE sponsorship.

Finally, unending thanks to Mum and Dad for their constant support, especially in the eight full years since I left for university. I hope this new doorstop helps persuade you it was worth it; it's as much your achievement as mine.

Chapter One

INTRODUCTION

1.1. PREAMBLE

This PhD project is concerned with the potential for deployment of liquid crystal based devices in photonic systems, particularly fibre-optic communication systems.

Liquid crystal materials have been exploited very successfully for use in display applications, but their potential in telecommunications devices for optical fibre systems has only recently become the focus of extensive research. Liquid crystals have advantages over conventional electro-optic telecoms materials such as Lithium Niobate in that they have high birefringence, high optical transparency, low power consumption, non-mechanical operation, and are cheap and simple to manufacture.

The telecoms industry is in a situation at the present whereby optical fibre systems carry the all the long-distance and national backbone data traffic at huge data rates, but the city-wide and local exchange networks are still electronically operated, with a data bottleneck between the end user and the local exchange: the "last mile". As the optical architecture penetrates further through the network towards the home and the end-goal of an all optical network, the number of network nodes increases exponentially, so the requirements for optical components shifts from very high performance devices to very cheap ones. It is in this area therefore, where cost is paramount and tolerance of device weaknesses such as optical attenuation, dispersion and channel cross talk is slightly greater, that liquid crystal based components may find their niche.

The main area in which liquid crystals suffer in comparison to solid-state electro-optical devices is their relatively low switching speeds, typically tens of milliseconds. It is for this reason that the more promising liquid crystal telecommunications devices attempt to either utilise faster liquid crystal electro-optic effects than the simple Freedericksz transition, such as the ferroelectric and electroclinic effects, or address applications which require switching at well below the bit-rate of the system, such as switchable interconnects,[1,2] add/drop multiplexers,[3] or polarisation controllers.[4-6]

The flexoelectro-optic effect[7] is a relatively recently discovered electro-optic switching process observed in chiral nematic liquid crystals. It has the dual benefits of fast, typically 100-500μs, response times and analogue field dependence allowing greyscale control of transmitted optical

intensity through the device. These properties mark it out as a prime candidate for telecoms applications, but due to the relatively small research output on the effect so far, it remains unexplored for use in photonic communication components. The recent development of bimesogenic liquid crystals[8] with very high flexoelastic coefficients, however, provides a new opportunity for development of the effect into these areas. This project aims to assess the potential of the flexoelectric effect in such high tilt angle samples for photonics applications by investigating the characteristics of flexoelectric devices at the telecommunications wavelength of 1550nm, and developing both the device designs and liquid crystal mixtures utilised in them to improve device performance.

1.2. OUTLINE OF THE THESIS

Following this introduction to the thesis, Chapter Two introduces the theoretical background to liquid crystal electro-optic effects relevant to this work, particularly those in chiral nematic liquid crystals. Further emphasis is placed on outlining the current knowledge of the flexoelectro-optic effect and citations of the key works in this area to date. It is the flexoelectro-optic effect with which this work is primarily concerned, and in particular a novel geometry in which to examine the effect. Some numerical calculations are also detailed at this stage, which were performed to provide an expectation of the electro-optic response in this new geometry.

In Chapter Three, the experimental techniques and apparatus schematics used in the work presented here are introduced. Three principal experiments were developed to effect the investigations reported, and each of these are outlined in turn, with their particular aims and methods.

The first observations of the flexoelectro-optic effect in Grandjean textured, chiral nematic liquid crystals under the influence of in-plane electric fields are reported in Chapter Four. Observations of the magnitude and response time magnitude of the effect are made in several liquid crystal mixtures.

The work of the previous chapter is developed in Chapter Five with the extension of the effect into polymer stabilised samples. This improves the ruggedness of texture, allowing a.c. fields of varying frequency to be applied to the samples. The contributions to the observed response from

dielectric and flexoelectric coupling are now separable, and the magnitude and speed of the response in a range of monmesogenic and bimesogenic mixtures are directly compared. The flexoelectric characteristics of the mixtures used are also examined in the ULH texture, providing a correlation of the observed response in the two geometries.

Further investigations are performed into the flexoelectro-optic response of polymer stabilised ULH textured samples in Chapter Six. Quantitative measurements of the effect of varying the concentration of reactive mesogen used on the field-induced tilt angle and response time are obtained, and the relative influences of polymer curing temperature and device operating temperature are examined.

In Chapter Seven, the electro-optic effect detailed in chapters five and six is re-applied to produce fast, electrical tuning of dye-doped, chiral nematic, photonic band edge lasers. This is observed for the first time, and the initial results are detailed along with attempts to develop the effect.

Chapter Eight concludes the thesis with a summary of the experimental results obtained and presented in the thesis and an analysis thereof, along with some suggestions for future development and directions in which the work could be progressed.

1.3. REFERENCES

[1]H. Yamazaki, M. Yamaguchi, Optics Letters, **16**, (18), 1415, (1991).

[2]W.A. Crossland, et al, IEEE *Journal of Lightwave Technology*, **18**, (12), 1845, (2000).

[3]M.C. Parker, A.D. Cohen, R.J. Mears, IEEE *Journal of Lightwave Technology*, **16**, (7), 1259, (1998).

[4]S.H. Rumbaugh, et al, IEEE *Journal of Lightwave Technology*, **8**, 3, p.459, 1990.

[5]Ohtera Y., et al, IEEE *Photonics Technology Letters*, **8**, 3, p.390, 1996.

[6]Chiba T., et al, IEEE *Journal of Lightwave Technology*, **17**, 5, p.885, 1999.

[7]J. S. Patel and R. B. Meyer, *Physical Review Letters*, **58**, (15), 1538, (1987).

[8] H. J. Coles, M. J. Coles, S. P. Perkins, B. M. Musgrave and D. Coates, Patent: *GB2356629.*,

Chapter Two

THEORY

2.1. INTRODUCTION

Having introduced the liquid crystalline state of matter in the previous Chapter, along with the potential applications for materials exhibiting these mesophases in telecommunications devices, this Chapter will outline the theory of electro-optic effects in liquid crystals, with particular emphasis on the chiral nematic liquid crystals investigated in this study. This will lay the foundation for understanding the effects observed in this work, particularly the flexoelectro-optic effect, results from the investigation of which are presented subsequently in Chapters Four to Seven.

In the following section, the treatment of liquid crystals as a continuous medium is outlined, along with the concept of elastic deformation of the nematic director field. This provides the basis for an equilibrium state for the director in certain boundary conditions, deformations from which are countered by a restoring force. The inherent microscopic anisotropy of nematic liquid crystals is discussed in section 2.3, and the resulting macroscopic dielectric and optical anisotropy of nematic media are outlined. This is shown to provide the basis for electro-optical effects in liquid crystals. The chiral nematic phase is discussed in detail in section 2.4. The optical properties in the equilibrium state of this phase are unusual enough to merit attention, and the dielectric and flexoelectric mechanisms of coupling of the chiral nematic director field to an applied electric field are also presented in this section.

The principal direction of the work presented in this thesis is development of the flexoelectro-optic effect to provide operation in a novel geometry, whereby the helical axis of the chiral nematic is aligned vertically in the cell, known as the Grandjean texture. Initial theoretical predictions as to the nature and magnitude of the effect in the type of cells that will be used are therefore made at the end of section 2.4.

As a by-product of the results presented on the flexoelectro-optic effect in the Grandjean texture (Chapters Four and Five), it became possible to start an investigation into the possibility of tuning the emission from chiral nematic photonic band edge lasers (PBE's), via means of the flexoelectro-optic effect. The theory behind the operation of chiral nematic PBE's is laid out roughly in section 2.5, as a precursor to the results presented in Chapter Seven. The key points to the theoretical

descriptions laid out in this Chapter, as they apply to the work subsequently presented, are then summarised.

2.2. ELASTIC CONSTANTS AND THE FREE ENERGY

The concept of liquid crystalline order and the use of an order parameter to describe the degree of orientational order in a nematic material were introduced in the previous Chapter. We will now discuss the possibility of disruptions from this equilibrium order, caused by surface or field effects on the material. These result in deformations to both the director direction and the order parameter, causing them to change on moving through the material.

These types of deformation to the nematic order can be described by considering the liquid crystal as a continuum medium.[1-4] In such an approach, distances over which deformations occur are assumed to be much larger than the molecular length of the material constituents, so the material can be considered "smooth" and molecular scale details ignored. The key parameter is therefore the free energy of the system, which is described as a function of the vector field based on the director **n**, itself an average of the preferred molecular orientation.

The general free energy density for an elastic system is given by:

$$f = \frac{U}{V} = \frac{1}{2}k\left(\frac{x}{l}\right)^2 \qquad 2.1$$

where U/V is the free energy per unit volume, k is the elastic constant and x/l is the strain. In anisotropic media, such as liquid crystals, the stress and the strain become second-rank tensor values, and the elasticity tensor which relates the two, and is required for the free energy, is a fourth rank tensor.[5,6] As nematics have no resistance to pressure and shear, there is no such thing as conventional strain as derived above, but the strain tensor can be replaced by a torsional analogue in which the change in relative position of two particles is replaced by the change in angular displacement of the director: $n_i' = n_j + \left(\frac{dn_j}{dr_j}\right)r_j$. If n at the origin is taken to be along the z-axis, there are six non-zero values in the torsional strain tensor, which can be said to represent the three fundamental distortions of the liquid crystal director, splay, twist and bend.

Torsional strain tensor: $e_{ij} = \begin{pmatrix} dn_x/dx & dn_y/dx & 0 \\ dn_x/dy & dn_y/dy & 0 \\ dn_x/dz & dn_y/dz & 0 \end{pmatrix}$ 2.2

The relationship of these strain elements to the elastic deformation is illustrated below:

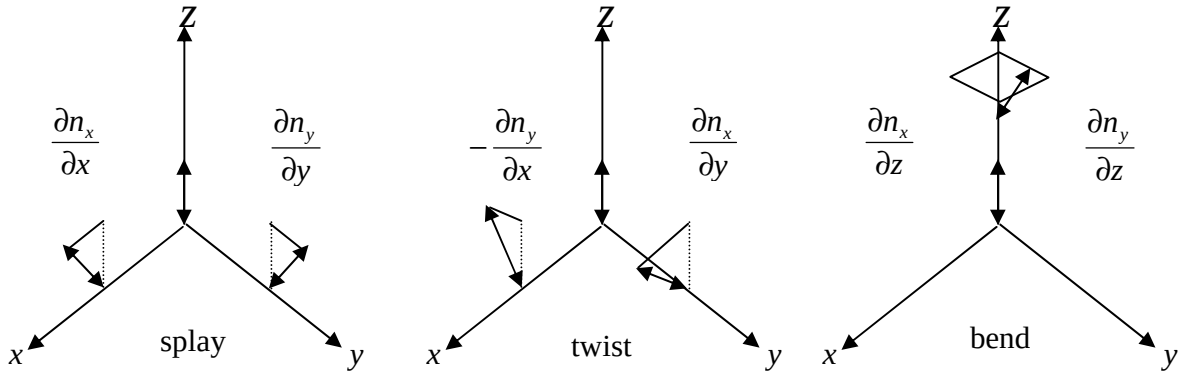

Figure 2.1: *Illustrative diagram of the splay, twist and bend deformations in nematics.*

The torsional strain tensor can be reduced to a first rank tensor of six elements simply by forming a column of the six non-zero values and remembering the convention. This reduces the elasticity tensor to one of second rank, and the free energy density can be expressed as:

$$f = \frac{1}{2} k_{ij} e_i e_j \qquad \text{i,j,= 1-6, summation implied.} \qquad 2.3$$

The tensor k_{ij} has ten non-zero components, of which four are independent, and are known as the torsional elastic constants, k_{11}, k_{22}, k_{33} and k_{24}. These represent the elastic constants for the splay, twist, bend and saddle-splay torsional deformations respectively, and can be written in co-ordinate free notation to give the equation for the free energy density:

$$f_{elastic} = \frac{1}{2}\left[k_{11}(\underline{\nabla}\cdot\underline{\mathbf{n}})^2 + k_{22}(\underline{\mathbf{n}}\cdot\underline{\nabla}\times\underline{\mathbf{n}})^2 + k_{33}(\underline{\mathbf{n}}\times\underline{\nabla}\times\underline{\mathbf{n}})^2 - (k_{22}-k_{24})(\underline{\nabla}\cdot\{\underline{\mathbf{n}}\underline{\nabla}\cdot\underline{\mathbf{n}} + \underline{\mathbf{n}}\times\underline{\nabla}\times\underline{\mathbf{n}}\})\right]$$

2.4

The above equation assumes that the lowest energy state is that with a uniform director, and it can be modified for conformations with spontaneous twist such as a chiral nematic. Also k_{24} can be ignored for simple 1-d deformations providing further simplification.

This equation therefore provides the energetic basis for an orientationally aligned liquid crystal medium, and provides definition of the elastic constants corresponding to the four independent director strains, which any deformation in a nematic liquid crystal can be described as a combination of. This is then the foundation of the restoring force in liquid crystals that have been deformed under the action of an applied electric or magnetic field. The basis of such action is the topic of the next section.

2.3. DIELECTRIC AND OPTICAL ANISOTROPY

As has been discussed, by definition, a liquid crystalline medium has to have a preferential axis of orientation, the basis of which is founded on molecular shape. All thermotropic liquid crystals have some shape anisotropy in their constituent molecules, the most common being "rod-shaped" or calamitic.[7] This shape anisotropy provides not only the preferential alignment due to greater Van der Waals interactions for side-to-side molecules, but can also result in dielectric anisotropy due to differing freedom of the electrons to produce dipoles along the long molecular axis and perpendicular to it.

2.3.1. Dielectric Coupling

An insulating material's dielectric constant, ε, describes its ability to electrically polarise under the influence of an applied field. This polarisation is the result of dipoles which form in the bulk of the material, reducing the effective field strength in the bulk.[8] This polarisation is given by:

$$\mathbf{P} = \varepsilon_0 \varepsilon_r \cdot \mathbf{E} = \boldsymbol{\varepsilon} \cdot \mathbf{E} \qquad 2.5$$

In a nematic liquid crystal, the dielectric constant varies with direction relative to the director, **n,** so we have the tensor relation,

$$\underline{\mathbf{P}}_i = \varepsilon_{ij} \underline{\mathbf{E}}_j \qquad 2.6$$

where i,j are the three orthogonal directions x, y, z, and summation over all three is implied. If **n** is defined as lying in the z direction, the principal values of the dielectric tensor are $\varepsilon_\perp, \varepsilon_\perp$ and $\varepsilon_\parallel$ in the x, y and z directions respectively.

The components of an electric field parallel and perpendicular to the director are:

$$E_{\parallel} = \mathbf{E} \cdot \mathbf{n} \tag{2.7}$$

$$E_{\perp} = \left|\mathbf{E} - (\mathbf{E} \cdot \mathbf{n})\mathbf{n}\right| \tag{2.8}$$

The overall polarisation is then given by:

$$\mathbf{P} = \varepsilon_{\perp}\mathbf{E} + \Delta\varepsilon(\mathbf{n} \cdot \mathbf{E})\mathbf{n} \tag{2.9}$$

where $\Delta\varepsilon = \varepsilon_{\parallel} - \varepsilon_{\perp}$. The free energy density is then obtained, as the result of the integration of **P** with respect to **E**:

$$f_{dielctric} = -\frac{1}{2}\left[\varepsilon_0 E^2 + \Delta\varepsilon(\mathbf{E} \cdot \mathbf{n})^2\right] \tag{2.10}$$

The first term of this result is independent of **n**, but the second term reveals the source of the dielectric torque. If the material has positive dielectric anisotropy ($\varepsilon_{\parallel} > \varepsilon_{\perp}$) then the lowest energy state is that with the director aligned with the applied field (a negative $\Delta\varepsilon$ produces the opposite result, the director being compelled to lie at 90º to the field. If we take the director to lie at an angle θ to the applied field, the torque, Γ,on the director is:

$$\Gamma = -\frac{\partial f}{\partial \theta} = \Delta\varepsilon E^2 \sin\theta\cos\theta \tag{2.11}$$

The torque is therefore zero when the field is parallel or perpendicular to the director, but one of these states is an unstable equilibrium, dependent on the sign of $\Delta\varepsilon$. The torque is greatest at θ = 45º.

If the liquid crystal is held in a cell which holds the director in a certain direction at the boundaries, the electric field therefore competes with elastic restoring force to deform the director alignment. This is known as the Freedericksz transition. The expression for the total free energy density in this situation is now:

$$f_{elastic} + f_{dielctric} = -\frac{1}{2}\left[k_{11}(\nabla \cdot \mathbf{n})^2 + k_{22}(\mathbf{n} \cdot \nabla \times \underline{\mathbf{n}})^2 + k_{33}(\mathbf{n} \times \nabla \times \underline{\mathbf{n}})^2 + \varepsilon_0\Delta\varepsilon(\mathbf{E} \cdot \mathbf{n})^2\right] \tag{2.12}$$

There will be a threshold field at which the dielectric torque is sufficient to deform the director from uniform alignment. This will depend on the elastic constant for the particular deformation being induced, but is in general given by:

$$E^{threshold}_{splay,twist,bend} = \frac{\pi}{d}\sqrt{\frac{k_{11,22,33}}{\varepsilon_0\Delta\varepsilon}} \tag{2.13.}$$

where d is the sample thickness. The Freedericksz transition, with its electrically induced director deformation and elastic restoring force is the basic mechanism for many liquid crystal electro-optic

effects. This is because, as the director of a sample is rotated, the optical properties of the sample change. This is described in the next section.

2.3.2. Optical Anisotropy

Having outlined the dielectric anisotropy of liquid crystals resulting from the molecular shape anisotropy, it follows that this also results in optical anisotropy, as in non-ferromagnetic materials,

$$n_i = \sqrt{\varepsilon_{ii} / \varepsilon_0} \qquad 2.14$$

where n is the principal refractive index in the i = x, y, z orthogonal directions such that the components of the dielectric permittivity tensor ε_{ii} are diagonalised, and ε_0 is the permittivity of free space.[9] The dielectric anisotropy therefore results in a molecular birefringence that, if the molecules are on average aligned in a particular direction as in a liquid crystalline state, results in a macroscopic birefringence. This birefringence can be represented by an ellipsoid optical indicatrix. The distance of the a point on the surface of this ellipsoid from the origin gives the refractive index for light travelling through the material which has an electric field vector polarized in the direction of the point from the origin. The semi-major and semi-minor axes of the ellipsoid therefore give the principal refractive indices for the material, parallel and perpendicular to the director. The indicatrix ellipsoid for a positive and negative uniaxially birefringent material are shown in Figure 2.2.

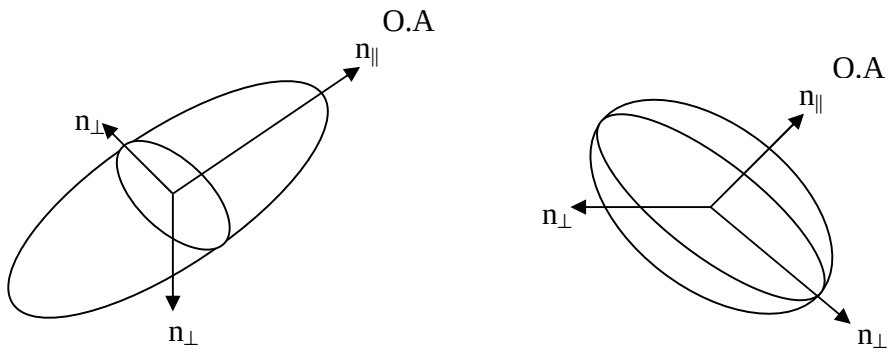

Figure 2.2: *The optical indicatrix ellipsoids for a positive (left) and negative (right) uniaxial material.*

In a material that is defined as having positive birefringence, the ordinary ray (that which does not experience a polarisation dependent refractive index, i.e. propagates along the optic axis)

experiences a smaller birefringence than the extraordinary ray. The extraordinary ray then has an electric field vector oriented perpendicular to that of the ordinary ray. This case is reversed for a negative uniaxial material. Light travelling along the optic axis always experiences $n = n_{\perp}$, while light travelling at an angle θ to the optic axis will have an ordinary ray experiencing $n_{\perp}$, and an extraordinary ray experiencing:

$$\frac{1}{n_e^2} = \left(\frac{\cos\theta}{n_{\perp}}\right)^2 + \left(\frac{\sin\theta}{n_{\parallel}}\right)^2 \qquad 2.15$$

These differing refractive indices lead to differing propagation speeds through the medium, depending on E-vector direction, which can be visualised using a wave surface diagram. These describe the wavefront propagation distances for a set travel time from a point source at the origin for the ordinary and extraordinary rays. Wave surfaces for positive and negative uniaxial media are shown in Figure 2.3.

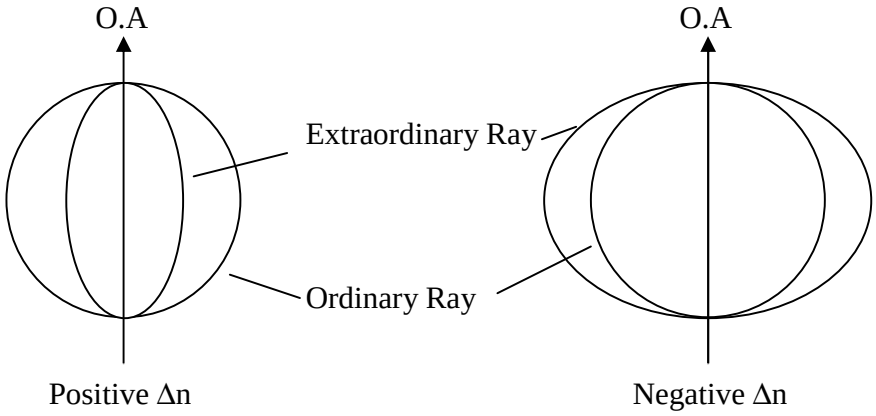

Figure 2.3: *Wave surface diagrams for positive and negative birefringent media*

A material with a birefringence $\Delta n = n_{\parallel} - n_{\perp}$, will then cause a phase difference to be imparted between the ordinary and extraordinary rays. This phase difference is given by:

$$\delta = \frac{2\pi\Delta n d}{\lambda} \qquad 2.16$$

where d is the length the light travels through the medium and λ is the wavelength of the light. If the Δn and the thickness of the material are such that δ = π, then the sample is a half waveplate, and the phase difference will be such that light initially polarised at 45° to the optic axis will be rotated by 90°, allowing it to pass through crossed polarisers unhindered. The general formula for the intensity of light transmitted through crossed polarisers containing a birefringent sample is:

$$I = I_0 \sin^2(2\psi)\sin^2\left(\frac{\pi\Delta nd}{\lambda}\right) \qquad 2.17$$

where I_0 is the intensity of the light passed through the initial polariser, and ψ is the angle between the transmission axis of the initial polariser and the optic axis of the sample. It can be seen from the above equation that, for a birefringent material to provide 100% modulation of an input light, either the effective retardance of the sample has to be switchable from $\delta = 0$ to $\delta = \pi$, or the optic axis of the sample with $\delta = \pi$ has to be rotatable from $\psi = 0^{o}$ to $\psi = 45^{o}$.

This relationship, in conjunction with the dielectric properties outlined in the previous section, which allow both the effective Δn and/or ψ in the above equation to be rapidly altered by the application of an electric field, which changes the director alignment, provide the basis for many electro-optic effects in liquid crystals. There are several other mechanisms by which the director orientation of a liquid crystal can couple to an applied field and produce a change in the samples optical properties however, including flexoelectric coupling.

2.3.3. Flexoelectric Coupling

In addition to dielectric coupling, in which an applied field induces a dipole in the constituent molecules of the liquid crystal, if the molecules have a significant spontaneous electric dipole, the field can couple to this. A liquid crystalline material can have spontaneous molecular dipoles, but no overall spontaneous polarisation, due to the $\mathbf{n} = -\mathbf{n}$ director property allowing the molecules to be aligned antiparallel, on average having their dipoles cancel out. An applied field will then align all the dipoles with the field, causing the molecules to align parallel. If the molecules also have a degree of shape anisotropy along the long axis of the molecule, this alignment will result in a curvature strain in the material. This process can also be inverted, allowing a curvature strain imposed on the material by boundary conditions to induce a spontaneous polarization in the bulk. This process was first described by Meyer,[10] and is illustrated below.

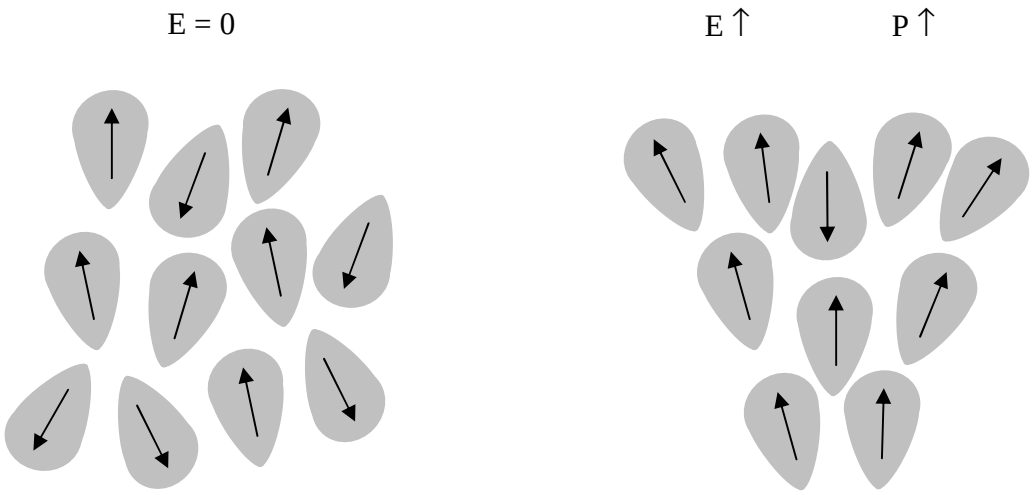

Figure 2.4: *Illustration of flexoelectric coupling inducing a splay deformation in pear-shaped molecules in addition to aligning the molecular dipoles with the applied field to cause a bulk polarisation.*

In the illustration above, the "pear" shape of the molecules causes a splay deformation to occur if the spontaneous dipole of the molecules lie along the director. This polarises the material and removes the $\mathbf{n} = -\mathbf{n}$ symmetry. A bend deformation can also be induced in "banana" shaped molecules, in this case a transverse molecular dipole is required to remove the symmetry.[11]

If the molecules possess a degree of both "pear" and "banana" asymmetry, the development of a bulk polarisation causes the formation of a periodic splay-bend deformation. This is illustrated below, as described by Meyer, and has been observed experimentally.[12]

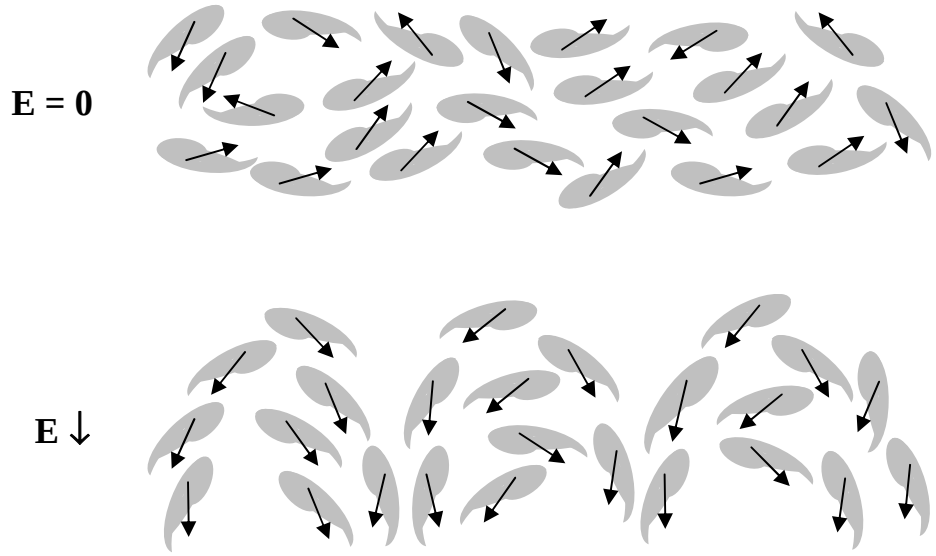

Figure 2.5: *The development of a periodic splay-bend deformation upon inducing a bulk polarisation in a liquid crystal with spontaneous molecular dipoles and "pear" and "banana" shape asymmetry*

The induced polarisation in the bulk of a flexoelectric material can therefore be linked to the degree of splay and bend deformations induced in the material, according to the following equation:[11]

$$\mathbf{P}_{flexo} = e_s \mathbf{n}(\nabla \cdot \mathbf{n}) + e_b (\mathbf{n} \times \nabla \times \mathbf{n}) \qquad 2.18$$

where e_s and e_b are the flexoelectric coefficients for splay and bend deformations respectively, according to the convention laid out by Rudquist et al.[11,13] The importance of the molecular shape in this effect has been demonstrated by the dependence of the flexoelectric coefficients on trans-cis isomerisation of the constituent molecules.[14]

Flexoelectricity can also arise in materials without dipoles and the particular shape anisotropies mentioned. It has been shown by Prost et al that quadrupolar flexoelectric coupling is also possible.[15] This allows the possibility of a degree of flexoelectric coupling in all nematic liquid crystals.

The flexoelectric coefficients have been studied experimentally, chiefly by Murthy[16] and theoretically by Osipov.[17] The former study concluded that the flexoelectric coefficients are generally proportional to the square of the order parameter ($(e_s+e_b) \sim S^2$), but that some nematics appear to have some component of the flexoelectric coefficients linearly dependent on S. This is in

line with the theory presented by Osipov. In this study, the degree of flexoelectric coupling is observed via the optical response it produces in chiral nematic samples, rather than directly via the polarisation induced by a given deformation. This is known as the flexoelectro-optic effect, and is discussed in the subsequent section.

2.4. THE CHIRAL NEMATIC PHASE

The physical basis for electro-optical effects in nematic (N) liquid crystals has been outlined in the preceding sections of this chapter. These principles are all applicable in chiral nematic (N*) materials, but an added complexity is introduced by the fact that the molecular chirality results in a material which exhibits a helical director configuration macroscopically. The chirality of the system can be an inherent property of the liquid crystalline material, as with the cholesteric samples in which liquid crystalline phase was first observed[18-20], or can be introduced into an achiral nematic material by the addition of a chiral additive.[21] Either method results in the same liquid crystalline geometry: a degree of nematic orientational order locally, with the nematic director orientation rotating on moving through the sample in a direction perpendicular to the local alignment direction. This arrangement can be described in a Cartesian frame as follows: If the director **n** is confined to the x-y plane,

$$n_x = \cos(\theta),\ n_y = \sin(\theta),\ n_z = 0 \qquad 2.19$$

where θ is the angle of the director in the x-y plane, with respect to its angle in the z = 0 plane, and is given by:

$$\theta = \frac{2\pi}{P} z = kz \qquad 2.20$$

where P is the pitch length of the material, defined as the distance in the z direction taken for the director to rotate through 2π radians, and k is the modulus of the helical wavevector of the material. This arrangement is illustrated below.

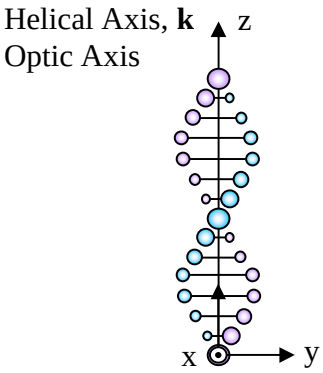

Figure 2.6: *Diagram showing the director structure in the chiral nematic phase.*

This helical director structure can be thought of as a stack of thin nematic plates, each exhibiting the same material birefringence, but with the director rotated by a small amount going from one plate to the next. This inherent twist in the director structure requires a modified free energy equation, taking into account the twist in the lowest energy state, giving the following expression:[22]

$$f_{elastic} = \frac{1}{2}\left[k_{11}(\nabla\cdot\mathbf{n})^2 + k_{22}(\mathbf{n}\cdot\nabla\times\mathbf{n} + k)^2 + k_{33}(\mathbf{n}\times\nabla\times\mathbf{n})^2\right] \qquad 2.21$$

This director configuration gives rise to some very unusual optical properties, which are discussed below.

2.4.1. Optical Properties

When considering the optical properties of the chiral nematic phase, two situations have to be considered, that of light propagating along the helical axis, and that of light propagating perpendicular to it, as the interactions between the light and the medium is very different for each of these. For the former case, the two defining features of chiral nematics, selective reflection and large optical activity with anomalous dispersion are observed. These can be explained both analytically, [23] and numerically[24-26] using the "dielectric stack" model as a basis for a matrix approach. For the latter case, the length of the material pitch relative to the wavelength of the light determines whether a simple macroscopic birefringence is experienced, or a diffracting structure of periodic refractive index.

2.4.1.1 Macroscopic Birefringence

When a chiral nematic sample is observed under a polarising microscope from a direction orthogonal to the helical axis, usually in a cell aligned in the uniform lying helix (ULH) texture, a so-called fingerprint texture is observed.[7] This is a striped texture resulting from the periodic change in refractive index, the period of the stripes corresponding to a π rotation of the director, or a P/2 length of helix, due to the $\mathbf{n} = -\mathbf{n}$ symmetry of nematics. This striping can only occur if $P > \lambda$, and the light can effectively sample the different refractive regions of the helix, as the refractive index experienced by the light polarised orthogonal to the helical axis changes from $n_{\parallel}$ to $n_{\perp}$ with the helical director rotation. This is not the case if $P < \lambda$, in which case an average refractive index of $n_{o,N^*} = \sqrt{\frac{n_{\perp}^2 + n_{\parallel}^2}{2}}$ is experienced for light polarised perpendicular to the helical axis.[27] Light polarised parallel to the helical axis experiences $n_{e,N^*} = n_{\perp}$ for all regions of the helix. The material therefore exhibits a macroscopic birefringence, with negative Δn and optic axis perpendicular to the director planes, i.e. parallel to the helical axis in an undeformed sample. The optical texture in this case appears relatively uniform and coloured, though in most cases not monodomain due to the changing surface alignment conditions for the different regions of the helix.

This straightforward birefringence is drastically affected however, as the light propagates along the optic axis. In this situation, the light is best considered as being decomposed into two components of oppositely rotating circularly polarised light.

2.4.1.2 Selective Reflection

If the period of the helix matches that of the wavelength of the light in the medium, a Bragg-like reflection occurs for the light with the circular handedness which matches that of the helix. i.e. a right-handed helix, defined as that which exhibits a clockwise rotation of the director upon moving

along the helix axis, reflects right circularly polarised light, defined as light which exhibits a clockwise rotation of the electric field vector as seen by an observer having the light propagate towards them. This result is predicted from theory[24,26], and has been observed experimentally in many instances.[24,27,28] The band of wavelengths which experience reflection is given by:

$$\Delta\lambda = P\Delta n \qquad 2.22$$

and the reflected band is centred on the wavelength given by:

$$\lambda_C = \bar{n}P \qquad 2.23$$

where $\bar{n} = \frac{n_{\parallel} + n_{\perp}}{2}$.

The transmission spectra for unpolarised light input to a chiral nematic sample, as taken in the laser lab by Steve Morris, is shown in Figure 2.7.

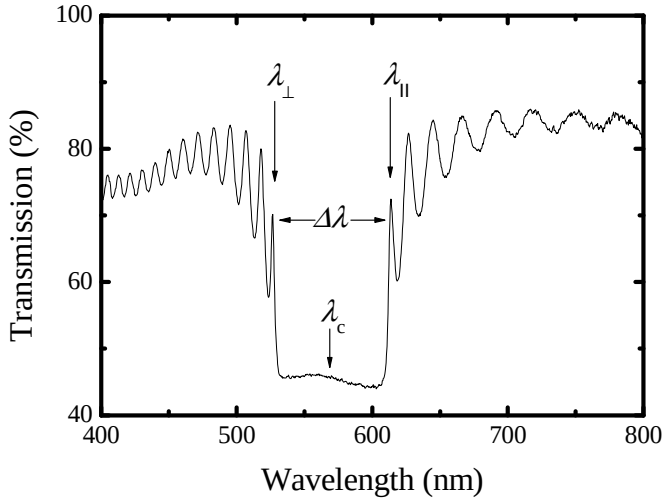

Figure 2.7: *Transmission of unpolarised white light through a chiral nematic sample.*

The figure shows the short and long wavelength band edges, $\lambda_\perp$ and $\lambda_\parallel$ respectively. The overall loss of approximately 20% is due to the reflection by the glass surfaces and ITO electrodes on the cell walls, after which it can be seen half the light (that with a circular polarisation component corresponding to the sense of rotation of the material helix) is reflected, as expected. There are also reflection side-lobes, which are predicted by the theory for the chiral nematic sample alone, but are probably enhanced by etalon reflections from the glass walls.

2.4.1.3 Optical Activity and Anomalous Dispersion

If the wavelength of the incident light is outside the reflection band, both right and left circular components are transmitted. The helical refractive index configuration still results in differing effective refractive indices for the two different components however. This is circular birefringence or optical activity. Unlike the case of linear birefringence, the phase excursion introduced between the two circularly polarised components does not change the degree of ellipticity of shape of the output light, but simply rotates the angle of polarisation of the linearly polarised light which re-forms on exiting the medium.

The rotatory power of an optically active medium is given by the angular rotation of the input light per unit length, ψ / d, and has been found to be extremely high in liquid crystals, over 10^3 deg/mm,[22] compared to 24 deg/mm in quartz. The rotation is also highly and anomalously dependent on wavelength. The degree of rotation per unit length, as a function of the material refractive indices and pitch length, was derived by De Vries,[29] and can be written as follows:

$$\frac{\psi}{d} = \frac{\pi}{16}\left(\frac{n_{\parallel}^2 - n_{\perp}^2}{n_{\parallel}^2 + n_{\perp}^2}\right)^2 \frac{P^3}{\lambda^2\left(P^2 - \lambda^2\right)} \qquad 2.24$$

This equation reveals that the degree of rotation is strongest closest to the reflection band, where the wavelength is closest to the pitch, and that the direction of rotation changes on going from one side of the reflection band to the other. For $\lambda < P$ the polarisation is rotated in the same sense as the helix, and this is reversed for $\lambda > P$. For $\lambda >> P$, the polarisation direction follows the director, known as the Mauguin regime.[30] This waveguiding configuration is that used by the very successfully commercialised twisted nematic and super-twisted nematic cell types.

The chiral nematic phase, viewed along the helical axis always looks coloured, due to the selective reflection, and will also appear coloured through crossed polarisers due to the reflection and rotatory dispersion effects. Monodomain samples are easily achieved as uniform planar alignment layers on the glass surfaces provide good anchoring for sample with the helical axis vertical in the cell, and the material will alter slightly its natural pitch in order to allow the director to rotate to the preferred direction of alignment on the substrate. This smooth coloured appearance is known as the Grandjean texture. If the cell is not of uniform thickness, disclination lines appear where the director at the surface twists through 180º to change from a slightly stretched helix to a slightly

compressed one in order to minimise the free energy while still maintaining a local surface director along the rubbing direction. These are known as Grandjean-Cano steps.

2.4.2. Dielectric Coupling

The behaviour of chiral nematic materials under the influence of an electric field is dependent on the direction in which the field is applied relative to the helical axis. In a Grandjean textured cell with a positive $\Delta\varepsilon$ material, with the field applied from top to bottom in the cell via transparent ITO electrodes, as is the usual case, as the field amplitude is increased the helix will break up and a focal conic texture nucleates, this is a scattering state with many small domains of randomly oriented helices. These will then begin to unwind under the dielectric coupling influence on the individual molecules eventually resulting in an achiral homeotropic texture. This chiral nematic to nematic phase transition occurs at the critical unwinding field:[3]

$$E_{crit} = \frac{\pi}{2}\sqrt{\frac{k_{22}}{\varepsilon_0 \Delta\varepsilon}} \qquad 2.25$$

This process is illustrated below:

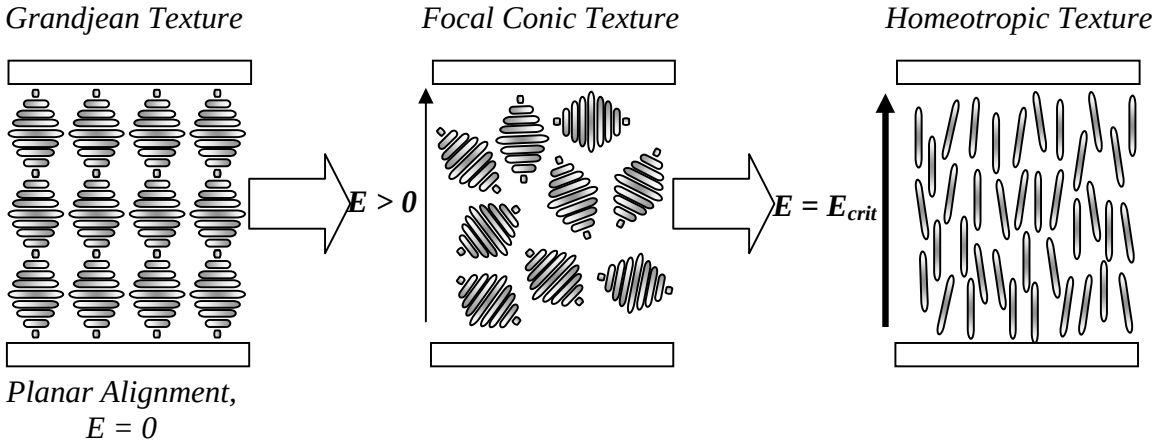

Figure 2.8: *Diagram illustrating the change in director configuration as an applied field of increasing strength is applied parallel to the helical axis of a chiral nematic sample.*

This transition can be viewed with a polarising microscope, simultaneously as the throughput intensity is monitored with a photodiode. The resulting trace reveals the transition from the transmissive grandjean to the scattering focal conic, and eventual complete unwinding at E_{crit} to the very clear homeotropic state. This is shown for a chiral nematic mixture in Figure 2.9.

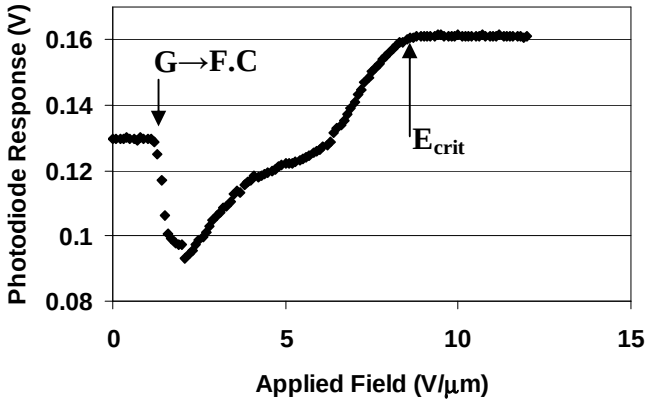

Figure 2.9: *The photodiode response for a Grandjean textured chiral nematic mixture subject to an increasing field applied parallel to the initial helical axis, showing the transitions to the focal conic state (G→F.C. and eventual helix unwinding (E_{crit}).*

On reduction of the field from the homeotropic state, the focal conic again nucleates and this state then remains stable in the absence of further inducement to adopt the Grandjean texture, such as a shear.[31]

If the field is applied orthogonally to the undeformed helical axis, in a positive $\Delta\varepsilon$ material, the helix is not compelled to break up, but can begin to unwind from its initial state, undergoing a direct N* → N transition. The exact process by which the chiral nematic state becomes an unwound nematic has not been described in a manner which satisfies all experimental data, but two models provide the likely possibilities. These are the gradual and continuous extension of the material pitch, which reaches infinity at E_{crit}, as proposed by De Gennes,[3] and the Kawachi-Kogure model,[32] in which the pitch remains constant, but the helix regions of director parallel to the field are extended, sharpening the twist zones at the P/2 points, before these twists are annihilated from disclinations. Which of these mechanisms dominates in an actual sample appears dependent on the ratio of pitch to cell thickness, and the material parameters such as dielectric anisotropy and flexoelectric coefficients.

2.4.3. The Flexoelectro-optic Effect

As with the achiral nematics discussed previously, as well as dielectric coupling to the unequal dipoles induced by an applied field along and perpendicular to a nematogen's long axis, flexoelectric coupling can occur to a molecule's spontaneous electric dipole, and cause splay and bend deformations in the material according to the molecule's shape anisotropy. In the case of a periodic splay-bend deformation being induced, as in Figure 2.5, the chiral nematic director configuration allows an unusual helix deformation to occur to satisfy this condition with minimal cost to the elastic free energy when the field is applied orthogonal to the helical axis. The deformation is a rotation of the director in the sections of the helix in which it lies perpendicular to the applied field, around the direction of the applied field. This causes the director planes of the helix to lie at an angle to the helical axis. Bouligand originally showed that such an angled slice through a helical material resulted in the required splay-bend deformation being observable in the cross-section of the slice.[33]

The resulting optical effect was first discovered by Patel and Meyer[34] in ULH aligned cells with a field applied vertically via transparent ITO electrodes on the cell surfaces, and takes the form of an in-plane rotation of the optic axis of the birefringent cell.[35] This deformation is illustrated in Figure 2.10.

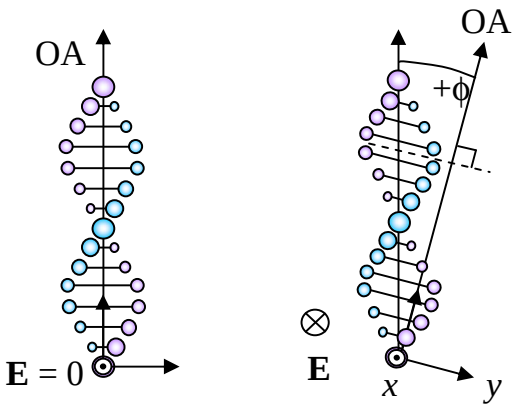

Figure 2.10: *Helix deformation and consequent rotation of the optic axis resulting from the flexoelectro-optic effect.*

The key points of interest in the flexoelectro-optic effect, as well as the in-plane rotation of the optic axis in the plane orthogonal to the applied field, are that the characteristic response time of the effect is fast, being generally of the order 100-500μs.[36] Also the degree of optic axis rotation, ϕ, is linear with the applied field, therefore the direction of ϕ (positive or negative in Figure 2.10)

is dependent on the polarity of the applied field.[37] A change in field from +E to –E, therefore produces a rotation of the optic axis from $+\phi$ to $-\phi$, a total switch of 2ϕ.

The basis of the relationship between the tilt angle and response time to the applied field and material parameters has been outlined by Rudquist et al, as development on the original theory of Patel and Meyer.[13,38,39] The total free energy density for the chiral material is now given as:

$$f = f_{elastic} + f_{dielectric} + f_{flexoelectric} \qquad 2.26$$

where
$$f_{flexoelectric} = \mathbf{E}\cdot\mathbf{P}_{\mathbf{flexo}} = e_s\left(\mathbf{E}\cdot\mathbf{n}(\nabla\cdot\mathbf{n})\right) + e_b\left(\mathbf{E}\cdot\mathbf{n}\times\nabla\times\mathbf{n}\right) \qquad 2.27$$

and the preceding terms are given by equation 2.12. Taken in Cartesian co-ordinates, the director components are:

$$\mathbf{n} = \cos(kz)\hat{\mathbf{x}} + \sin(kz)\cos(\phi)\hat{\mathbf{y}} - \sin(kz)\sin(\phi)\hat{\mathbf{z}} \qquad 2.28$$

where $k = \frac{2\pi}{P}$ as in equation 2.20. With this convention, the vector descriptions of the director deformations used in the free energy equation are:

$$\nabla\cdot\mathbf{n} = -k\cos(kz)\sin(\phi)$$

$$\nabla\times\mathbf{n} = -k\cos(kz)\cos(\phi)\hat{\mathbf{x}}$$

$$\mathbf{n}\cdot\nabla\times\mathbf{n} = -k\cos(\phi)$$

$$\mathbf{n}\times\nabla\times\mathbf{n} = \left(-k\sin^2(kz)\sin(\phi)\right)\hat{\mathbf{x}} + \left(k\cos(kz)\sin(\phi)\cos(\phi)\right)\hat{\mathbf{y}} + \left(-k\sin(kz)\cos(kz)\sin^2(\phi)\right)\hat{\mathbf{z}}$$

$$\mathbf{n}(\nabla\cdot\mathbf{n}) = -k\cos(kz)\sin(\phi)\left[\cos(kz)\hat{\mathbf{x}} + \sin(kz)\cos(\phi)\hat{\mathbf{y}} + \sin(kz)\sin(\phi)\hat{\mathbf{z}}\right]$$

$$(\mathbf{n}\times\mathbf{n}\times\mathbf{n})^2 = k^2\sin^2(kz)\sin^2(\phi) \qquad 2.29$$

Taking these relations and the applied field in the negative x direction, we have:

$$f = \frac{1}{2}k_{11}\left(k^2\cos^2(kz)\sin^2(\phi)\right) + \frac{1}{2}k_{22}k^2(1-\cos(\phi))^2 + \frac{1}{2}k_{33}\left(k^2\sin^2(kz)\sin^2(\phi)\right) - Ek\sin(\phi)\left(e_b\sin^2(kz) + e_s\cos^2(kz)\right) \qquad 2.30$$

The free energy then has to be averaged over the whole helix, i.e. $\langle\sin^2(\theta)\rangle = \langle\cos^2(\theta)\rangle = \frac{1}{2}$, where the angled brackets represent a thermal average, therefore:

$$\langle f\rangle = \frac{1}{4}k_{11}\left(k^2\sin^2(\phi)\right) + \frac{1}{2}k_{22}k^2(1-\cos(\phi))^2 + \frac{1}{4}k_{33}\left(k^2\sin^2(\phi)\right) - \frac{1}{2}Ek\sin(\phi)(e_b + e_s) \qquad 2.31$$

which becomes

$$\langle f \rangle = \frac{1}{2} K k^2 \sin^2(\phi) + \frac{1}{2} k_{22} k^2 (1 - \cos(\phi))^2 - \bar{e} E k \sin(\phi) \qquad 2.32$$

where $K = \frac{(k_{11} + k_{33})}{2}$ and $\bar{e} = \frac{(e_s + e_b)}{2}$. Equation 2.32 can then be minimised by setting the derivative with respect to ϕ to zero:

$$\frac{\partial \langle f \rangle}{\partial \phi} = k^2 \sin(\phi)\cos(\phi)(K - k_{22}) + k_{22} k^2 \sin(\phi) - \bar{e} E k \cos(\phi) = 0 \qquad 2.33$$

and approximated for small angles to give:

$$\tan\phi = \frac{\bar{e}E}{kK} = \frac{\bar{e}E}{K}\frac{P}{2\pi} \qquad 2.34$$

This equation therefore shows the degree of optic axis tilt induced in a chiral nematic sample by the flexoelectro-optic effect to be linearly dependent on the applied field, and inversely on the pitch. Any temperature dependence of the tilt angle must also be contained in the temperature dependence of the pitch, elastic constants, and flexoelectric coefficients. The equation can also be seen to provide a figure of merit for flexoelectric materials, namely the flexoelastic ratio, $\bar{e}/K$. This has units of $CN^{-1}m^{-1}$, and is typically valued at less than 0.6 $CN^{-1}m^{-1}$ in flexoelectro-optic materials.[40]

The response time for the effect can be characterised by the time taken to for the optic axis to return to equilibrium on the removal of an applied field. This is given by:[36,41]

$$\frac{\partial \phi}{\partial t} = \frac{1}{\gamma}\frac{\partial \langle f \rangle}{\partial \phi} \qquad 2.35$$

where γ is the relevant effective viscosity for the distortion. Again, substitution from equation 2.33, and assuming a small angle gives:

$$\gamma \frac{\partial \phi}{\partial t} = K k^2 \phi - \bar{e} E k \qquad 2.36$$

If the optic axis is assumed to return to equilibrium from its initial field dependent angle exponentially, then $\phi = \phi_0 e^{-t/\tau}$, and the characteristic response time is approximated to:

$$\tau = \frac{\gamma}{K k^2} = \frac{\gamma}{K}\frac{P^2}{4\pi^2} \qquad 2.37$$

This shows a field independent response time, with the temperature dependence again being limited to that of the viscosity and the elastic constants.

2.4.4. Bimesogens for the Flexoelectro-optic Effect

From the equations derived in the preceding section, it can be seen that the desired physical parameters for a large and fast flexoelectro-optic switch are:

1. High flexoelectro-optic coefficient and low splay and bend elastic constants to maximise the flexoelastic ratio and therefore the induced tilt angle in a given field.
2. Low viscosity to minimise the response time of the pitch.
3. Pitch short enough to allow a smooth texture when viewed in the ULH configuration (i.e. $P<\lambda$), and minimise the response time according to equation 2.37, but long enough so as not to compromise the tilt angle according to 2.34. Clearly a trade-off is required in this case, but maximisation of $\bar{e}/K$ allows the shortest possible pitch to be selected for the required tilt angle.
4. High birefringence to allow the sample to be made as thin as possible to reduce operating voltages. For example, if full light modulation is required, the higher the material birefringence, the thinner the sample can be made and still provide a half waveplate, so the lower the voltage required to provide the applied field which gives an optic axis rotation of $2\phi = 45^{o}$, according to equation 2.17.
5. Low dielectric anisotropy, in order to prevent dielectric helix unwinding and allow higher strength fields to be applied before the ULH texture is disrupted, maximising the achievable tilt angle.

The synthesis of a liquid crystal optimised for the flexoelectric effect has been attempted with the development of bimesogenic liquid crystals.[42-44] Bimesogens are so called due to their molecules possessing two mesogenic moieties, such as cyanobiphenyl units, attached with a flexible alkyl chain. If these units are attached at opposite ends such that the connecting unit holds them antiparallel, the individual spontaneous dipoles of the units on average oppose each other, and this is believed to lead to a reduction in the dielectric anisotropy without significant loss of material birefringence.[45]

The degree of reduction of the dielectric anisotropy can depend on whether the bimesogens are symmetric, i.e. have identical mesogenic units, or non-symmetric – in possession of non-identical mesogenic units, and also on the length of the alkyl chain spacer, as this determines the average

angle of the mesogenic units to each other with an odd-even effect resulting from the change from -trans to -cis conformation.[46,47]

In addition to the reduction in dielectric anisotropy without loss of birefringence, which address points 4 and 5 above, bimesogens, when mixed with a chiral dopant, have been shown to exhibit extremely high flexoelectric coefficients, therefore also addressing point 1.[48] The flexoelastic ratio, as mentioned before has been valued at typically < 0.6 $CN^{-1}m^{-1}$, has been measured at up to 2.35 $CN^{-1}m^{-1}$ in chiral mixtures of odd spacer-length bimesogens.[39] In this work, several bimesogen liquid crystal mixtures are investigated, both symmetric and non-symmetric, including the ester-linked symmetric difluorinated bimesogens which have been shown to have the strongest flexoelectro-optic response.[49]

2.4.5. The Flexoelectro-optic Effect in the Grandjean Texture

As discussed in the previous Chapter, the flexoelectro-optic effect as so far only been investigated in the original configuration, outlined by Patel and Meyer,[34] i.e. with a chiral nematic aligned in the ULH texture, and an electric field applied between transparent electrodes on the cell surfaces. The central idea of this thesis is to attempt to observe the effect in a new geometry in which the liquid crystal is aligned in the Grandjean texture with the field applied in the plane of the cell, and then to asses the potential of the effect in this configuration for telecoms applications.[50] As this arrangement has not been previously tested, a consideration of the optics of the switch is required, and some basic calculations of the expected magnitude of the electro-optic response.

Fibre-optic communication systems generally operate with a signal carrier lightwave at 1550nm wavelength in order to minimise absorption in the silica medium. For this reason, the electro-optics of the proposed cell were tested at this wavelength in this work. The idea behind the proposed device is that operation at these wavelengths will allow relatively long pitch (≈500nm) materials to be used, maximising the flexoelectro-optic tilt angle, while maintaining a pitch much shorter than the wavelength of the infrared light, removing any optical rotation effects, according to equation 2.24, and preventing any selective reflection. At equilibrium with no field applied the cell should therefore appear optically neutral, the optic axis of the macroscopically birefringent sample lying perpendicular to the cell walls, giving extinction when placed between crossed polarisers. Between parallel polarisers, the sample should be highly transparent.

A field applied in the plane of the cell should tilt the optic axis in a direction perpendicular to the applied field, as in Figure 2.10, resulting in the optic axis having a component in the polarisation plane of the light, and an effective birefringence appearing in the sample. If the direction of the applied field within the plane of the cell is at some angle $\psi > 0$ to the transmission axes of the crossed polarisers, some optical throughput will then occur. This throughput should reach 100% if $\psi = 45°$, and the effective birefringence is such that the sample becomes a half waveplate. This mode of operation is illustrated in Figure 2.11.

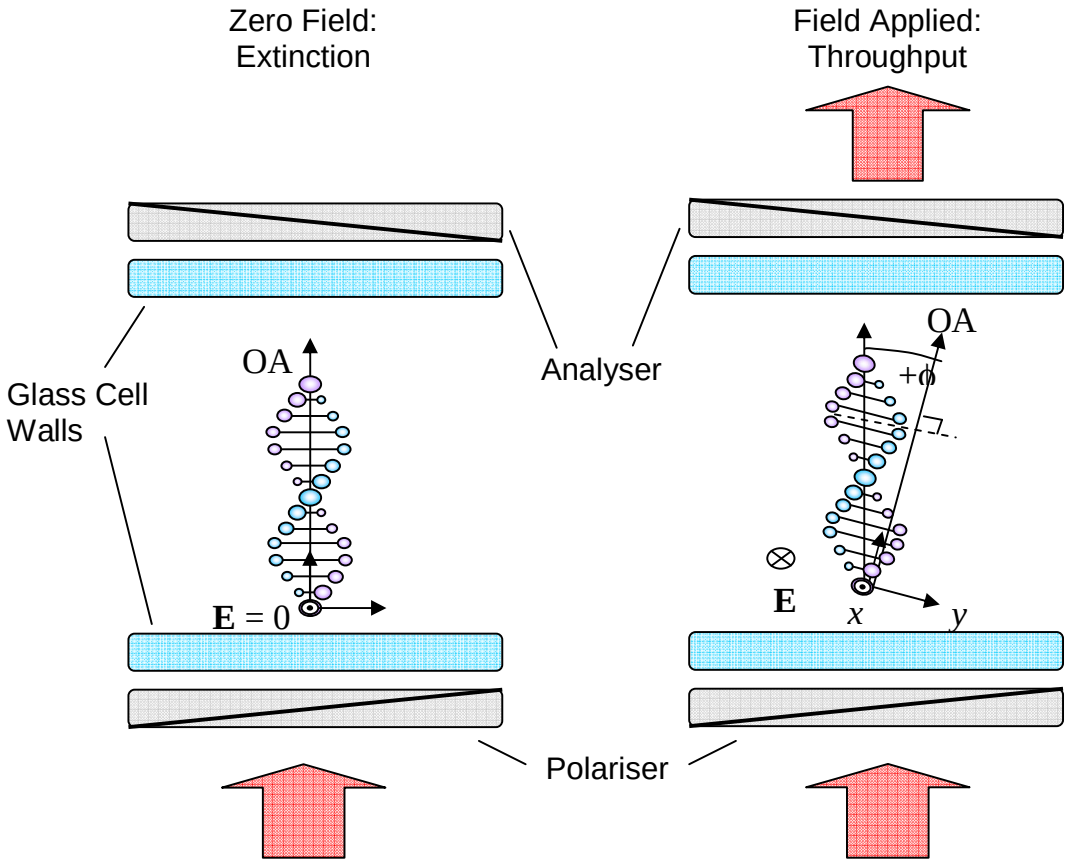

Figure 2.11: *Diagram illustrating the operation of a Grandjean flexoelectro-optic device. The direction of applied field is into the page to allow clear illustration of the deformation, which occurs in the plane perpendicular to the applied field.*

As the optic axis is tilted at an angle to the direction of light propagation, it is thought that some anomalous refraction will occur, and as well as a variable waveplate, the cell will also act as a walk-off element for the beam. This effect should be negligible however for the type of cell thicknesses anticipated (10-40µm).

The basis for this induced birefringence is clear, if the director configuration is considered from the direction of the incoming light. The undeformed helix exhibits full-circle precession of the director on going through a pitch length of material. As the polarisation direction of the input light experiences no rotation, the effective birefringence experienced by the light, averaged over the whole helix, is the same for all directions of polarisation. Under an applied field, the flexoelectro-optic deformation causes the director planes to tilt out of the polarisation plane of the light, in a direction perpendicular to the applied field. This reduces the effective birefringence, averaged over the whole helix, for light polarised in the direction of tilt. The circular director pattern as viewed along the helix becomes squashed into an ellipse, and a birefringence results. This is illustrated in Figure 2.12.

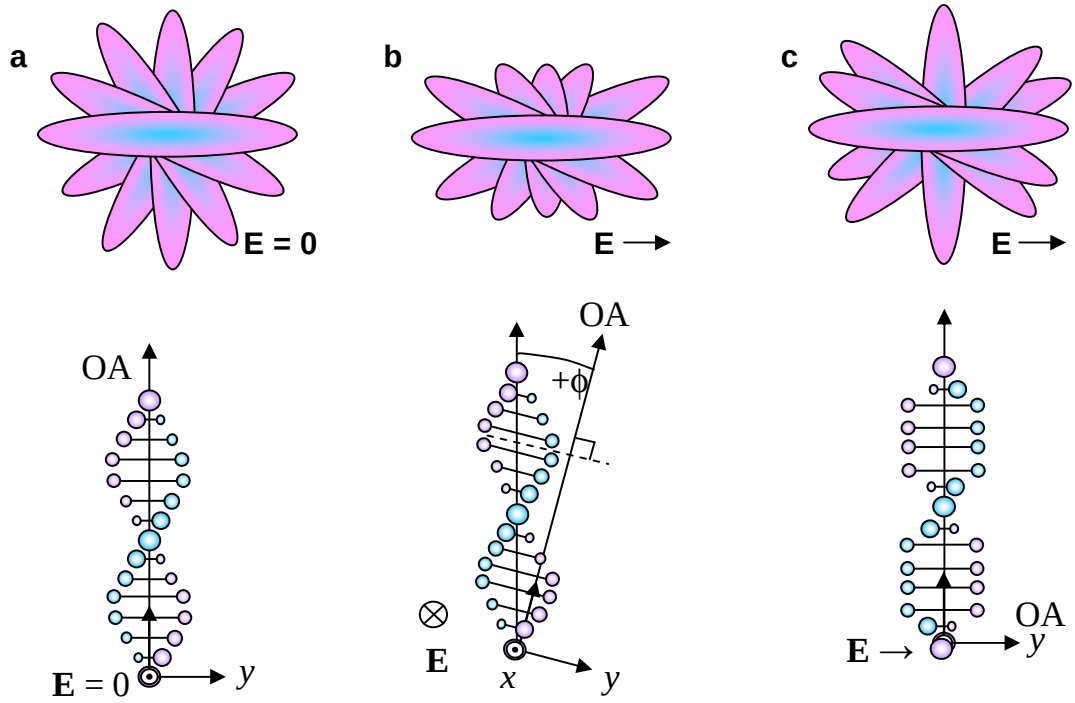

Figure 2.12: *Schematic illustration of the deformation of the chiral nematic helical director structure (a) due to flexoelectro-optic (b) and dielectric (c) coupling to an electric field applied orthogonal to the helical axis. The effect of the deformation is viewed along (upper figure) and perpendicular (lower figure) to the helical axis to illustrate the source of the resulting birefringence. Note in the flexoelectric example the differing electric field direction for the two views, necessary for illustrative purposes.*

It also can be seen from the figure that dielectric coupling of the applied field to the director will result in a degree of helix unwinding which contributes to the birefringence and produces an optic axis parallel to the projection of the flexoelectrically tilted optic axis in the polarisation plane of the light. These effects will therefore be complementary, and indistinguishable by the birefringence they produce.

In order to estimate the magnitude of the electro-optic response resulting from the flexoelectro-optic deformation in the Grandjean texture at 1550nm, a calculation was carried out of the expected induced birefringence. This was done by treating the cell as a stack of thin birefringent plates, the effective birefringence and optic axis direction of each plate being determined by the estimated material birefringence, and the director direction, as prescribed by the chiral rotation of **n** with distance along the helical axis, and the flexoelectric tilt angle.

To calculate the effective birefringence from each of these plates, the ellipsoid refractive index for each plate is calculated in Cartesian co-ordinates, having undergone the required rotations, around the z axis due to the natural helix progression, and around the x axis due to the flexoelectric tilt (the helix is taken to have it's axis in the z direction, as for equations 2.19 and 2.20, and the field is taken to be applied in the x direction). An ellipsoid indicatrix with semi-major axis along the x direction is described by the equation:

$$\frac{x^2}{n_{\parallel}^2}+\frac{y^2}{n_{\perp}^2}+\frac{z^2}{n_{\perp}^2}=1 \qquad 2.38$$

This can be written in matrix form as $\mathbf{X}^{+}\cdot\mathbf{V}\cdot\mathbf{X}=1$, or:

$$(x,y,z)\begin{pmatrix} 1/n_{\parallel}^2 & 0 & 0 \\ 0 & 1/n_{\perp}^2 & 0 \\ 0 & 0 & 1/n_{\perp}^2 \end{pmatrix}\begin{pmatrix} x \\ y \\ z \end{pmatrix}=1 \qquad 2.39$$

For each plate, depending on it's position in the stack along z, the long-axis of the indicatrix is rotated by θ about the z axis, where θ is given by equation 2.20. This is represented in the matrix description of the ellipsoid by multiplying by the rotation matrix $\mathbf{R_1}$. The rotation of the ellipsoid due to the flexoelectro-optic tilt is included by multiplying by the rotation matrix $\mathbf{R_2}$. The new ellipsoid equation is then $\mathbf{X}^{+}\cdot\mathbf{R}_2^{+}\cdot\mathbf{R}_1^{+}\cdot\mathbf{V}\cdot\mathbf{R}_1\cdot\mathbf{R}_2\cdot\mathbf{X}=1$, where:

$$\mathbf{R_1} = \begin{pmatrix} \cos\theta & \sin\theta & 0 \\ -\sin\theta & \cos\theta & 0 \\ 0 & 0 & 1 \end{pmatrix} \quad \text{and} \quad \mathbf{R_2} = \begin{pmatrix} 1 & 0 & 0 \\ 0 & \cos\phi & \sin\phi \\ 0 & -\sin\phi & \cos\phi \end{pmatrix} \tag{2.40}$$

The flexoelectro-optic rotation $\mathbf{R_2}$ must be effected on the right hand side of $\mathbf{R_1}$ in order for the tilt to be performed around the original x axis, i.e. the direction of applied field. This produces the desired effect of tilting the indicatrix ellipsoid in the layer planes in which the director is perpendicular to E by ϕ, and merely rolling the ellipsoid around its long axis when **n** is parallel to **E**, reproducing the helix deformation illustrated in Figure 2.10.

In order to calculate the effective refractive indices for each of the plates in the stack after these rotations, the projection of the rotated ellipse in the x-y plane must be found. This is done as follows. The matrix equation for the ellipsoid will now have 9 non-zero elements, as the ellipse is no longer aligned with the principal axes, so the matrix is not diagonalised. The generalised ellipsoid equation can then be written as a quadratic in z:

$$m_{33}z^2 + 2(m_{13}x + m_{23}y)z + (m_{11}x^2 + 2m_{12}xy + m_{22}y^2) - 1 = 0 \tag{2.41}$$

where m_{ij} are the matrix elements of the rotated ellipsoid. The solutions of the above equation give two z values for any point in the x-y plane, representing the top and bottom of the ellipsoid at that point. The solutions are given by the general equation for solutions to quadratics:

$$z = \frac{-B \pm \sqrt{B^2 - 4AC}}{2A} \tag{2.42}$$

where $A = m_{33}$, $B = m_{13}x + m_{23}y$ and $C = M_{11}x^2 + 2m_{12}xy + m_{22}y^2$. If $\sqrt{B^2 - 4AC = 0}$ then z is single valued, and the point x-y is at the extreme edge of the ellipsoid when viewed in the x-y plane. The locus of these points is given by the equation:

$$ax^2 + 2bxy + cy^2 = 1 \tag{2.43}$$

where $a = m_{11} - \frac{m_{13}^2}{m_{33}}$, $b = m_{12} - \frac{m_{13}m_{23}}{m_{33}}$ and $c = m_{22} - \frac{m_{23}^2}{m_{33}}$. This equation describes an ellipse, and is the projection of the rotated ellipsoid in the x-y plane. A series of plots of this projected ellipse for plates at varying distances along the z axis, from z = 0 to z = P/4 is shown in Figure 2.13. The ellipsoid has been given an exaggerated difference between long and short axes for clearer illustration of the effect.

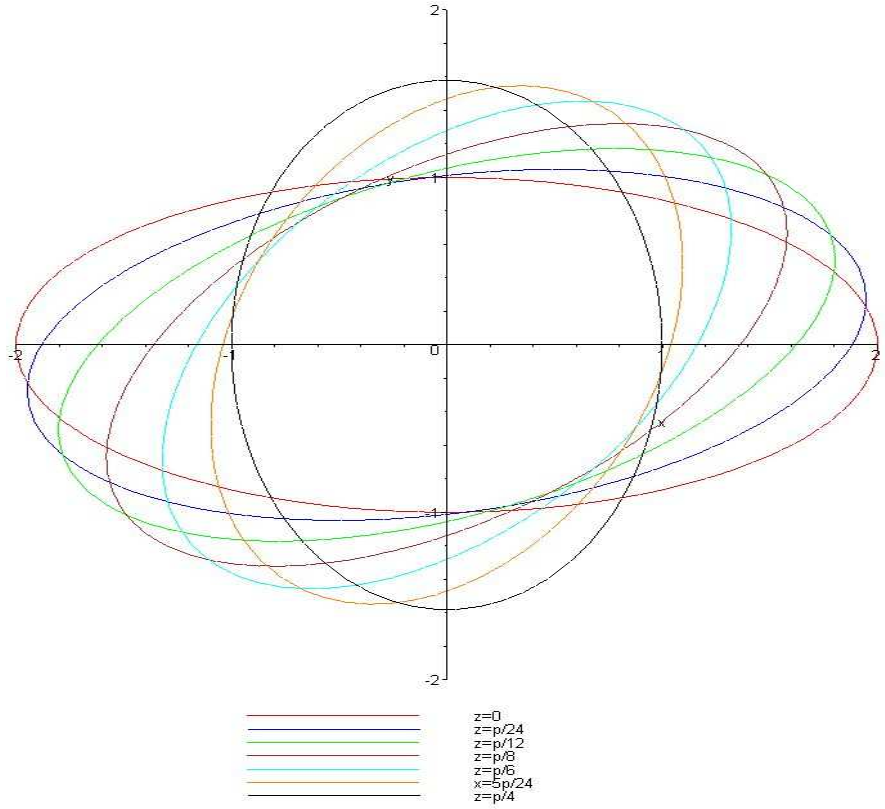

Figure 2.13: *Projections in the x-y plane of a series of ellipsoids having undergone rotations of θ = 0 to θ = 90º about the z axis, and ϕ = 45º about the x axis.*

The above figure shows that the rotations do indeed produce the expected change in effective refractive indices in the polarisation plane of the light as the plane moves along the z direction: as the director rotates through the helix, the long axis of the ellipse is shortened. It is also worth noting that due to the $\mathbf{R_2}$ rotation being about the original x axis, the ellipsoid is skewed when viewed along z, so the angle of the long axis of the projected ellipse for any given plate with respect to the original axes, does not always match the value of θ for that plate.

These birefringences, calculated as a function of z and ϕ for each plate, can then be used to create a Jones matrix for each birefringent plate. For this calculation, the material pitch was taken to be 500nm and the material birefringence at 1550nm was estimated to be 0.077. A Jones matrix was generated for every 5º rotation of θ, and matrices only need to be produced for 0º to 180º, as **n** = -**n**, so resulting matrices for a stack making up half a pitch length can be multiplied by itself 40 times, to produce a total path length of 10µm. This overall matrix for the cell was then combined

with the Jones matrices for crossed polarisers either side of the stack with transmission axes at 45º to the x axis (and therefore the applied field), and the Jones vector for input light linearly polarised along the transmission axis of the first polariser. The resulting output Jones vector gives the components of the E-vector of the output light in the x and y directions, the magnitude of which is squared to give the intensity transmitted by the system.

This output intensity was calculated for a series of systems with flexoelectro-optic tilt angles ranging from $\phi = 0$ to 60º. The expected intensity transmission as a function of induced tilt angle according to this method, ignoring dielectric effects is shown below. The figure shows the optical throughput for input light polarised parallel and at 45º to the applied field.

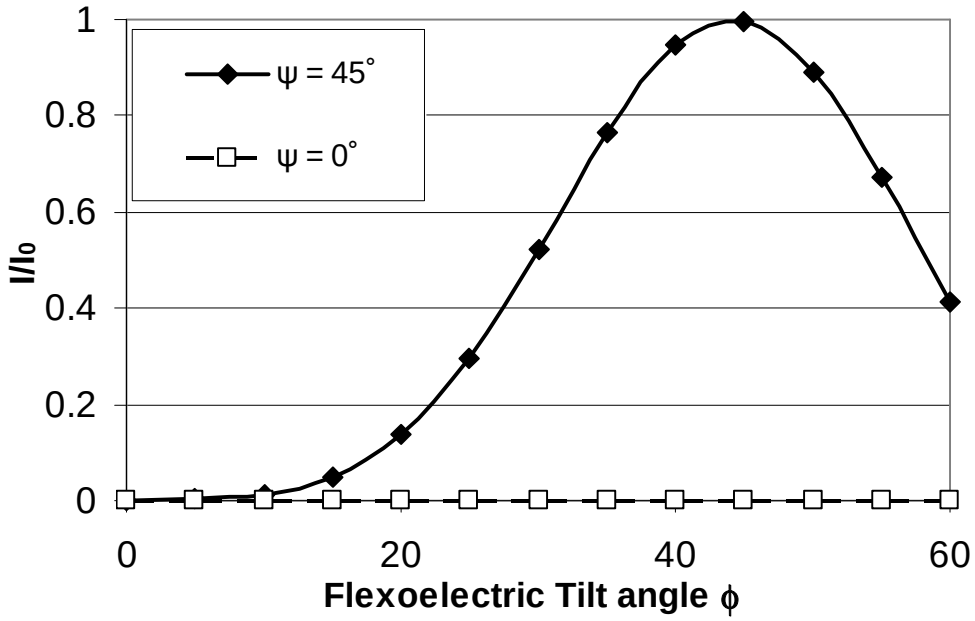

Figure 2.14: *The expected optical throughput of a Grandjean textured chiral nematic 10µm thick, with material $\Delta n = 0.77$ at 1550nm, between crossed polarisers, as a function of induced flexoelectro-optic tilt angle. The throughput is shown for input light polarised parallel ($\psi = 0$) and at $\psi = 45º$ to the applied field.*

The figure shows that in a 10µm thick sample, a tilt angle of approximately 45º is required to produce a half-waveplate, and that as expected, the transmission begins to drop after the retardance increases beyond half a waveplate. It also shows the expected dependency on the polarisation direction of the input light relative to the applied field. Input light polarised along the field direction produces no throughput.

The important result however, is that the bimesogen mixtures, which have been shown to have high flexoelectro-optic tilt angles, should provide a switch of significant magnitude with the fields available, so an effect ought to be visible. It appears from the plot that a tilt angle of at least 15º is required before a significant switch is observed. The experimental details of the investigation into this effect are detailed in the next chapter, and the first observations of the flexoelectro-optic effect in Grandjean textured chiral nematics are shown in Chapter 4.

2.5. PHOTONIC BAND EDGE LASING

It is thought that the flexoelectro-optic deformation in Grandjean textured chiral nematic materials, as detailed above may have an effect on the pitch of the material undergoing deformation, due to the tilting of the nematic layer planes changing the layer spacing. If this is the case, then the flexoelectro-optic deformation ought to provide a means of electrically tuning the output of dye-doped chiral nematic liquid crystal lasers with very fast response time.

Lasing at the edge of the reflection (or stop) band of a dye doped Grandjean textured chiral nematic liquid crystal was first observed by Kopp et al,[51] having been predicted several years earlier.[52] Lasing in these systems results from stimulated fluorescence emission from dye molecules which are dissolved in the liquid crystal host and then excited by a pump laser beam. The emission is amplified by feedback resulting from the increased density of photon states, and increased photon dwell time at the edges of the reflection band (see Section 2.4.1.2), which can be considered as a one dimensional photonic band gap, and is hence known as photonic band edge (PBE) lasing.[53,54]

This amplification, of course, only occurs if the pitch of the material is engineered by careful control of the concentration of chiral dopant in the material to have one or both of the reflection band edges in the emission peak of the dye used. As it is the inherent liquid structure that provides the feedback mechanism, the lasing is said to be mirrorless, and the properties of the host liquid crystal (e.g. birefringence, order parameter) have been shown to strongly affect the lasing characteristics such as pump threshold energy and slope efficiency.[55,56] The measured reflection band of a chiral nematic sample and the spectral position of the laser line that results from pumping the sample are shown below.

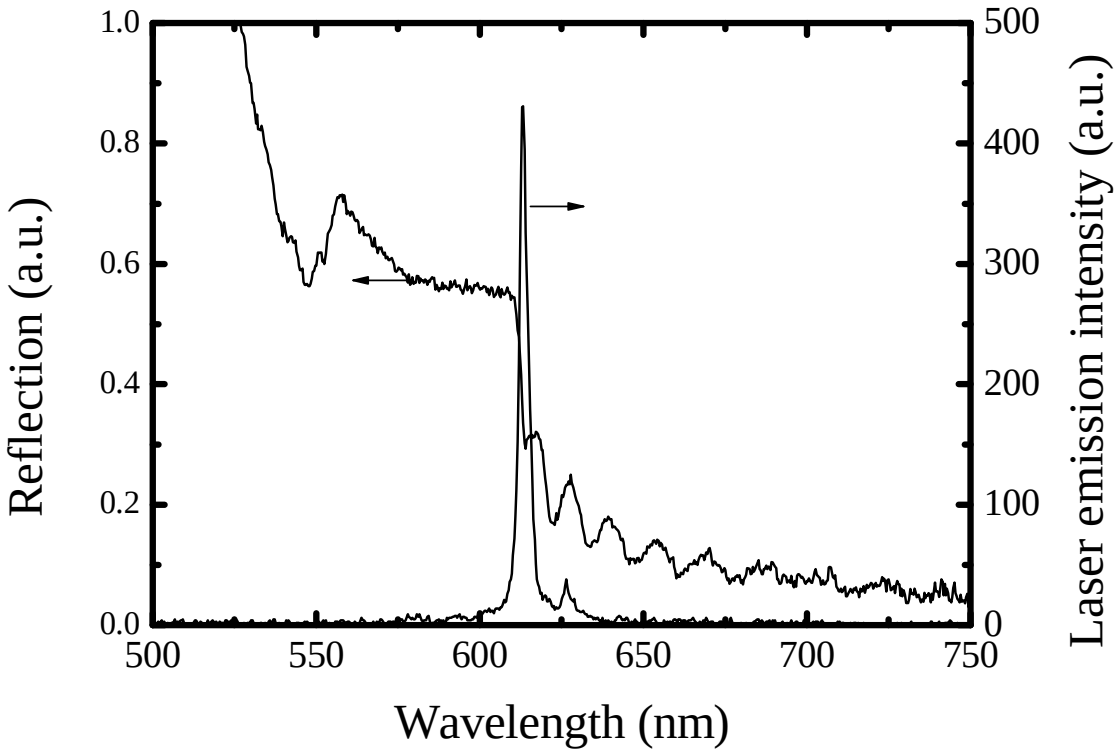

Figure 2.15: *Reflection spectrum of a chiral nematic sample and resultant laser line produced by an incident pump pulse, showing the precise positioning of the laser output at the long-wavelength band edge. (Figure courtesy of S. Morris.)*

The laser line is seen to be very narrow bandwidth, and therefore acts as a very accurate marker of the edge of the reflection band, which otherwise is not always clear due to side-lobes and reflections from the cell substrates (see the above plot and Figure 2.7). Any mechanism which can adjust the position of the edges of the reflection band in the sample therefore, will tune the laser output, as long as the edge of the reflection band remains within the emission spectrum of the dye.

Several mechanisms of achieving this manipulation of the reflection band have been demonstrated, such as the temperature variation of the pitch length, optical tuning via photoiosmerisation of the chiral dopant to alter its effectiveness[57], mechanical translation of a cell with a pitch gradient to physically change the area of the cell being pumped,[58] and even stretching of an elastomeric chiral nematic sample in two directions to compress the pitch.[59] These methods all require some slow mechanical or temperature movement however, and a fast electronic mechanism with no moving parts would be far preferable. Electronic tuning of liquid crystal lasers has been achieved in devices composed of a photonic bandgap with a switchable ferroelectric or nematic defect layer,[60,61] but not to date in a simple monodomain chiral nematic sample. It is this effect the work

reported in Chapter 7 was aimed at achieving via utilisation of the flexoelectro-optic effect in the Grandjean texture.

2.6. REFERENCES

[1]C. W. Oseen, *Transcripts of the Faraday Society*, **29**, 883, (1933).

[2]H. Zocher, *Transcripts of the Faraday Society*, **29**, 945, (1933).

[3]P. De Gennes and J. Prost, *The Physics of Liquid Crystals*, Oxford: Clarendon Press, (1993).

[4]F. C. Frank, *Discuss. Faraday. Soc.*, **25**, 19-28, (1958).

[5]D. R. Lovett, *Tensor Properties of Crystals*, IOP Publishing Ltd., (1989).

[6]D. Demus, J. W. Goodby and G. W. Gray, *Physical Properties of Liquid Crystals*, Wiley-VCH, (1999).

[7]P. J. Collings, *Liquid Crystals: Nature's delicate phase of matter*, Princeton University Press, (2002).

[8]P. J. Collings and M. Hird, *Introduction to Liquid Crystals, Chemistry and Physics*, Taylor and Francis Ltd., (1997).

[9]S. J. Elston and J. R. Sambles, *The Optics of Thermotropic Liquid Crystals*, Taylor and Francis Ltd, (1998).

[10]R. B. Meyer, *Physical Review Letters*, **22**, (18), 918, (1969).

[11]P. Rudquist and S. T. Lagerwall, *Liquid Crystals*, **23**, (4), 503, (1997).

[12]I. Dozov and I. Penchev, *Journal de Physique (Paris)*, **47**, 373-7, (1986).

[13]P. Rudquist, PhD, Chalmers Technical University, (1997).

[14]D. S. Hermann, P. Rudquist, K. Ichimura, K. Kudo, L. Komitov, et al., *Physical Review E*, **55**, (3), 2857, (1997).

[15]J. Prost and J. P. Marcerou, *Journal de Physique (Paris)*, **38**, 315-24, (1977).

[16]P. R. M. Murthy, V. A. Raghunathan and N. V. Madhusudana, *Liquid Crystals*, **14**, (2), 483-96, (1993).

[17]M. A. Osipov, *Journal de Physique (Paris) Lettres*, **45**, 823, (1984).

[18]F. Reinitzer, *Monatsh. Chem*, **9**, 421, (1888).

[19]F. Reinitzer, *Liq. Cryst.*, **5**, 7, (1989).

[20]O. Lehmann, *Z. Phys. Chem.*, **4**, 462, (1889).

[21]L. N. Lisetski and A. V. Tolmachev, *Liq. Cryst.*, **5**, (3), 877-88, (1989).

[22]H. J. Coles, *Chiral Nematic Liquid Crystals,* in *Handboook of Liquid Crystals*,**2a**, D. Demus, J. W. Goodby and G. W. Gray, Wiley-VCH, (1998).

[23]E. I. Kats, *Sov. Phys. JETP.*, **32**, 1004-7, (1971).

[24]D. W. Berreman and T. J. Scheffer, *Phys. Rev. Lett.*, **25**, (9), 577-&, (1970).

[25]D. W. Berreman, *Journal of the Optical Society of America*, **62**, (4), 502-&, (1972).

[26]D. K. Yang and X. D. Mi, *J. Phys. D-Appl. Phys.*, **33**, (6), 672-6, (2000).

[27]R. Dreher and G. Meier, *Phys. Rev. A*, **8**, (3), 1616-23, (1973).

[28]S. Chandrasekhar, G. S. Ranganath and K. A. Suresh, *Acta Crystallographica Section A*, **31**, S161-S, (1975).

[29]H. L. de Vries, *Acta Cryst.*, **4**, 219-26, (1951).

[30]M. C. Mauguin, *Bull. Soc. Fr. Mineral.*, **34**, 71, (1911).

[31]M. Kawachi, O. Kogure and K. Kato, *Japanese Journal of Applied Physics*, **17**, (2), 391-4, (1978).

[32]M. Kawachi and O. Kogure, *Japanese Journal of Applied Physics*, **16**, (9), 1673-8, (1977).

[33]Y. Bouligand, *Journal De Physique*, **30**, (C4), 90, (1969).

[34]J. S. Patel and R. B. Meyer, *Physical Review Letters*, **58**, (15), 1538, (1987).

[35]J. S. Patel and R. B. Meyer, Patent: *EP0281341*, (1988).

[36]J. S. Patel and S. D. Lee, *J. Appl. Phys.*, **66**, (4), 1879-81, (1989).

[37]L. Komitov, S. T. Lagerwall, B. Stebler and A. Strigazzi, *J. Appl. Phys.*, **76**, (6), 3762-8, (1994).

[38]B. Musgrave, PhD, University of Southampton, (2000).

[39]M. J. Clarke, PhD Thesis, University of Southampton, (2004).

[40]P. Rudquist, M. Buivydas, L. Komitov and S. T. Lagerwall, *J. Appl. Phys.*, **76**, (12), 7778, (1994).

[41]S. D. Lee, J. S. Patel and R. B. Meyer, *J. Appl. Phys.*, **67**, (3), 1293-7, (1990).

[42]H. J. Coles, M. J. Coles, S. P. Perkins, B. M. Musgrave and D. Coates, Patent: *GB2356629.*,

[43]B. Musgrave, P. Lehmann and H. J. Coles, *Liq. Cryst.*, **26**, (8), 1235-49, (1999).

[44]H. J. Coles, B. Musgrave, M. J. Coles and J. Willmott, *J. Mater. Chem.*, **11**, (11), 2709-16, (2001).

[45]B. Musgrave, M. J. Coles, S. P. Perkins and H. J. Coles, *Mol. Cryst. Liq. Cryst.*, **366**, 2587-94, (2001).

[46]D. A. Dunmur, G. R. Luckhurst, M. R. de la Fuente, S. Diez and M. A. P. Jubindo, *J. Chem. Phys.*, **115**, (18), 8681-91, (2001).

[47]A. Ferrarini, G. R. Luckhurst, P. L. Nordio and S. J. Roskilly, *Chemical Physics Letters*, **214**, (3-4), 409-17, (1993).

[48]H. J. Coles, M. J. Clarke, S. M. Morris, B. J. Broughton and A. E. Blatch, *J. Appl. Phys.*, **submitted**, (2005).

[49]M. J. Clarke, A. E. Blatch and H. J. Coles, *Mol. Cryst. Liq. Cryst.*, **434**, 367-75, (2005).

[50]H. J. Coles, B. J. Broughton, M. J. Coles and S. M. M. Morris, Patent: *PCT/GB2005/002630*, (2004).

[51]V. I. Kopp, B. Fan, H. K. M. Vithana and A. Z. Genack, *Optics Letters*, **23**, (21), 1707-9, (1998).

[52]L. S. Goldberg and J. M. Schnur, Patent: *U.S. 3,771, 065*, (1973).

[53]V. I. Kopp and A. Z. Genack, *P. Soc. Photo-Opt. Ins.*, **3623**, 71-9, (1999).

[54]B. Taheri, A. F. Munoz, P. Palffy-Muhoray and R. Twieg, *Mol. Cryst. Liq. Cryst.*, **358**, 73-82, (2001).

[55]S. M. Morris, A. D. Ford, M. N. Pivnenko and H. J. Coles, *J. Appl. Phys.*, **97**, (2), art. no.-023103, (2005).

[56]S. M. Morris, A. D. Ford, M. N. Pivnenko and H. J. Coles, *P. Soc. Photo-Opt. Ins.*, **5289**, 236-45, (2004).

[57]A. Chanishvili, G. Chilaya, G. Petriashvili, R. Barberi, R. Bartolino, et al., *Appl. Phys. Lett.*, **83**, (26), 5353-5, (2003).

[58]A. Chanishvili, G. Chilaya, G. Petriashvili, R. Barberi, R. Bartolino, et al., *Appl. Phys. Lett.*, **86**, (5), (2005).

[59]H. Finkelmann, S. T. Kim, A. Munoz, P. Palffy-Muhoray and B. Taheri, *Advanced Materials*, **13**, (14), 1069-+, (2001).

[60]M. Ozaki, M. Kasano, K. Funamoto, R. Ozaki, T. Matsui, et al., *P. Soc. Photo-Opt. Ins.*, **5213**, 111-22, (2003).

[61]R. Ozaki, Y. Matsuhisa, M. Ozaki and K. Yoshino, *Molecular Crystals and Liquid Crystals*, **433**, 237-45, (2005).

Chapter Three

Experimental Techniques

3.1. INTRODUCTION

This chapter will introduce the experimental apparatus, its arrangement and the procedures used to obtain the various measurements performed during the course of the work presented in this thesis.

Three principal experiments form the basis of this thesis:

1. The measurement of the flexoelectro-optic properties (tilt angles and response times) of a series of chiral nematic mixtures aligned in the uniform lying helix (ULH) texture. This is a polarising microscope based experiment using visible light and a fast photodiode detector.

2. The measurement of the electric-field induced birefringence of a series of Grandjean textured chiral nematic mixtures at infra-red wavelengths. This is an optical fibre based experiment arranged on an optical breadboard using a 1550nm laser source and an infra-red power meter.

3. The measurement of laser output from dyed Grandjean textured chiral nematic liquid crystals, and the electric field tuning of that output.

The following section will detail the experimental apparatus and arrangement used in these experiments. Section 3.3 will describe the liquid crystal test cells used and their preparation, as well as the preparation of the chiral nematic liquid crystal samples themselves. The operational methods used in obtaining the results for each experiment, and the expected form of the electro-optic responses are outlined in section 3.4.

3.2. APPARATUS

3.2.1. The Microscope and Visible Electro-optic Equipment

The polarising microscope is a fundamental tool of liquid crystal science. It is used to identify phases, characterise phase transition points, observe textures and detect defect structures. It is used here in conjunction with an electrical signal generator, fast photodiode and oscilloscope to perform electro-optical studies, and also in conjunction with a spectrometer to measure cell thicknesses and chiral nematic reflection bands.

Sample cells are placed on a temperature controlled stage which is positioned in the microscope light-path between the polarisers. With the polarisers crossed therefore, only samples which are optically anisotropic are visible, and regions of the sample imparting different phases excursions on the white light, or different optical rotations, appear differently coloured. The sample can be observed through the eyepieces, as well as simultaneously through the phototube aperture with a camera or photodiode. The polarising microscope used here is an Olympus BH-2 model,[1,2] a schematic of which is shown in Figure 3.1. This microscope allows fine focus adjustment, free rotation of both the polarizer and analyser (to 0.1º accuracy in the case of the analyser), and optional direction of the light throughput to either the eyepieces, the phototube, or split between the two. A range of objectives were used, between 4x and 50x magnification, which, along with the 10x magnification of the eyepieces, gives a total magnification of up to 500x.

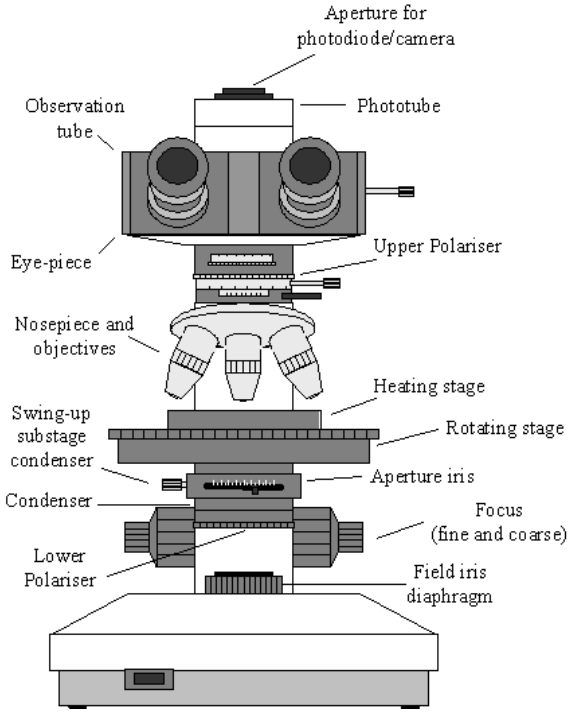

Figure 3.1: *The Olympus BH-2 polarising microscope.*

The hot stage used was manufactured by Linkam,[3] and was connected to a Linkam temperature controller which allowed temperature control of the sample between room temperature up to approximately 250ºC, with 0.1ºC accuracy. Heating and cooling at specified rates was also possible, a useful feature when attempting to align liquid crystal samples by cooling under an applied field. The hot-stage itself was mounted on the microscope's rotation stage. This allowed 360 degree rotation of the sample relative to the polarisers, with 0.5 degree accuracy.

In order to utilise the microscope for electro-optic measurements, the sample cell was connected to a signal generating apparatus. This consisted of a Thurlby Thandar[4] programmable waveform generator, the output of which was input to a wide-band high-voltage amplifier (made in-house). The signal generator was capable of producing standard square, sinusoidal and triangular waveforms of up to 20V peak to peak, with dc offsets of up to ±10V. The waveform frequency could be varied between 1mHz to 13MHz. The amplifier had a continuously variable level of amplification, with a maximum output of 240V peak to peak.

The output from the amplifier was connected to the sample and, in parallel, a Hewlett-Packard[5] 54503A 500 MHz digitizing oscilloscope to allow visualisation and measurement of the output.

This oscilloscope allowed simultaneously viewing of up to four input channels, averaging of up to 2048 waveforms and waveform capture. It also allowed automatic measurement of waveform features such as maximum and minimum voltages, 10-90% rise and fall times and R.M.S. voltages. Also input to the oscilloscope was the voltage response from the photodiode positioned in the microscope phototube. This was a Thorlabs[6] silicon photodetector with a gain of up to 40dB and an active area of approximately 13mm^2. The photodiode provided a linear response to the light intensity input to it: rotation of the microscope analyser with no sample present revealed the expected cos^2 dependency of output voltage on analyser angle. In this way the light intensity from the microscope phototube was measurable as a function of the applied electric field, providing a straightforward electro-optic measurement mechanism. The experimental set-up as described above is illustrated in Figure 3.2.

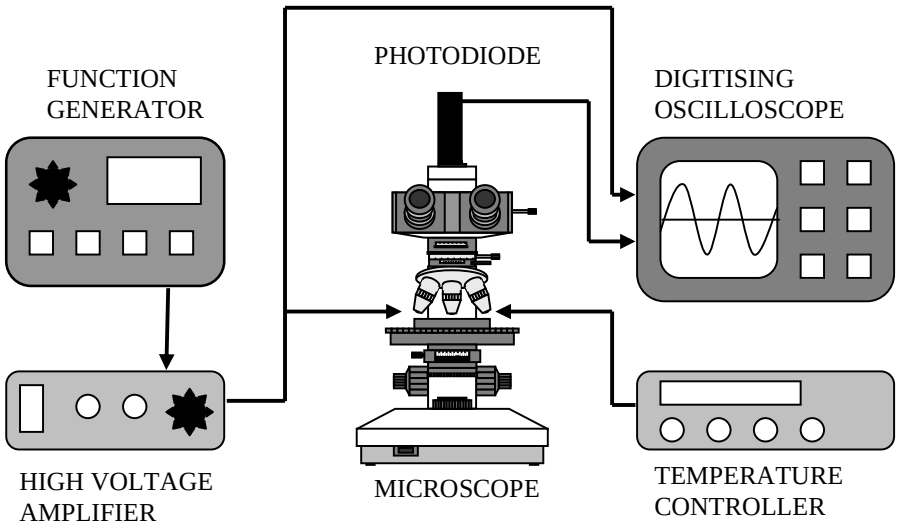

Figure 3.2: *Experimental arrangement for visible light electro-optic measurements.*

As mentioned previously, the photodiode can be replaced in the phototube by a camera for recording of liquid crystal textures. The camera used was an Olympus C4040Z digital camera with 4.2 megapixel resolution. This allowed digital images of textures and video of switching effects to be recorded easily. The camera was used in conjunction with an additional lens (Olympus) inside the phototube, and a mount to allow focusing and fix the camera in place.

3.2.2. The Fibre based Infra-red Electro-optic Equipment.

One of the principal aims of this study is to assess the potential of liquid-crystal based devices, particularly those utilising the flexoelectro-optic effect in optical communication systems. As discussed in Chapter 1, fibre-optic cables now carry the bulk of the world's long distance information transmissions. For reasons of fibre absorbtion and dispersion, they do this on several very closely spaced wavelength channels centred on 1550nm. Therefore, any potential device for utilisation in such a system has to be tested for its electro-optic properties at these wavelengths. This section outlines the experimental arrangement used to perform these tests on the cells and liquid crystal materials examined in this study.

The key performance factors of the device prototype outlined in Chapter 4 are the electric field induced birefringence and the response times required for the birefringence to manifest and remove itself on application and removal of the field. These features can be measured in the same manner as the visible electro-optic characteristics of the previous section, i.e. with the cell between crossed polarisers and the light throughput being input to a digitizing oscilloscope alongside the applied voltage. The only real difference being that, as most infra-red sources and detectors are fibre launched and gathered, fibre alignment devices and infra-red optics had to be used to arrange the light path on an optical breadboard.

This breadboard was a 60x60cm Newport[7] board, creating the requirement for quite a compact experiment. This was another reason for using fibre to deliver the light, removing the need for bulky beam-steering optics.

The source was an Agilent[8] 81640A external cavity tuneable laser module housed in an 8164A lightwave measurement system. This outputs a maximum of 2dBm power at a wavelength tuneable from 1510 to 1640nm, with 0.015nm resolution. The output is fibre launched via an FC ferrule connector. The 8164A also housed the 81634B In GaAs power sensor module. This has -110dB sensitivity ±0.005dB polarisation dependent loss. The light could be input to the sensor directly via an FC fibre ferrule, or via an 81624A optical head. The power reading was displayed on the LC display of the lightwave measurement system, and also output via a BNC connector and coaxial cable to the oscilloscope. The oscilloscope in this case was and Tektronix[9] TDS 3014B digital phosphor oscilloscope, which allowed easy capture of the electro-optic response even to pulses

with large spacing, and export to a computer for analysis, as well as the required automatic measurements.

The light emerging from the source fibre was collimated, sent through an infra-red polariser, focused through the active area of the liquid crystal cell under investigation, re-collimated through the second polariser, and focused into the collection fibre to the power meter. This was achieved with Melles Griot[10] optical components. Specifically, "microblock" 3 axis positioning stages (4mm travel, 50nm resolution with differential drives), 10x infra-red microscope objectives, 12.5mm diameter infra-red polarisers (10^{-3} extinction) and rotatable holders (0.5º accuracy), as well as the required posts and post holders were used. The experimental arrangement described here is illustrated in Figure 3.3:

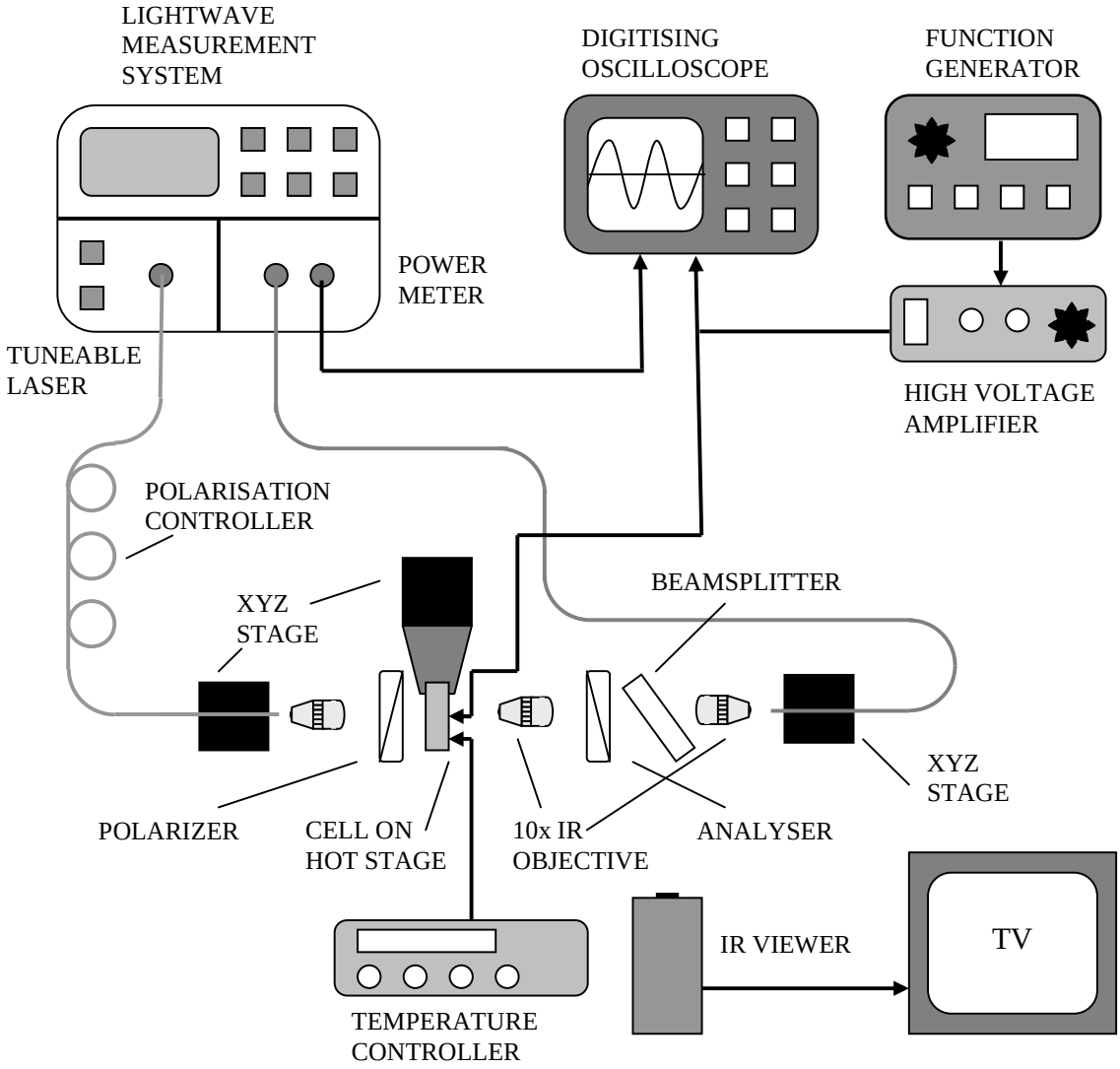

Figure 3.3: *Experimental arrangement for the infra-red electro-optic experiment.*

A beamsplitter could be positioned in the beam path after the second polariser to deflect a small portion of the light into an infrared viewer (Electrophysics[11] 7290A). As the objective immediately behind the cell in the beam path acted as the front lens for the viewer, the image of the cell could be viewed on the television which the viewer output to, and the beam accurately positioned in the active region of the cell by adjustment of the XYZ stage on which the cell was mounted. With the cell at the focal point for the IR viewer, the beam waist could be adjusted to coincide with the cell by adjustment of the first XYZ stage and observation of the spot size on the TV.

Finally, the third objective re-focused the beam back into the fibre for input to the power meter. The collection fibre was mounted on a rotation stage on the XYZ stage to allow optimal positioning for a maximum input of light to the fibre. The power throughput of the system with all the optics in place and the polarisers uncrossed was found to have an optimum of -15dB. This is a tiny fraction, but is to be expected in a fibre-to-fibre coupling set-up with such an amount of free-space optics between fibres. The small amount of light received does not limit the measurements either, as it is still well within the sensitivity of the power meter and all measurements are relative to this measured throughput. The fibre-to-fibre set-up, however, did leave the system extremely sensitive to vibration and use of an isolating optical bench would have afforded greater accuracy. For this reason, when available from the project CASE sponsors Pi Photonics, the 81624A optical head was used in preference to the collecting fibre, providing greater throughput and greatly reduced vibration sensitivity. The experimental set-up thus described then provided a highly sensitive method of detecting fast changes in birefringence at 1550nm, as required.

3.2.3. The Lasing Equipment

All the experiments involving dyed chiral nematic liquid crystal samples, and attempts to observe wavelength tuning of their output by means of the flexoelectro-optic effect were carried out in collaboration with Alison Ford and utilised her well developed experiment[31] to measure lasing performance.

Photonic band-edge (PBE) lasing in chiral nematic liquid crystals is a mirrorless dye laser phenomenon, whereby the inherent 1-dimensional photonic band gap of the helical chiral nematic structure creates an enhanced photon dwell time for light of a wavelength at the band-edge with

the correct circular polarisation. This provides an in-built feedback mechanism, and light emitted into these modes, from excited laser dye molecules dissolved in the liquid crystal, will induce stimulated emission in neighbouring dye molecules. This results in laser amplification and an output beam from both sides of the cell in the direction of the helical axis.

In order to observe such effects, a dyed chiral sample with a helical pitch engineered to match the fluorescence peak of the dye is pumped into an excited state by an external pump laser with a wavelength corresponding to the dye absorbtion peak. The resulting laser emission is collected, the remainder of the pump pulse filtered out, and the PBE emission directed to either an energy meter for threshold power and slope efficiency measurements, or a spectrometer for peak wavelength and full-width-half-maximum measurements.

As alluded to above, the aim of the experiment presented here was to observe electrical tuning of the output wavelength from the liquid crystal, so the energy meter was not required, and the sample cell was connected to apparatus for applying and electrical field to the sample at the time of the input pulse from the pump laser. The experimental arrangement therefore was as illustrated in Figure 3.4.

The laser used was a New Wave Research[12] Polaris model. This is a Q-switched, frequency doubled Nd:YAG laser with pulsed output at 532nm. The device was capable of producing 5ns pulses at up to 20Hz repetition rate and 30mJ pulse energy maximum. For these measurements however, the laser was pulses at only 1HZ to avoid optically induced reorientation of the chiral nematic director[13], and with the spot size at the cell (approximately 100µm), 60µJ was the maximum pulse energy required.

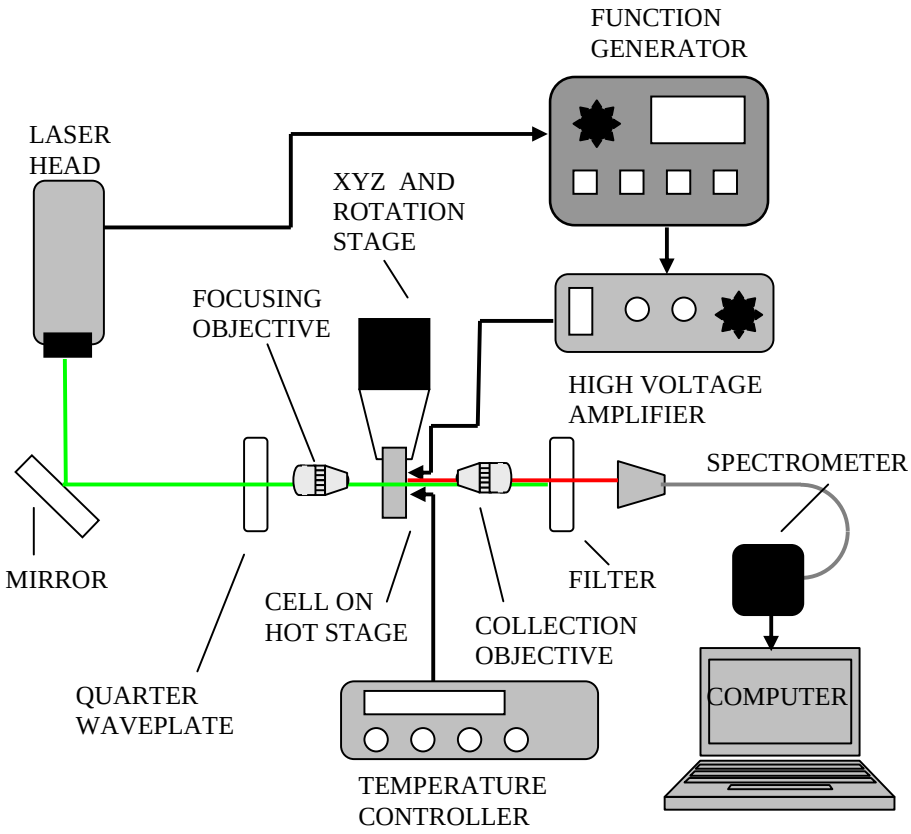

Figure 3.4: *Experimental arrangement for the laser tuning experiment*

The laser output had two voltage trigger pulses for timing purposes, one coinciding with the flashlamp trigger, and one 220µs later, coinciding with the Q-switch release, at which point the laser pulse is emitted. In this experiment, the first pulse was used to trigger the function generator to emit a 2ms bipolar square pulse of the desired voltage. This allowed 220µs for the dyed chiral nematic sample to deform under the applied field before the pump pulse arrived at the sample. The results obtained for the Grandjean flexoelectro-optic effect and presented in Chapter 4 indicate that this is ample time for the material to respond fully to the field before the structure is probed via the pump pulse. The timing of the pump pulse from the Nd:YAG laser within the applied voltage pulse was observed by placing a photodiode in the beam path and observing its response on the oscilloscope alongside the voltage output from the function generator. The resulting trace is shown in Figure 3.5.

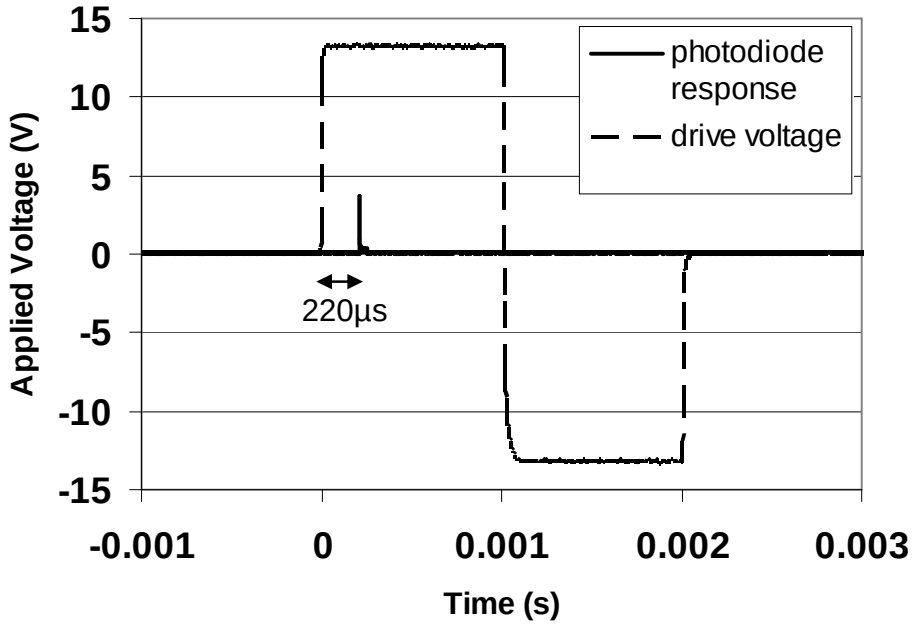

Figure 3.5: *The timing of the pump pulse incident on the sample cell within the voltage pulse applied to the cell.*

In the polymerised samples, which are described in Chapter 5, the material is able to withstand constant a.c. applied fields, so the synchronised pulse of the E-field is not required.

The spectrometer utilised to analyses the output light from the liquid crystal laser was an Ocean Optics[14] USB2000 model desktop spectrometer with fibre input and built-in collection optics. This provided 1.2nm wavelength resolution over a range of 200-800nm input light. Each pulse was analysed by the spectrometer and the information output to a computer with dedicated software to display the pulse spectrum. This software was the OOIBase32 spectrometer operating software, also from Ocean Optics, running on a standard PC.

The function generator, amplifier, temperature controller and optics were all as used in the infra-red birefringence experiment above. This experiment then allowed the generation and characterisation of laser light from dyed chiral nematic samples.

3.3. SAMPLE PREPARATION

3.3.1. Cell Construction, Alignment Layer Application and Characterisation

A liquid crystal electro-optic sample cell is essentially a pair of glass slides which are glued together with a small separation to allow a liquid crystal material to be contained between them. Most common types of cell will be glued only down two parallel sides of the glass to allow the liquid crystal to be capillary filled between the slides from one end to the other. Most will also be coated on their inner surfaces with some kind of alignment layer, usually a thin layer of polymer, which induces a preferential direction for the director to align itself with, in relation to the cell walls, creating a uniform, monodomain sample. Cells which induce an alignment of the director which is parallel to the cell walls are said to provide planar alignment, and those which provide an alignment whereby the director is perpendicular to the cell walls are known as homeotropic.

In order for electro-optic studies to be carried out, the cell must also provide a means for electric fields to be applied to the liquid crystal, and this can either be achieved by placing metallic bulk electrodes between the glass slides and having the liquid crystal between these and the glass, or by having a layer of transparent conductor (usually indium tin oxide, ITO) deposited on the inner surfaces of the glass. The former option allows field to be applied within the plane of the cell, and the latter allows for applied fields in the direction perpendicular to the cell walls. ITO can also be deposited onto the glass surfaces in very accurate patterns by means of photolithography. This allows for the application of fields in a variety of directions, in or out of the plane of the cell.

Three general types of cell were used in the course of the work presented in this thesis; The “Lucid” cell, the cartwheel cell and the patterned ITO electrode cell. Their differing geometries, construction and applications are outlined below:

3.3.1.1 The Lucid Cell.

The Lucid cell is so called after the name given to the cell model by its commercial manufactuer.[15] The cells were 0.55mm thick glass with a ready-made ITO coating on each inner surface and a planar alignment layer (rubbed polyimide). The cell walls were glued down two parallel sides, allowing for capillary filling, and contained glass spacer beads in the glue to regulate the thickness of liquid crystal which they contained. Cells were available with 5, 7.5 and 10µm thicknesses. The walls were glued with an overhang to allow soldering of contacts wires onto the ITO on each side. The ITO on each side was arranged so that an overlap of the electrodes provided a 0.25cm^2 active region. A schematic of the cell type is shown in Figure 3.6.

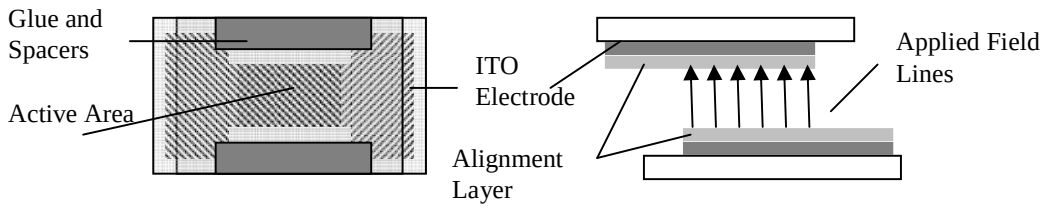

Figure 3.6: *Schematic showing plan and side view of Lucid cell.*

Cells were available with the rubbing direction of alignment layer on each side arranged antiparallel (for uniform planar texture) or at 90º to each other (for twisted nematic alignment). The cells were made with antiparallel alignment because with a parallel geometry, any small pretilt in the surface director direction (angle out of the plane of the cell wall) would otherwise result in a permanent splay deformation in the director field through the cell.

The antiparallel cells could be used to obtain a uniform lying helix texture in the active region, when the chiral nematic material inside cooled from the isotropic phase to the N* under the influence of an applied field. For this reason, they were used for flexoelectro-optic measurements in the visible regime on ULH textured samples, as detailed in Chapter 6. Once filled, the cells were sealed by lining the edges of the cell gap with UV curing adhesive (Norland 65[16]), and exposing to UV light from a Macam flexicure device.[17]

3.3.1.2 The Cartwheel Cell

The defining feature of the cartwheel cell is the presence of multiple bulk metallic electrodes converging on an active region aperture in a radial fashion. The electrodes are patterned onto the base wall of the cell via photolithography to a given thickness, and therefore also act as spacers onto which the lid of the cell can be glued. The reason for the radial patterning is to allow, by variation of the voltage on each of at least four electrodes, the resulting field in the central aperture to be directed at any angle within the plane of the cell. The field in the active region can then be rotated providing a mechanism for an endlessly rotatable, reset-free active waveplate device.[18,19]

The cartwheel cells used in this work were obtain from the project CASE sponsors, Pi Photonics[20] who had them professionally manufactured to their own specification.[21] These cells measured 2mm x 3mm and had electrodes of deposited gold with a 50µm diameter active region and an electrode thickness of 10µm. The electrode pattern is shown in Figure 3.7.

Although it is such a device that the studies outlined in Chapters 4 and 5 are aimed towards providing an improved mechanism for, the effect characterisation that constitutes this work did not require the extra field rotation freedom and these cells were used as a mechanism for applying a uniform field in the plane of the cell. For this reason, the light incident on the cell was directed not at the central aperture, but at a region of uniform 50µm electrode separation between the two central electrodes.

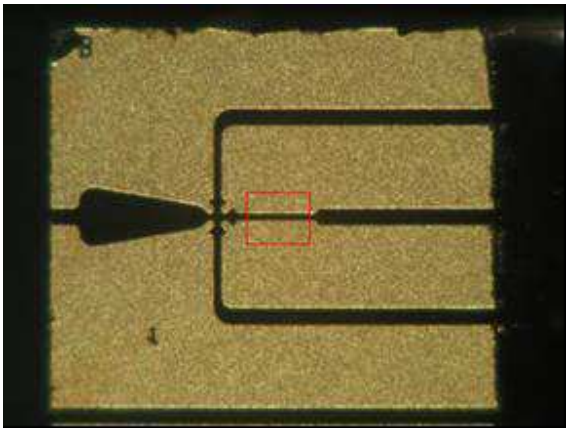

Figure 3.7: *Photomicrograph of Pi Photonics' cartwheel cell showing electrode pattern, and red box indicating uniform field region utilised in this study.*

The cells were received as a base substrate with the deposited electrodes, and were finished in house. This involved the cleaving of 100µm cover slip glass into 2mm x 2mm squares to form lids, application of an alignment layer to the cell and lid, and the gluing of the cell to the lid.

As the bulk electrodes protruded above the base substrate, and the region to be filled with liquid crystal was very thin (mostly 50µm channels) rubbing of a traditional polymer alignment layer to obtain the desired planar alignment and subsequent Grandjean texture was impossible. In order to overcome this problem, a linearly photopolymerisable polymer (LPP) was obtained from Rolic Ltd.[22] This allowed spin-coating of the monomer onto the cell and lid, which had been cleaned by soaking in acetone, then deionised water, then blown dry with nitrogen. The coated surfaces were then exposed to UV light which was polarised along the direction of the central electrode channel by sheet UV polarizer (Comar Instruments[23]). The LPP then crosslinked under the UV with a preferential direction along the direction of light polarisation, providing a uniform planar alignment layer.

This alignment layer could then be viewed with a Nomarski Prism in a differential interference contrast (DIC) microscope set-up, to highlight the uniformity of thickness and any defects in the layer. Images of the resulting alignment layer taken in this way are shown in Figure 3.8.

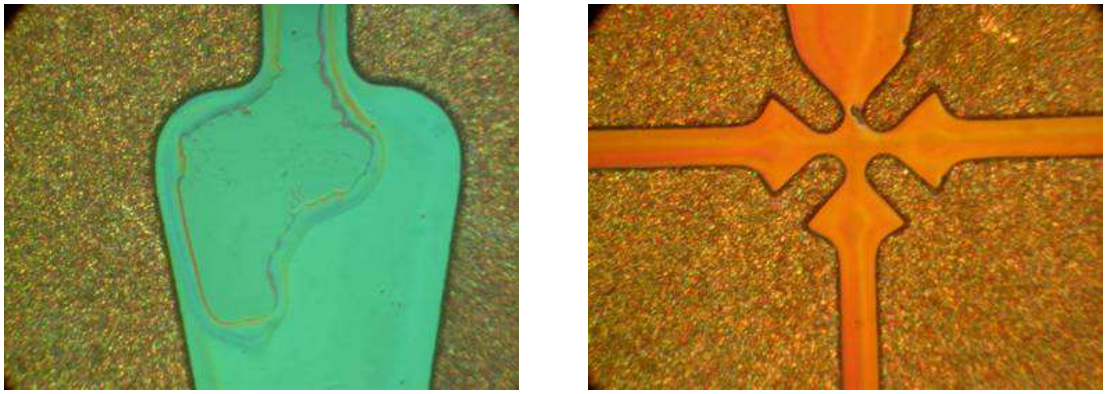

Figure 3.8: *DIC microscopy images of the LPP alignment layer used in the cartwheel cells.*

In the DIC images, the transparent alignment layers appears brightly coloured with shading indicating areas of differing optical thickness. The image on the left shows a large region of substrate uncovered by the layer, and the right-hand image shows a successfully aligned cell with uniform coverage and only slight build-up of thickness at the edges of the channels.

Once coated, the lid was glued onto the cell by placement onto the electrode surfaces and allowing UV curing adhesive (Norland 65) to capillary fill along the electrode surfaces before exposing to UV to cure. Care had to be taken with this process to ensure that both the cell and lid remained completely clean, otherwise the lid would not sit flush to the electrode surfaces and after gluing the cell thickness would be much more than the expected 10µm. A cell in which this had occurred was set in epoxy, sawn across the active area and polished. The resulting cross-section, shown in Figure 3.9, clearly shows the extended gap between the top of the gold electrodes and the bottom of the lid.

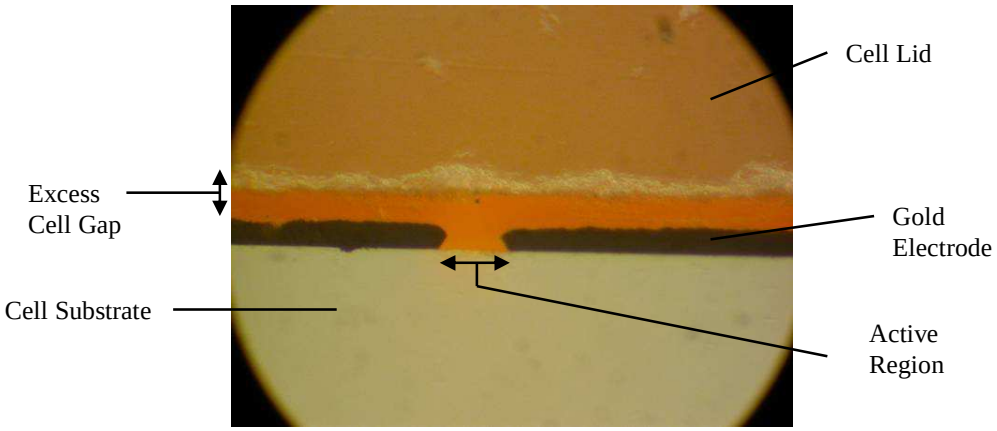

Figure 3.9: *Photomicrograph of a polished cross-section through the cell active region, showing an extended cell gap thickness.*

It can be seen from the polished cross-section that the gold electrodes do not appear to have ideally vertical walls at the boundary to the active region. This is important, as the electrode walls have to be parallel to provide a uniform field. It was thought that the irregular walls could be simply due to "smearing" of the gold due to the sawing of the cell, so to check the electrode quality, a complete cell was examined using a Wyko NT 3300 optical profiler.[24] The image of the electrode pattern obtained with this method is shown in Figure 3.10.

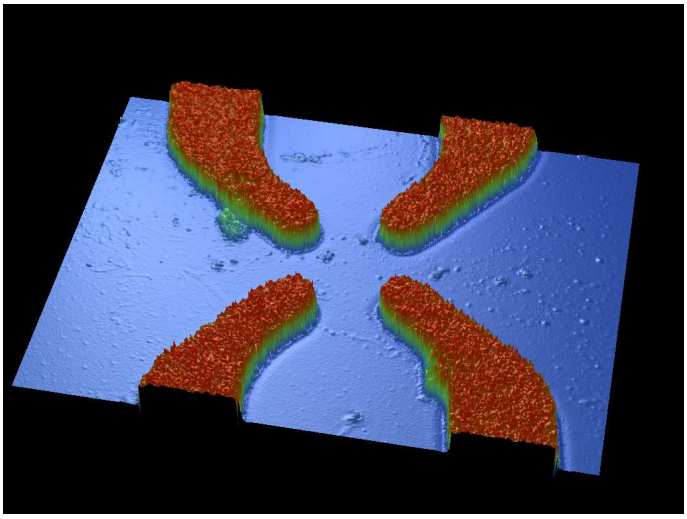

Figure 3.10: *Optical profile image of the cartwheel cell electrode pattern.*

The profile obtained shows that in a complete cell, the walls are indeed sufficiently vertical to allow full confidence in the uniformity of the field.

With the lid successfully fixed, the liquid crystal was capillary filled into the cell between the electrodes, before sealing with Norland 65. With the cell glued and aligned, and only the channel between the two central electrodes being probed, the effective cell geometry is as in Figure 3.11 below.

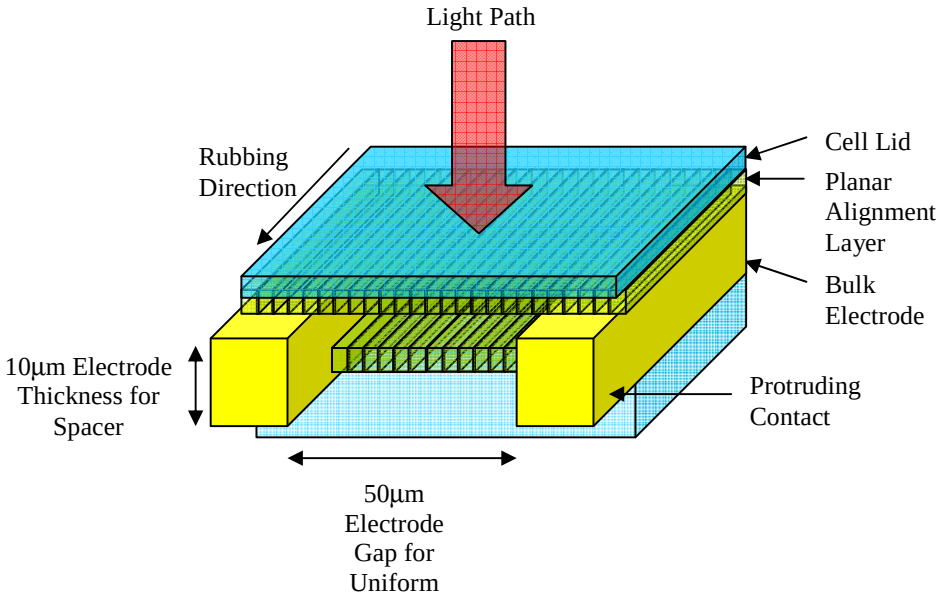

Figure 3.11: *Schematic of the active region of the cartwheel cell as used in this study.*

3.3.1.3 The Patterned ITO electrode Cell.

The supply of cartwheel cells to this project was limited, and although they provided a very uniform in-plane field, this could also be achieved to a good approximation by the use of patterned ITO glass slides. In these cells, stripes of ITO with a fixed separation are present on both the top and bottom substrates of the cell. If these are aligned exactly parallel and on top of each other when the cell is constructed, the top and bottom electrodes can be paired and a field applied between an adjacent pair. As the cells are roughly 10µm thick, with a 50 or 100µm electrode separation, the field which fringes into the bulk of the cell is reasonably uniform and will provide a reliable switching mechanism. The cell geometry as described is illustrated in Figure 3.12.

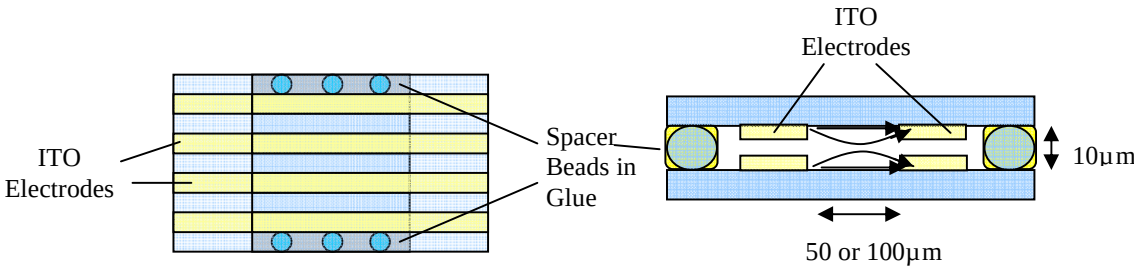

Figure 3.12: *Plan and cross-section schematics of the patterned ITO electrode cell.*

The patterned ITO glass with 100µm electrode spacing was available within the group. These substrates could be coated with an alignment layer with the LPP as with the cartwheel cell, or with the much simpler method of rubbing PVA solution onto the glass and allowing it to evaporate on a hot-stage. The most effective method for promotion of a Grandjean texture once filled with chiral nematic, however, was found to be polytetrafluoroethylene (PTFE) coating. This is achieved by the dragging of a PTFE bar over glass cleaned in acetone and blown dry with nitrogen, heated to 300ºC.[25] A machine for this purpose exists in the group as the result of a previous project.

Once aligned, the substrates were glued together using Norland 91 optical adhesive, mixed with 10µm diameter “dynosphere” spacer beads[26] to set the desired cell gap. The two substrates were aligned under the microscope to ensure the correct positioning of the electrodes relative to each other, and then cured with UV. A photograph of a complete pattered ITO electrode cell, with the light angles to show the electrode stripes, is shown in Figure 3.13.

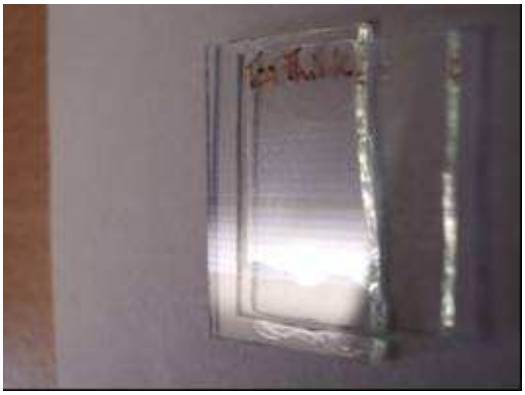

Figure 3.13: *Photograph of a complete patterned ITO electrode cell showing aligned ITO stripes.*

As the electric field that can be applied to a liquid crystal sample in these cells is limited by the electrode spacing, a further set of patterned ITO electrode cells was produced with a 50µm electrode gap. These cells were ITO patterned, alignment layer coated and constructed by Dr. Tim Wilkinson of the Department of Engineering at Cambridge University.

3.3.1.4 Cell Thickness Determination.

As illustrated by Figure 3.9, the cell thickness of the cells constructed in-house is not always easily predicted from the spacers used. Even the Lucid cells exhibit a small variance in their thickness from that quoted by the manufacturers. For this reason, a method of accurately measuring the thickness of a cell once constructed is required. This is done by examination of the empty cell in a microscope with an Ocean Optics spectrometer[14].

The light propagating through the cell experiences a small amount of reflection from both cell surfaces. In the cavity of the cell, these reflections interfere with each other either constructively or destructively according to the cell thickness and the wavelength of the light, according to etalon theory. The white light throughput from the microscope will then be modulated and the spectrometer displays an oscillating spectrum with peaks occurring for wavelengths at which twice the cell thickness is an integer number of wavelengths:

$$m\lambda_m = 2nd \qquad 3.1$$

where m = 1,2,3 etc is the number of the peak on the spectrum, λ_m is the wavelength at which the successive peaks occur, d is the cell gap and n is the refractive index within the cell (=1 for an empty cell). Note this equation is simplified for normal incidence. If the wavelength values of a series of successive peaks is measured, a plot of peak number, m ,against λ_m ,therefore has a gradient equal to 1/2d, and the cell gap is derived. This method is accurate to approximately 0.01µm. Lucid cells are found to vary in thickness over the cell area by approximately 0.1µm. The home made cells can vary by much more than this, according to the care with which they were constructed. Nevertheless, the cells constructed in this study have an active region of only 100µm at the most, so very little variation occurs over this distance, and this method allows the cell thickness in the relevant region to be known very accurately. This allows measured optical retardances of sample cells to be converted into material birefringence for general classification.

3.3.2. Mixture Preparation

The liquid crystal mixtures examined in this work were all composed of commercially available compounds and bimesogenic materials synthesised in house. In order to obtain reproducible results considerable care has to be taken in the making of mixtures so their constituent proportions are known to a fraction of a percent. This is important since some components have a profound impact on the liquid crystal structure and electro-optic properties with very little change in their proportion, e.g a change in the proportion of chiral dopant of 0.5% of the total mixture weight can change the chiral nematic pitch length by the order of 100nm, and dramatically alter the flexoelectro-optic tilt angle. The fact that total mixture weights are typically only 20-80mg means components have to be weighed very accurately.

This is done with a Mettler Toledo[27] AG245 balance, which allowed weighing of samples to 0.01mg accuracy. Samples were deposited into glass sample bottles, and their exact proportions as weight for weight (w/w) measures of the total mixture were noted. Samples were then left to mix in the isotropic phase for 48 hours before being filled into a cell. If the sample contained a UV reactive mesogen and photoinitiator to allow creation of a polymer stabilised system, the bottle was completely wrapped in black plastic tape to prevent uncontrolled UV polymerisation in the bottle. These samples also had to be examined under the microscope using a red transmissive sheet filter on the microscope source, again to prevent uncontrolled premature polymerisation.

3.3.3. Mesophase Characterisation

Once a fully mixed sample was introduced to a pre-prepared cell, the optical texture of the mesophase was observed in the polarising microscope. This allowed identification of the liquid crystal phase the sample adopted, characterisation of the phase transition points via observation of phase changes with temperature, and confirmation that the desired liquid crystal conformation had been achieved, prior to electro-optic measurements. The identification of liquid crystal phases by their characteristic optical textures in polarising microscopy is a well known science.[28] Samples can be viewed with planar alignment, or no alignment to obtain a variety of textures for identification. The chiral nematic liquid crystals used in this study have three characteristic textures, each the result of a different alignment of the helical axis of the material within the cell.

The Grandjean texture occurs when the sample is planar aligned and the helical axis is vertical in the cell. This texture is typically uniformly coloured, with defects occurring in the shape of “oily streaks” in the texture. It the cell is not of uniform thickness, pitch jumps may be visible, at the point the director at the cell surface rotates by 180º to minimise the free energy under counteraction influences from the twist elastic constant in the bulk and the alignment energy at the surface. These jumps are visible as a sudden change in colour across a disclination line with a gradual shading back to the original colour moving away from the disclination.

The uniform lying helix texture occurs when the helical axis of the material lies uniformly in one direction in the plane of the cell. This can be induced in planar aligned cells by cooling of the sample into the chiral nematic(N*) phase from the isotropic under the influence of an applied field, combined with a physical shearing of the sample. The texture is identified by the ellipsoidal domain formed with the long axis perpendicular to the rubbing direction of the cell alignment layer, and the fact it is only present in the area of the cell in which the electrodes are overlapping.

The focal conic texture occurs when the material is unaligned in many small domains with random orientation of the helical axis. This is a scattering texture and generally requires re-heating of the sample into the isotropic phase and/or shearing to be removed. Example of the three textures and illustration of their director conformations are given in Figure 3.14. In this figure, the Grandjean texture shows some oily streak disclinations, and the ULH texture is in the dark state with the helix axis parallel to the microscope polariser.

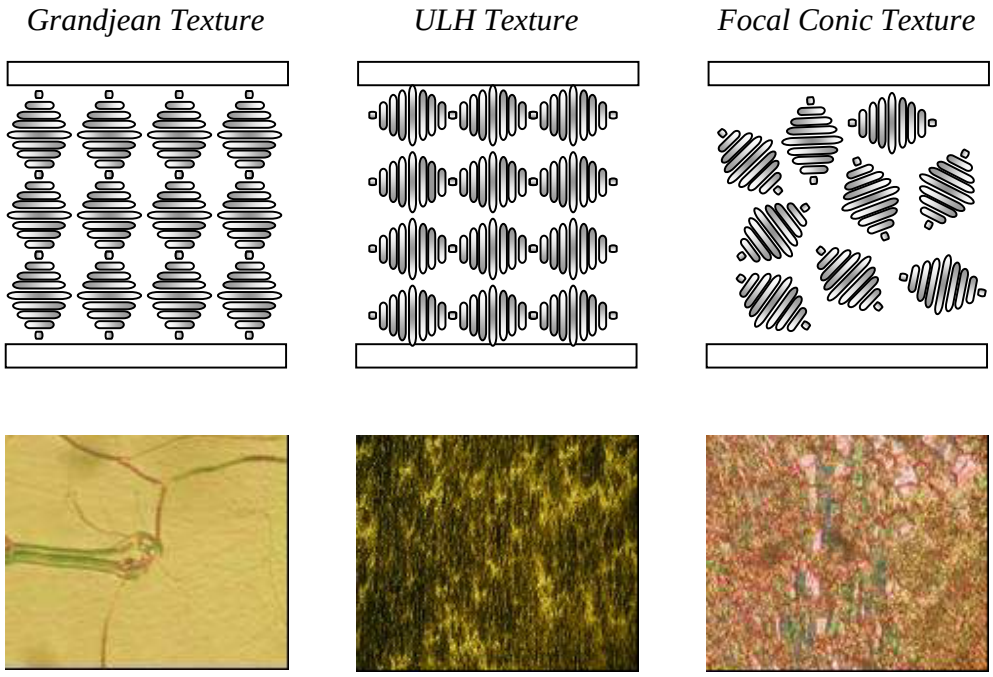

Figure 3.14: *Diagrams illustrating the director orientation in the three principal chiral nematic conformations, and their corresponding optical textures.*

Once a cell had been constructed to specification, filled with a sample mixture and the desired texture identified and confirmed, the sample was ready for electro-optic characterisation.

3.4. ELECTRO-OPTIC MEASUREMENTS

3.4.1. Flexoelectro-optic Tilt Angles and Response Times

The flexoelectro-optic characteristics of a particular material, namely the tilt angle and response times as a function of applied field and temperature, are measured using the visible light microscope based set-up outlined in Section 3.2.1, using the 5µm thickness Lucid cells described

in Section 3.3.1.1. In these cells, the chiral nematic liquid crystal is brought into the ULH texture by cooling the sample from the isotropic phase under the influence of an applied field of ≈3V/μm, at 80Hz. As the sample forms the N* phase, the ULH texture will be vaguely present, at which point rubbing of the cell surface will solidify the desired texture. The exact temperature at which the I→N* phase transition occurs (known as the clearing temperature, T_c) is noted, and all measurements are performed at temperatures relative to this, usually from Tc-5ºC down to room temperature in 5ºC steps.

As described in Chapter 2, Section 2.4.2, a chiral nematic sample with flexoelectric coefficients will, when an electric field is applied perpendicular to its helical axis, deform in such a way as to rotate the optic axis of the material in the plane perpendicular to the field. In the arrangement described here, this results in a rotation of the optical axis in the plane of the cell. The transmission of light intensity through crossed polarisers by a birefringent material is given by:

$$I = I_0 \sin^2(2\psi)\sin^2\left(\frac{\pi\Delta nd}{\lambda}\right) \qquad 3.2$$

where I_0 is the intensity of the polarised light incident on the sample, ψ is the angle the optic axis of the sample makes with the transmission axis of the first polariser, Δn is the sample birefringence, d is the sample thickness, and λ is the wavelength of the light. This equation shows that, if the sample is a half waveplate, i.e $\Delta nd/\lambda = 1/2$, then the second $\sin^2$ term becomes unity and rotation of the optic axis from ψ=0 to ψ=45º gives 100% intensity modulation. In fact, for any fixed sample retardance, the maximum and minimum transmission points will be at ψ=45º and ψ=0 respectively. Therefore even with white light, a clear intensity modulation will be visible with the electrically induced optic axis rotation of the sample. The extent of this rotation for a given applied field defines the flexoelectro-optic tilt angle ϕ(E). This is measured by the following method:

At zero field, the equilibrium (E = 0, ϕ = 0) optic axis position is aligned with the transmission axis of one of the polarisers by minimising the intensity throughput. The angle reading of the rotation stage on which the sample sits is noted. An a.c. square wave field at a given amplitude, and usually 80Hz frequency is then applied to the sample, and deflection of the optic axis from this minimum transmission position in either direction (E = +ve or –ve) results in an increase in transmission. The observed trace is then as shown in the left example of Figure 3.15.

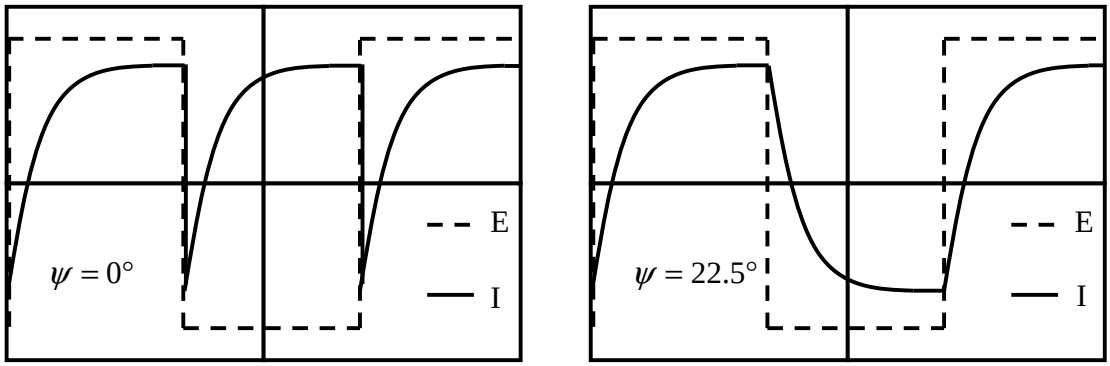

Figure 3.15*: Example traces of the flexoelectro-optic response with the zero-field optic axis position at 0º and 22.5º.*

The rotation stage is then rotated by 22.5º. The zero-field optic axis position is then at the mid-way to maximum transmission, and the E-field induced rotation produces an increase in transmission for one field polarity, and a decrease for the opposite polarity, the intensity response then being as shown in the right side of Figure 3.15. The mid point of this switch (equal to the zero-field position) is than marked with a cursor on the oscilloscope

The sample stage is rotated to bring the maximum transition value of the electro-optic response in line with the marking cursor. This corresponds to the optic axis of the material when fully switch to $+\phi$ lying at 22.5º to the polariser transmission axis. The rotation stage angle is noted. The stage is then rotated to bring the minimum transition point of the response level with the cursor. This corresponds to the sample optic axis in the $-\phi$ position lying at 22.5º to the polariser. The angle required to swing to this position from the previous measurement, when $+\phi$ was at 22.5º, is therefore 2ϕ. The rotation stage is accurate to 0.5º, so the tilt angle measurement is accurate to 0.25º

In order to measure the response times, the rotation stage is fixed with the zero-field optic axis at 22.5º. The timebase of the oscilloscope is increased so that one switch from $-\phi$ to $+\phi$ takes up almost the full screen, as well the display averaging is increased to 128 traces. The oscilloscope will then automatically read the time taken between the 10% and 90% levels of the switch. This measurement is taken for both the $-\phi$ to $+\phi$ switch and the reverse, and the average taken as the response time.

This measurement method is straightforward for tilt angles less than 22.5º. It becomes slightly more complex for higher tilt angles, as the intensity response goes to a maximum and back down to a lower level before settling at the ϕ value for the applied field, as the optic axis overshoots the maximum transmission point at ψ=45º. Tilt angle measurements are relatively unaffected, as the stage can still be rotated to place $+\phi$ then $-\phi$ at 22.5º, extra care just has be taken during the rotation to ensure the two ends of the switch are observed. Response times are more awkward, as the automatic 10-90% measurement is no longer valid. The cursors can be used to produce a manual measurement, but for most materials studied here, measurement of the response at fields which produce a switch below ϕ = 22.5º are sufficient for sample characterisation.

These measurements are then repeated for increasing field increments of 1V/µm until the sample texture can be seen to be disrupted due to unwinding of the chiral nematic helix at higher fields. The measurements are than repeated for the full range of applied fields at a lower temperature. If the pitch-lengths of the mixtures examined with this technique are also measured, the flexoelelastic ratio e/K, which is the figure of merit for flexoelectric materials, can be derived from the theory outlined in 2.4.2. This is complicated with many of the samples presented in this study however, because the pitch-lengths are too long to produce a visible reflection band. However, the principle aim of these measurements for this study is determination of the tilt angle for comparison with the response in the Grandjean flexoelectro-optic effect, rather than the flexoelectric coefficients. For these reasons, pitch length measurements were not performed.

3.4.2. Infra-red Birefringence and Response Times

The key value sought by the experiments outlined here was the birefringence induced by an applied electric field in Grandjean textured chiral nematic materials at telecoms wavelengths. This was achieved using the arrangement outlined in Section 3.2.2, and the “cartwheel cells” described in Section 3.3.1.2.

The cell for each sample had a well known thickness due to measurement with the etalon method (Section 3.3.1.4), therefore the cell retardance, measured via the transmission of light through crossed polarisers according to Equation 3.2, could be converted into material birefringence. The cell was positioned in the beam path such that the direction of applied field, and therefore optic axis of the induced birefringence was at 45º to the polariser transmission axis. This brings the first

$\sin^2$ term in Equation 3.2 to unity, and the intensity throughput is then solely a function of the retardance.

I_0 was measured as the intensity received at the power meter with the polarisers uncrossed and the cell in place in the isotropic phase. This removes any losses due to inherent polarizer absorbtion, light blockage by the cell electrodes and reflection at the cell surfaces, giving as true a measure as possible of the maximum throughput achievable by inducing birefringence with the polarizers crossed.

On cooling the sample into the N* phase and crossing the polarizers, extinction was observed, as the optical axis of the chiral nematic was in the direction of propagation of the light, resulting in zero birefringence. Optical activity due to the helical structure of the sample was also insignificant due to the wavelength of the light being greatly in excess of the helical pitch. This effect is described by the equation:

$$\frac{\psi}{d} = \frac{\pi}{16}\left(\frac{n_{\parallel}^2 - n_{\perp}^2}{n_{\parallel}^2 + n_{\perp}^2}\right)\frac{P^3}{\lambda^2\left(P^2 - \lambda^2\right)} \qquad 3.3$$

where ψ is the angular rotation of the linearly polarised light incident on the sample with wavelength λ, d is the sample thickness, $n_{\parallel}$ and $n_{\perp}$ are the refractive indices of the material parallel and perpendicular to the nematic director respectively, and P is the helical pitch length. Typical values of P, $n_{\parallel}$ and $n_{\perp}$ give a rotation of less than a degree.

Each sample was subjected to an applied field in the form of 2ms bipolar pulses at 5Hz. As any deviation of the optic axis from its vertical position in the cell results in a birefringence and increased intensity throughput, the expected response is similar to the ULH cell in the ψ=0º position in that both +ve and –ve polarity voltages produces a transmission increase, the difference being that as the sample is only pulsed, two response times are evident: the 10-90% “ON” response to the initial application of the field, and the 90-10% “OFF” response to the removal of the field. In the ULH set up, the sample as always in a driven state, responding only to changes in field polarity, never the removal of the field altogether. These two responses in this case then have to be treated separately. The expected trace is shown in Figure 3.16.

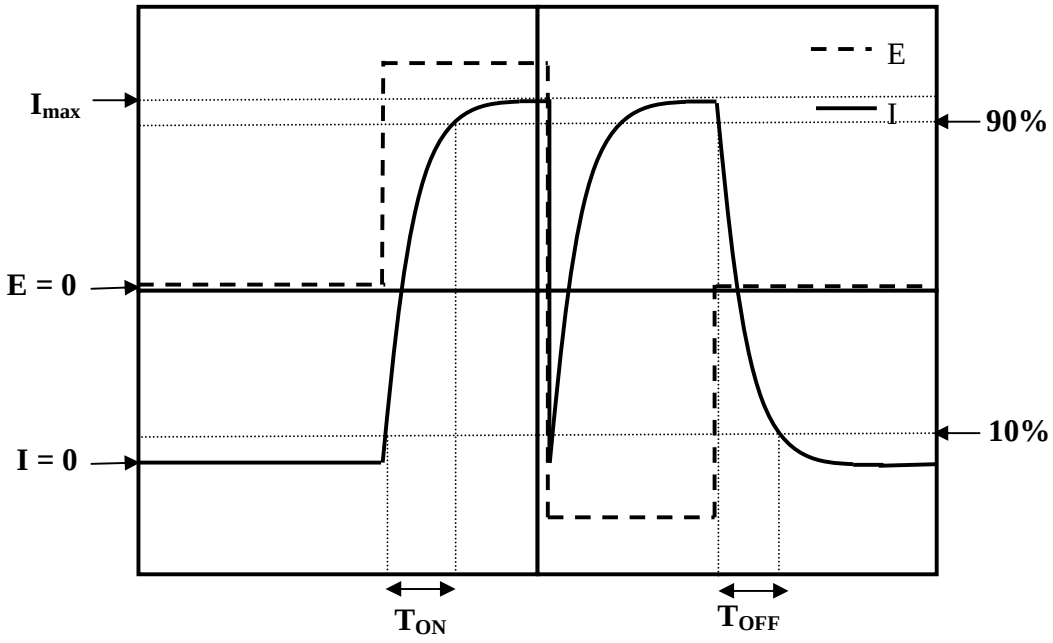

Figure 3.16: *Example trace of the Grandjean flexoelectro-optic response at 1550nm.*

The measurements required for characterisation are taken from this trace, i.e. the value of I at the top of the switch in comparison to I_0 gives the retardance and therefore birefringence, and the T_{ON} and T_{OFF} response times are taken as the 10-90% times from the front of the first peak and the rear of the second as discussed. For a purely flexoelectric switch, the transmission should drop to zero at the field polarity crossover point, as the optic axis swings back through the vertical position going from $+\phi$ to $-\phi$ or vice versa. If a significant degree of dielectric coupling is present however, some helix unwinding will take place and a residual birefringence will remain at the crossover point, as discussed in Section 2.4.3, due to the fact that dielectric effects couple to the R.M.S. field value.

In the case of significant dielectric coupling, the response times of the switch, as illustrated in Figure 3.16, will be due to both the flexoelectro-optic switch and helix unwinding, and the times measured will reflect this. In the polymerised samples of Chapter 5, constant square waves of varying frequency can be applied to the samples and the flexoelectro-optic and dielectric contributions to the switch distinguished. This is achieved by first observing the response under a low frequency (≈80Hz) field, in which the flexoelectro-optic switch has time to fully respond to each period of constant d.c. field and therefore large modulation of the transmission is observed at the field polarity change points. The response is then observed under a high frequency field (≈2kHz) of the same amplitude, in which case the d.c. periods of the waveform are too short for a

response to occur to them, and only coupling to the R.M.S. field i.e. dielectric effects can occur. This response provides a constant "baseline" birefringence on which the flexoelectro-optic effects are superimposed at low frequencies. The two responses can be compared as below.

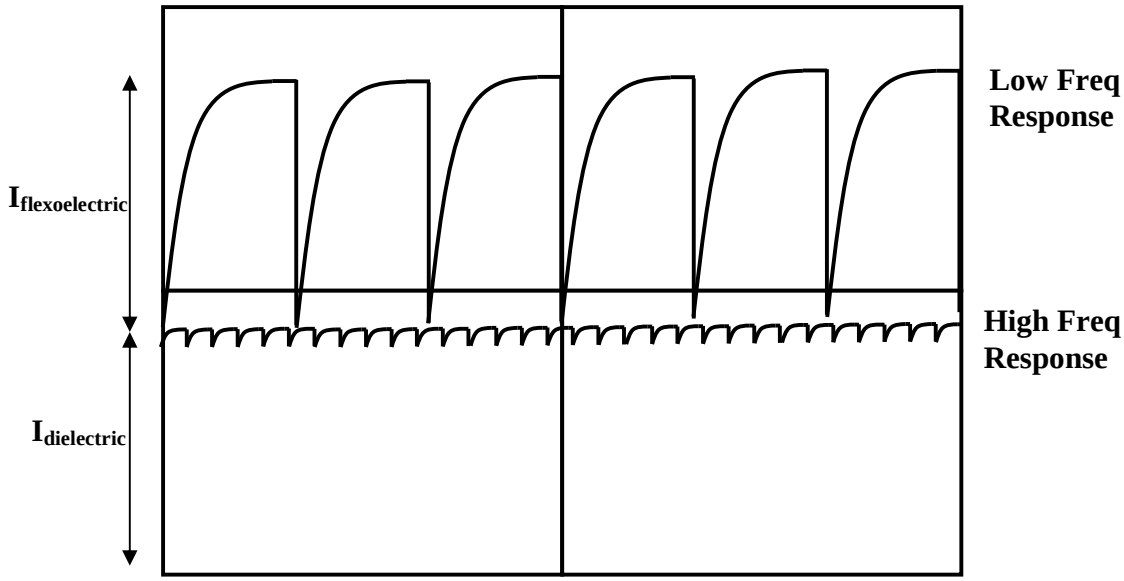

Figure 3.17: *Example trace of the Grandjean flexoelectro-optic response at 1550nm to a.c. square waves of high and low frequency.*

This "baseline" birefringence could then be subtracted from the combined low-frequency response to provide a measure of the induced birefringence resulting solely from flexoelectric coupling.

3.5. LASING MEASUREMENTS

3.5.1. Emission Spectra

The measurements of lasing output carried out with the arrangement described in Section 3.2.3, which produced the results outlined in Chapter 7, were performed with a view solely towards a proof of concept of flexoelectro-optic tuning of the laser output. All that was required, therefore, were emission spectra as sampled by the spectrometer and its custom software to be recorded for the output of a cell under a series of applied fields.

This was not entirely straightforward however. Firstly, samples were chosen and mixed based on their Grandjean flexoelectro-optic properties as investigated in this work, and their lasing

efficiencies as determined by Ali Ford and Steve Morris' work.[30,31] Samples were then mixed with the desired materials and the correct proportion of chiral dopant to produce a photonic band gap with the long-wavelength edge in the fluorescence band of the dye used in the mixture (either DCM or PM597).

Great care was then required in aligning the pump beam and collection optics to ensure the region of the cell experiencing the applied field was made to lase, and that given the restricted active area of the cartwheel and patterned electrode cells used, enough output light was collected to produce a spectrum. The output spectrum from the chiral nematic lasers is highly dependent on the quality of the Grandjean texture obtained in the cell. As this was more difficult to achieve in the home-made cells used, the output was subject to a random variation in spectrum shape and intensity from pulse to pulse. For this reason in some samples, the software was made to average up to 100 output pulses to make clear the effect of the applied field on the lasing.

3.6. REFERENCES

[1] Olympus UK Ltd. Great Western Industrial Park, Dean Way, Southall Middlesex, UB2 4SB.

[2] www.olympusmicro.com/

[3] Linkam Scientific Instruments Ltd, 8 Epsom Downs Metro Centre, Waterfield, Tadworth, Surrey, KT20 5HT. www.linkam.co.uk/

[4] Thurlby Thandar Instruments Ltd, Glebe Road, Huntingdon, Cambridgeshire. PE29 7DR. www.tti-test.com/

[5] Hewlett Packard Ltd, Cain Road, Bracknell, Berkshire. RG12 1HN. www.agilent.com/

[6] Thorlabs LTD, 1 Saint Thomas Place, Ely, Cambridgeshire. CB7 4EX. www.thorlabs.com/

[7] Newport Ltd, 4320 First Avenue, Newbury Business Park, London Road, Newbury, Berkshire, RG14 2PZ. www.newport.com/

[8] Agilent Technologies UK Ltd, Eskdale Road, Winnersh Triangle, Wokingham, Berkshire, RG41 5DZ. www.agilent.com/

[9] Tektronix UK, Western Peninsula, Western Road, Bracknell, RG12 1RF. www.tek.com/

[10] Melles Griot BV, Sovereign Court, Lancaster Way, Ermine Business Park, Huntingdon, PE29 6XU. www.mellesgriot.com/

[11] BFi OPTiLAS, Wolverton Mill South, Milton Keynes, MK12 5ZY. www.electrophysics.com/

[12] New Wave Research Co. Ltd, 8 Avro Court, Ermine Business Park, Huntingdon, Cambs, PE29 6XS. www.new-wave.com/

[13] S. M. Morris, A. D. Ford, M. N. Pivnenko and H. J. Coles, *J. Opt. A: Pure Appl. Opt.* ***7,*** *215-223* (2005).

[14] Geograaf 24, 6921 EW DUIVEN, The Netherlands. www.oceanoptics.com/

[15] EEV Ltd, Waterhouse Lane, Chelmsford, Essex.

[16] www.norlandprod.com/

[17] Macam Photometrics Ltd., 10 Kelvin Square, Livingston, EH54 5PF. www.macam.com/

[18] Y. Ohtera, T. Chiba and S. Kawakami, *IEEE Phot. Tech. Lett.*, **8** (3), 390, (1996).

[19] M. C. K. Wiltshire, Patent: *GB2255193*, (1994).

[20] Pi Photonics Ltd, 36 North End, Meldreth, Herts, SG8 6NT. www.piphotonics.com/

[21] R. A. Betts and T. Bricheno, Patent: *WO2004021073*, (2004).

[22] Rolic Technologies Ltd., Gewerbestrasse 18, CH-4123 Allschwil, Switzerland. www.rolic.com/

[23] Comar Instruments, 70 Hartington Grove, Cambridge, CB1 7UH.

[24] Veeco Instruments Ltd**.,** Nanotech House, Anderson Road, Buckingway Business Park, Swavesey, Cambridge, CB4 5UQ UK. www.veeco-europe.com/

[25] J. C. Wittmann and P. Smith, *Nature*, **352** (6334), 414-7, (1991).

[26] Agar Scientific Ltd, 66A Cambridge Road, Stansted, Essex CM24 8DA. www.agarscientific.com/

[27] Mettler-Toledo Ltd., 64 Boston Road, Beaumont Leys Leicester, LE4 1AW. www.mt.com/

[28] P. J. Collings, *Liquid Crystals: Nature's delicate phase of matter*, Princeton University Press, (2002); D. Demus and L. Richter, *Textures of Liquid Crystals*, Verlag Chemie, (1978).

[29] M. J. Clarke, *PhD Thesis*, University of Southampton, (2004).

[30] S. M. Morris, A. D. Ford, M. N. Pivnenko and H. J. Coles, J. Appl. Phys., 97, (2), art. no.-023103, (2005).

[31] A. D. Ford, S. M. Morris, M. N. Pivnenko, A. E. Blatch and H. J. Coles, *Proc. SPIE*, **5741**, 217-27, (2005).

Chapter Four

The Flexoelectro-optic Effect in Grandjean Textured Chiral Nematic Liquid Crystals

4.1. INTRODUCTION

This work is concerned with the potential utilisation of the flexoelectro-optic effect[1] in optical telecommunications devices. The principal benefits of the effect over other, more commercially developed, liquid crystal electro-optical mechanisms are fast response times[2] and analogue, linear electric field dependence.[3] These are of particular interest in optical communication systems where, due to the ever increasing data-rates of transmission systems, the switching speed of optical components is an important parameter.

The flexoelectro-optic effect in short-pitch chiral nematic liquid crystals has to date been observed only in samples in which the liquid crystal is aligned with a uniform helical axis lying in the plane of the cell (ULH texture), and the electric field is applied perpendicular to this axis via transparent electrodes on the inner cell surfaces. The resultant rotation of the optic axis in the plane of the cell allows the material to act as a waveplate with fixed retardation, but electrically controlled rotatability within a range limited by the maximum optic axis tilt angle.[4]

The aim of the work presented in this chapter is to demonstrate the existence of the flexoelectro-optic effect in a new geometry in which the liquid crystal is aligned in the Grandjean texture, with the helical axis perpendicular to the cell surfaces, and the electric field applied in the plane of the cell, still perpendicular to the helical axis. A flexoelectro-optic device operating in such a configuration would have several key advantages over the conventional device:

1. The Grandjean texture is easier to obtain than the ULH texture, as planar alignment of the cell surfaces provides uniform anchoring of the local nematic director in the vicinity of the surface in the desired direction. In the ULH configuration, the local director direction rotates 360º through the helical pitch length, so neither uniform planar nor homeotropic anchoring can provide ideal alignment for all regions along the helix. A periodically alternating alignment pattern scheme,[5] or electric field effects,[6] are therefore required to obtain and maintain the ULH texture. Although these alignment techniques have been shown to be reliable,[7] a uniformly planar aligned device would be simpler to manufacture and operate.

2. Application of the electric field in the plane of the cell allows, via a combination of radially converging electrodes, the field to be applied in any direction in the plane of the cell. As the flexoelectro-optic effect causes the optic axis of the material to rotate around the direction of the applied field, the optic axis can be deflected through a polar angle ϕ, defined by the material tilt angle for the given field. The ability to vary the direction of the applied field in the plane of the cell through 360º therefore allows complete and endless control of the azimuth, ψ, of the optic axis. This provides potential for an endlessly rotatable waveplate with electrically variable retardance. This is a device specification very much sought after for use in endless polarisation control devices, slower plain nematic versions of which have been previously demonstrated.[8,9]

3. At telecoms wavelengths (1550nm), the helical pitch of the chiral nematic materials used in the flexoelectro-optic effect is too short (typically 300-500nm), to give rise to any significant optical rotation of the input polarisation state of the light.[10] The illuminating wavelength is also too far from the chiral nematic reflection band for any selective reflection to occur.[11] At zero applied field, with the optic axis perpendicular to the cell surfaces, the device would therefore be optically neutral and extinction would occur between crossed polarisers. Without polarisers, the device would be nearly 100% transparent in a monodomain sample. This would allow for large contrast ratios to be obtained. This is the major drawback in the conventional ULH device, in which contrast ratios exceeding 10:1 are difficult to obtain due to the constant presence of disclinations in the texture.

The results presented here outline the development of the experiment described in Section 3.2.2, and detail the proof of concept of the flexoelectro-optic effect in the Grandjean texture with in-plane applied electric fields. Due to the novel nature of the experiment, considerable development in the measurements and liquid crystal composition occurred during the course of the work and some initial results are not directly comparable to later measurements, particularly the magnitude of the optical response. The preliminary results presented in this Chapter therefore provide only qualitative information since cell thickness measurement of the early cells was subject to error. This was a result of the bulk electrode layout of the cartwheel cells transmitting insufficient light for a measurement signal to be observed in either the UV-Visible spectrometer or microscope based experiments. Nevertheless, the author believes the results serve as a valuable document for the course of this work and the development of the effect in question, hence their reproduction

here. In the work described in the following chapter, these uncertainties have been removed, improvements to the experiment and the samples make the observations more repeatable, and a rigorous comparison of a series of samples possible.

4.2. TRIANGULAR WAVEFORM RESPONSE

Having prepared the planar aligned sample cells with bulk metallic in-plane electrodes, as described in Section 3.3.1.2, the cell was filled with a chiral nematic mixture based on the non-symmetric bimesogenic compound α-(2',4-difluorobiphenyl-4'-yloxy)-ω-(4-cyanobiphenyl-4'-yloxy)nonane, synthesised by Andrew Blatch,[12] and known by the acronym FFO9OCB. This material, whose structure is shown in Figure 3.1, was chosen as it has shown a large flexoelectro-optic effect in the ULH texture,[13] and a large switching material was thought to give the best chance of an observable effect. The bimesogen itself is achiral, which is why the high twisting power chiral dopant BDH1281 was added as a small percentage of the total weight of the mixture, to induce chirality into the system. The proportions of the mixture were: 98.05% FFO9OCB, 1.95% BDH1281 (all percentages given as weight for weight, as will be the convention throughout this study).

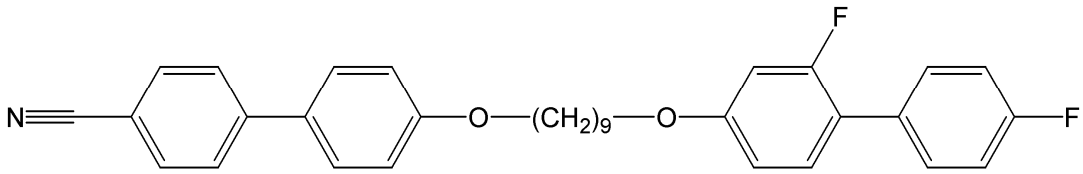

Figure 3.1: *The chemical structure of the non-symmetric bimesogen FFO9OCB*

The relevant material parameters of this mixture are shown in Table 4-I. This table uses the conventional values of Tc being the isotropic to nematic phase transition point, Δε the dielectric anisotropy at 1kHz and birefringence Δn at 550nm.

Tc	Δε	Δn
115˚C	3.9	≈0.2

Table 4-I: *Material parameters of the chiral FF09OCB mixture*

It was found that a Grandjean texture was most reliably obtained in the cell by filling the cell whilst in the chiral nematic temperature range, the flow of the material as it entered the cell creating a planar alignment. The sample was found to cool into the chiral nematic phase from the isotropic at 115ºC in the probe station, and the presence of the required Grandjean texture was

confirmed by optical microscopy. Once filled, the cell was placed in the infra-red electro-optic rig in order to test the electro-optic properties at 1550nm.

According to Equation 3.2, for any given induced birefringence in the cell, the transmission through crossed polarisers will be greatest if the optic axis of the material is at 45º to the polarisers' transmission axis. From flexoelectro-optic theory, the deflection of the optic axis in the cell should be at right angles to the applied field, so if the field is applied at 45º to the polariser, the projection of the deflected optic axis in the plane of the cell also ought to be at 45º to the polariser, and transmission maximised. As detailed in Section 3.4.2, for this reason the field was always applied at 45º to the polariser transmission axes in these experiments.

Square waveforms with field amplitudes up to 4 V/µm and frequencies of 80Hz to 1Khz were applied to opposite electrodes in the cell. It became apparent very rapidly that the sample could not withstand square waveforms of greater than a volt per micron in amplitude over any practical length of time. An intensity modulation was initially observable, but decayed into noise within the space of approximately 1 second. The sample texture was examined under a microscope before and after the application of the field, and was found to have degraded from the initial Grandjean texture to a scattering focal conic state. The textures observed are shown in Figure 3.2.

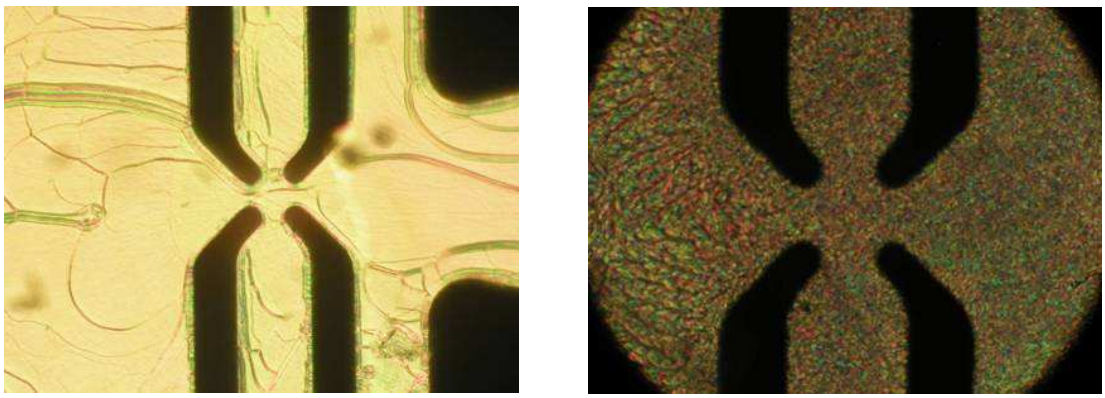

Figure 3.2: *Polarising microscopy images of the chiral FFO9OCB sample before (left) and after the application of an a.c. square waveform at 80Hz, 4V/µm and Tc-10˚C.*

It is thought that the electro-hydrodynamic instabilities (EHDI) arise as a result of the non-uniformity of the field around the active region. After the alteration of the texture due to EHDI, the Grandjean texture could not reliably be restored by thermal cycling.

While the application of square waveforms with field amplitude greater than 1 V/µm always led to EHDI, independently of field frequency and sample temperature, it was found that triangular waveforms did not have the same catastrophic effect, and that a useful signal could be observed. If the response is flexoelectric in origin, the optic axis will deflect from the vertical equilibrium position in the cell as the field is increased, and return to vertical as the field returns to zero. As the field then becomes negative, the optic axis should deflect in the opposite direction by an angle proportional to the field (see Section 2.4.2), again returning to vertical as the field returns to zero. A triangular waveform therefore ought to generate a metronomic movement of the optic axis, and as deflections from vertical in either direction produce an increase in transmission from extinction, the response ought to take the form of repeated "spikes" of transmission at twice the drive frequency. This expected response is shown in Figure 3.3, for the applied field making an angle of 45º with the polarisers.

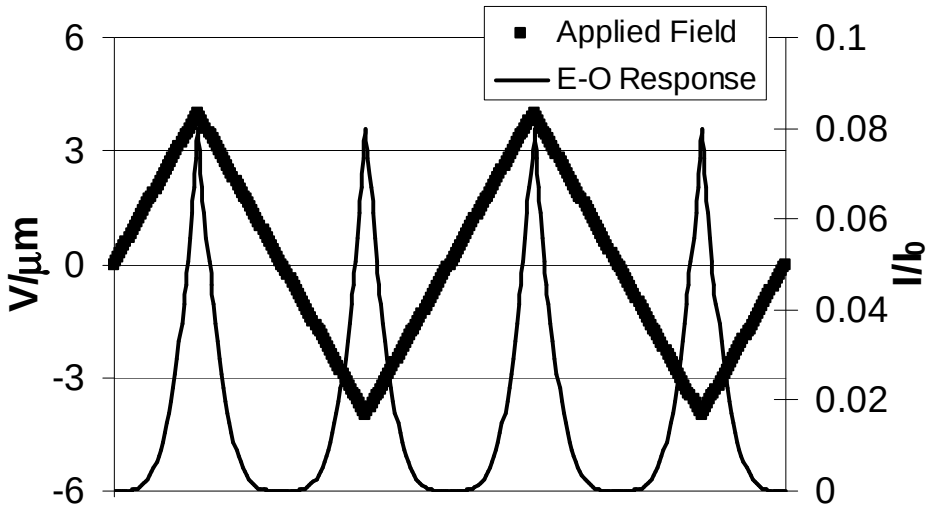

Figure 3.3: *The theoretically predicted electro-optic response of the cartwheel cell to a triangular a.c applied field.*

The I/I_0 values shown in the predicted trace are calculated from the theory laid out in Section 2.4.3, using typical material parameters ($\Delta n = 0.2$, $e/K = 1.2$ C/Nm).[13]

The observed response from the sample, subjected to a 1kHz triangular waveform applied at 45º to the polarisers, at 110ºC, is shown in Figure 3.4.

The observed response can be seen to very closely resemble the predicted response, both in shape and magnitude, giving strong evidence that a flexoelectro-optic distortion of the chiral nematic

helix is taking place. One interesting feature to note is the phase difference between the drive and response waveforms that does not appear in the prediction. This is a result of the response time required for the material to react to the applied field, of which no account was taken in the prediction. The lag is approximately 270μs, which is of the same order as the flexoelectro-optic response time of this material in the ULH texture,[13] a further sign that the observed optical response is indeed of flexoelectric origin.

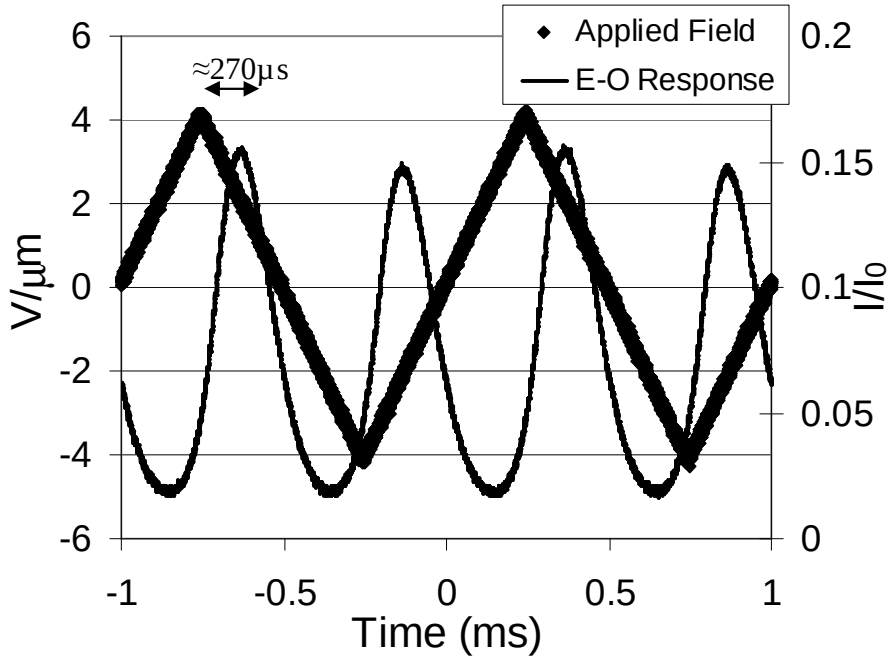

Figure 3.4: *The electro-optic response of the chiral FFO9OCB cell at T_C-10℃ to an applied triangular a.c. field of 1kHZ frequency and 4V/μm peak field.*

A series of these traces were taken at different drive frequencies to examine the frequency dependence of the response. It was expected that as the drive frequency was increased to the point that the period was reduced to the order of the material response time, the signal modulation would decrease as the optic axis would no longer have time to deflect to its full switching angle for the field, $\phi(E)$. As the frequency is increased, therefore, the optic axis movement, and consequently the signal modulation, should tend towards zero. The response signal for the same cell at an increased drive frequency of 4 kHz, i.e. a period similar to the response time, is shown below.

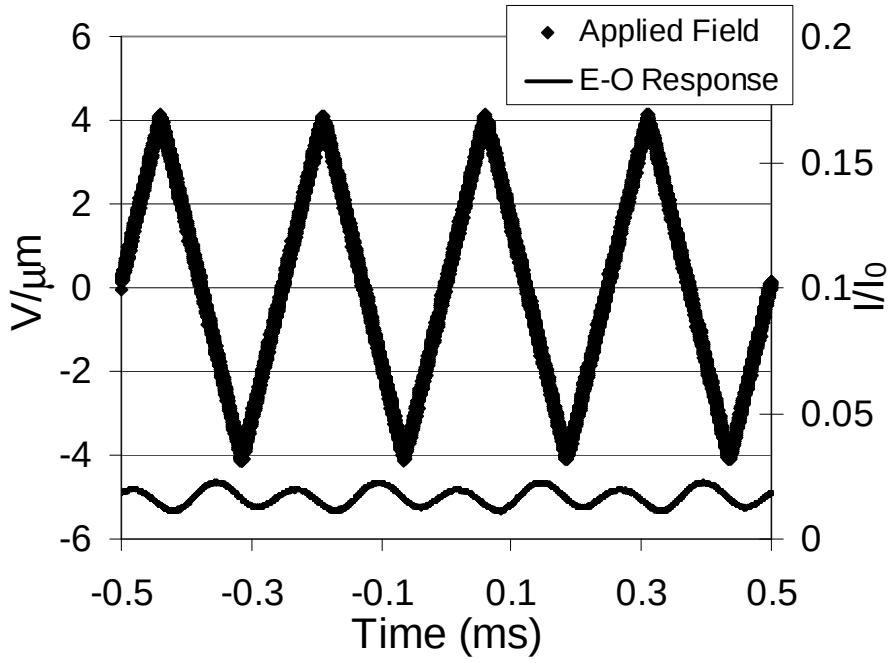

Figure 3.5: *The electro-optic response of the chiral FFO9OCB cell at T_C-10℃ to an applied triangular a.c. field of 4kHZ frequency and 4V/µm peak field.*

The expected reduction in signal modulation is clearly observed. The modulation as the change in % light transmission $I_{max} - I_{min}$ was measured at a series of drive frequencies, the results being shown in Figure 3.6. This figure shows the expected reduction in signal modulation with increase in drive frequency. In fact, the signal modulation was found to still be increasing at the lowest observed drive frequency of 0.8 kHz. It would be anticipated that once the drive frequency was reduced to the point that the optic axis had time to fully respond to the field before the field strength began to reduce and change polarity, further reductions in frequency would produce no further increase in signal modulation. It appears from the figure that this point has not yet been reached at 0.8 kHz. Further reduction in drive frequency resulted in damage to the cell texture though, so this point could not be ascertained.

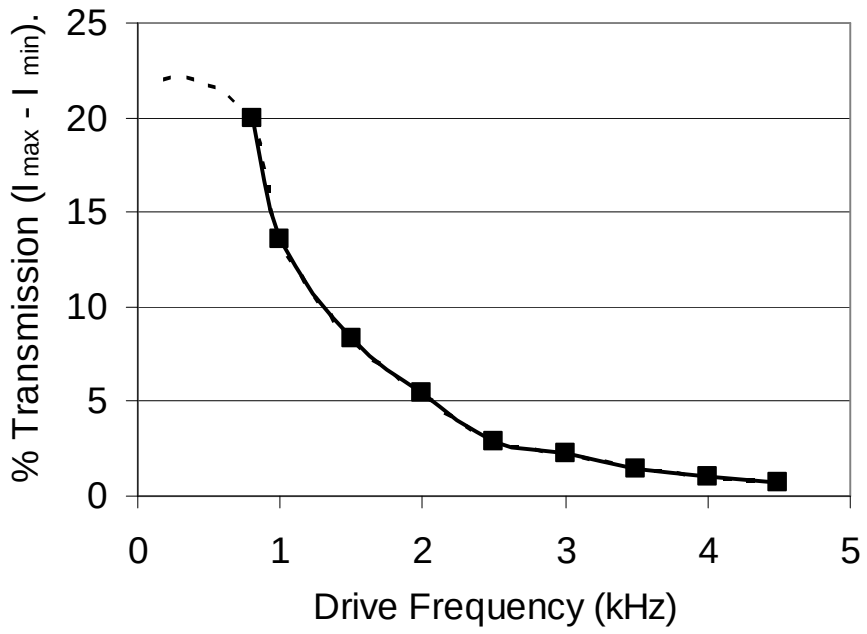

Figure 3.6: *The response signal modulation, measured as the change in I/I_0, as a function of frequency of the applied 4V/µm peak triangular waveform. The dotted line in addition to the solid line joining the measured data indicates the expected limiting of the response at lower frequencies.*

These results show clearly the presence of an electro-optic effect in grandjean textured chiral nematic samples with electric field applied in the plane of the cell. The nature of the observed traces correlates with the predicted response for a flexoelectro-optic deformation occurring in the sample, with both the magnitude and frequency dependence agreeing with the expected response, providing good evidence that the response is indeed flexoelectro-optic.

The limitation of the applied field to only high frequency triangular waveforms however prevents definite measurements of the amplitude and response time of the optical response, and therefore full characterisation of the effect. For this to be achieved, a bi-polar square pulses, separated in time by several tens of ms were applied to the cell, keeping the time the field was applied to a minimum.

4.3. SQUARE PULSE RESPONSE

4.3.1. FFO9OCB

A single one millisecond duration square pulse was applied to the cell, and a response observed. It was found that the isolated pulse had no adverse affect on the texture of the cell, and that using the triggered storage facility of the digital phosphor oscilloscope, the response could be captured and examined. The pulse could be repeated at up to 5 times a second and a reliable response maintained. The trace acquired from a 4 V/µm amplitude pulse at 110ºC (T_C-5ºC) is shown in Figure 3.7.

As the figure shows, the electro-optic response to the square pulse is as anticipated, and the magnitude of the switch as well as the response times on application and removal of the field can now be measured, as outlined in Section 3.4.2. This was done for a range of applied field strengths and operating temperatures, the results being shown in Figures 4.8, 4.9 and 4.10.

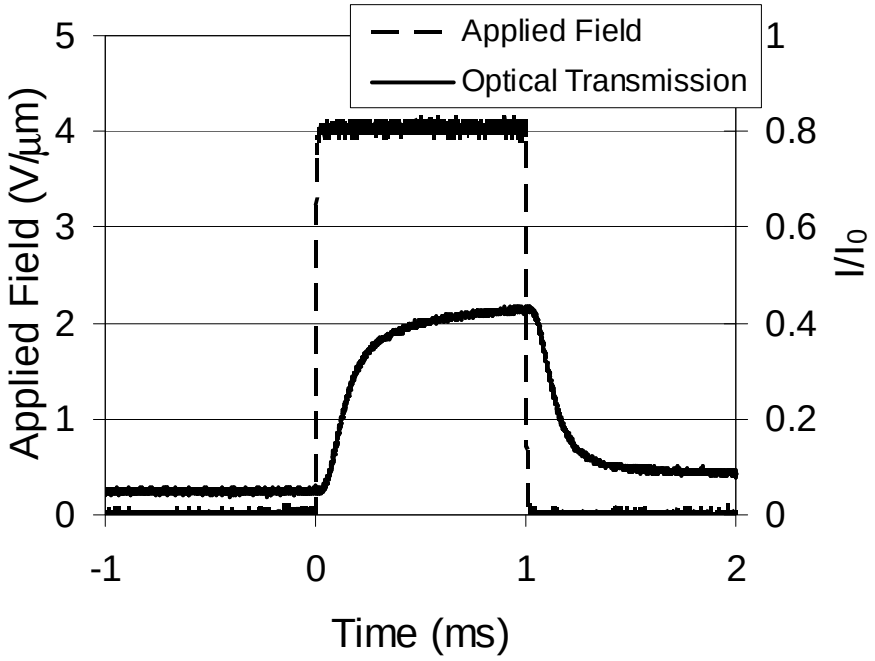

Figure 3.7: *The electro-optic response of the chiral FFO9OCBcell at T_C-10 ºC to an applied square pulse of 1ms duration and 4V/µm peak field.*

Two interesting features from the above trace are the fact that the relaxation time (T_{OFF}) appears to be considerably faster than the response time (T_{ON}). This is most unusual in liquid crystal electro-

optic effects,[14] as the director torque generated by an applied electric field is usually much larger than that of the opposing elastic deformation, so relaxation times which are driven solely by elastic forces tend to be slower. This behaviour is seen at all temperatures, as shown in the difference in the ON and OFF times in figures 4.9 and 4.10 respectively. Also, there appears to be a slight residual birefringence left over a millisecond after removal of the field, after 90% of the response has disappeared. This suggests a second, slower, mechanism contributing to the birefringence, which is likely to be dielectric helix unwinding. Overall however, the response times are very similar to those observed for the same material undergoing flexoelectro-optic switching in the ULH texture.[13]

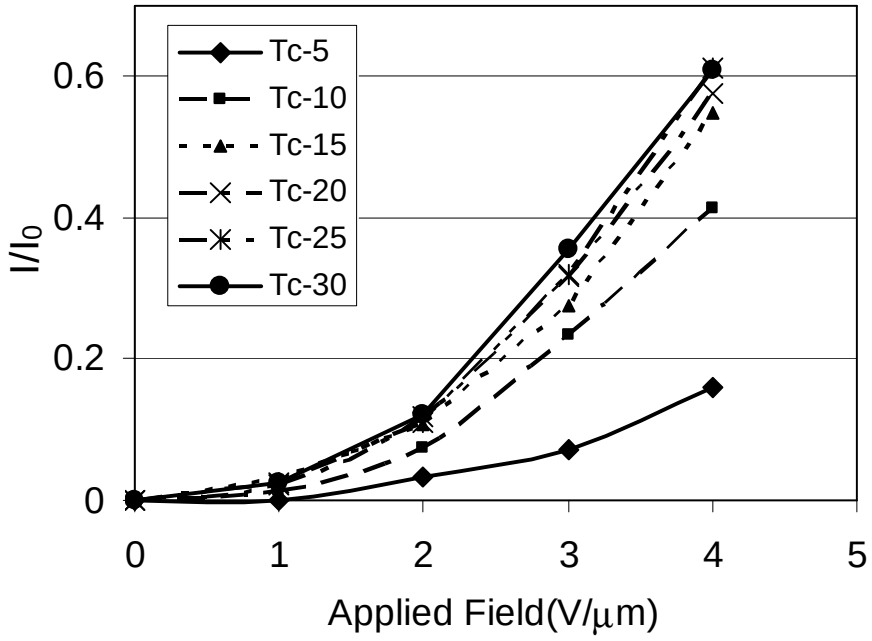

Figure 3.8: *The optical transmission of the chiral FFO9OCB cell as a function of applied field strength at a range of temperature.*

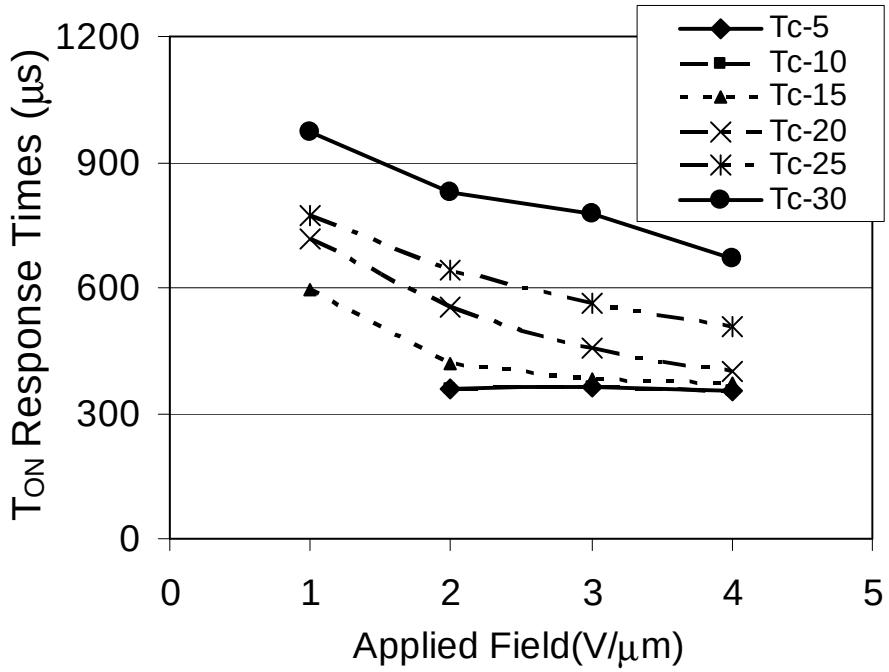

Figure 3.9: *The 10-90% (T_{ON}) response times of the chiral FFO9OCB sample as a function of applied field, at a range of temperatures below T_C.*

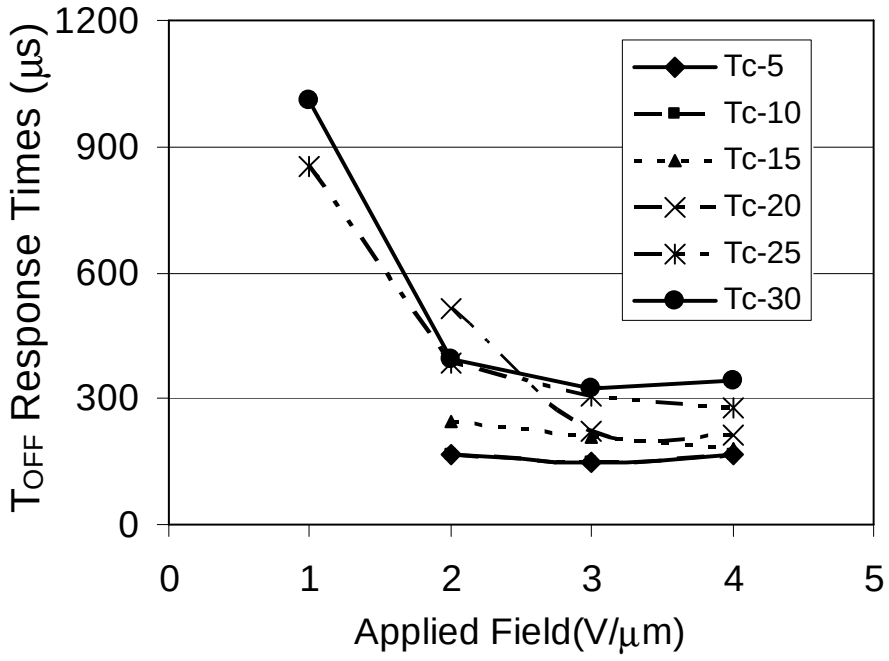

Figure 3.10: *The 90-10% (T_{OFF}) response times of the chiral FFO9OCB sample as a function of applied field, at a range of temperatures below T_C.*

In the above figures, where a data point does not appear in the response time plots for high temperature and low applied field it is because the optical response, although observed to be present, was not large enough to allow the digital oscilloscope to provide a reliable reading of the response time.

Having characterised the response at a range of field strengths and temperatures, and found the observed switch to be largely consistent with the predicted observations from a flexoelectro-optic deformation taking place, a further test was performed to confirm the expected dependence of the optical transmission on the angle of applied field with respect to the polarisers. Rotation of the E-field direction between the crossed polarisers ought to produce a $\sin^2$ dependency in the maximum optical transmission for a given field, according to equation 3.2. This was performed, and the results are displayed in Figure 3.11, alongside the theoretical response for the material according to the calculations laid out in Section 2.4.5.1, with values of the tilt angle as a function of applied field, $\phi(E)$, taken from those measured in the ULH[13]

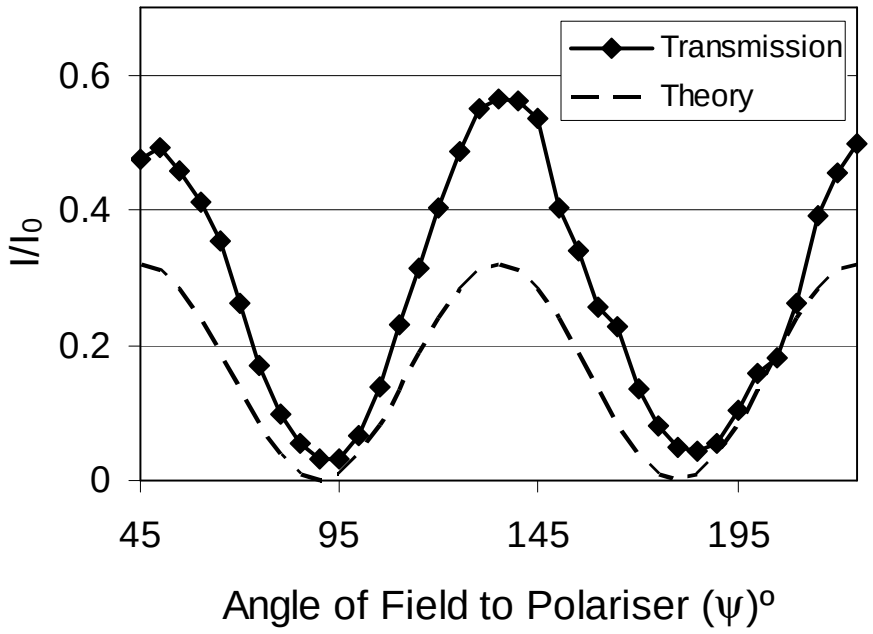

Figure 3.11: *The angular dependence of the optical transmission cell on the direction of the applied field with respect to the polariser's transmission axes, in comparison to the theoretical $\sin^2$ function.*

The above figure shows that, although the observed response is larger than that predicted, the expected $\sin^2$ dependency of the optical throughput on the applied field direction is clearly observed. This is further confirmation of the nature of the effect being as predicted.

One feature of the above trace, and the previous measurements on this sample with the square pulses, that has not so far been discussed, is the large magnitude of the optical response. Figure 3.8 shows fractional transmission of the cell as high as $I/I_0 = 0.6$ at high field strengths and low temperatures. This is a much higher throughput than expected in these cells, and several times that observed with the triangular driving waveform. This larger than anticipated response is believed to be due to the cell thickness being larger than the intended 10 µm. Unfortunately, no cell thickness measurement could be obtained from this cell so the transmission values could not be converted into birefringence (probably because it was too thick, e.g. > 20 µm, although an improved cell thickness measurement system was set up subsequently to the work in this chapter, but unfortunately a shortage of cells meant these measurements could not be repeated. These results still provide a full characterisation of the effect in other respects however, and allow qualitative analysis of the magnitude of the switch.

4.3.2. 7OCB

For comparison to the results detailed above, a second mixture was formed, based on the oxycyanobiphenyl monomesogen heptyl-alkyloxy-4'-cyanobiphenyl, known as 7OCB the structure of which is shown below. This was chosen as it has been previously examined for its flexoelectro-optic properties,[14,15] and although it is known to have only a small tilt angle in its chiral form, it would provide a good "control" material with which to compare the optical response from the bimesogenic mixtures.

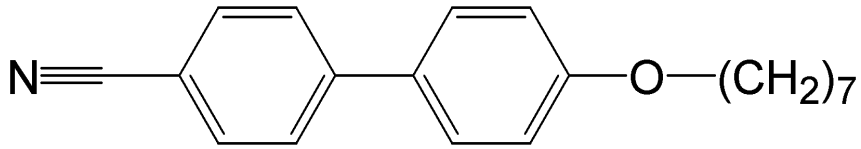

Figure 3.12: *The chemical structure of 7OCB.*

The nematic was mixed with 2.99% (weight/weight) BDH1281 to make the mixture chiral. The material was filled into a cartwheel cell and found to undergo the phase transition into the chiral nematic phase from the isotropic at 85ºC in the probe station.

Tc	Δε	Δn
85˚C	8.8	1.44

Table 4-II: *Material parameters of the 7OCB mixture*

Due to concerns over the repeated application of monopolar pulses to the samples effectively amounting to a d.c. field over time, and consequent charge injection problem this may induce, an isolated bipolar pulse waveform was applied to these cells. The measurements of optical response times with this bipolar pulse are still directly comparable to those from the monopolar pulse presented for FFO9OCB. The response of the chiral 7OCB sample to this bipolar pulse is shown in Figure 3.13.

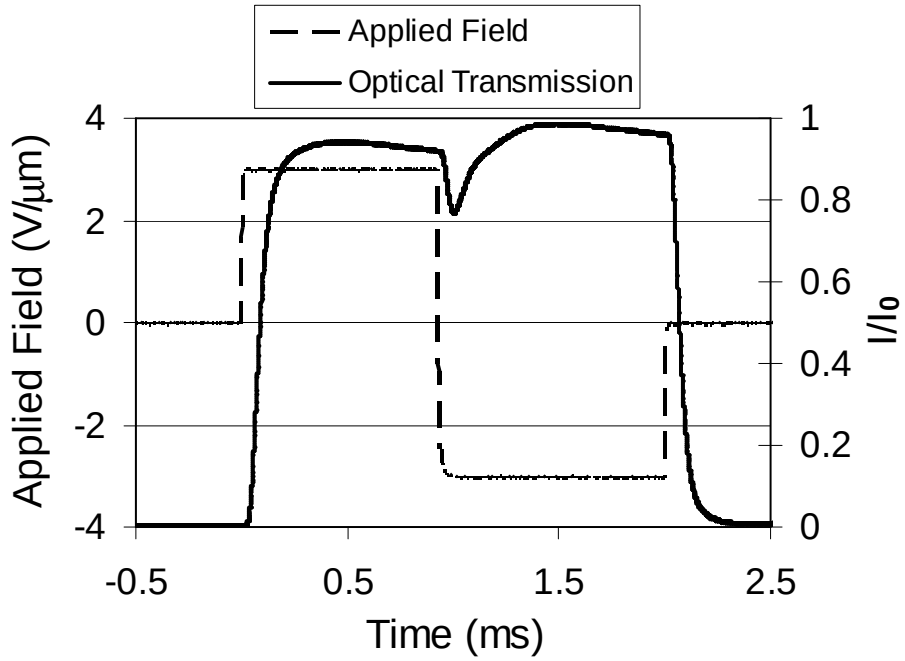

Figure 3.13: *The electro-optic response of the chiral 7OCB cell at T_C-10 ℃ to a +/-3V/μm 2ms duration bipolar square pulse.*

The above trace shows an even larger response than the previous bimesogen based sample, exhibiting almost 100% modulation of the light input. This remarkable result was highly unexpected, as the flexoelectric properties of these two mixtures were compared in the ULH texture and the bimesogenic FFO9OCB compound exhibited a tilt angle of ϕ = 22º at 4 V/μm compared with 5º from this sample. Again, the cell thickness was unknown for this sample, so only

qualitative comparison can be made with the magnitude of the switches, but subsequent destructive testing of the cell thicknesses (see section 3.3.1.2) revealed these cells to be of the order 40µm in thickness. This goes some way to explaining the larger than expected switch, as the optical path length is four times that anticipated form the cell construction.

An examination of the response times in this mixture shows that the optical response is slightly faster than in the previous mixture, for both T_{ON} and T_{OFF}, as displayed in Figure 3.14 and Figure 3.15.

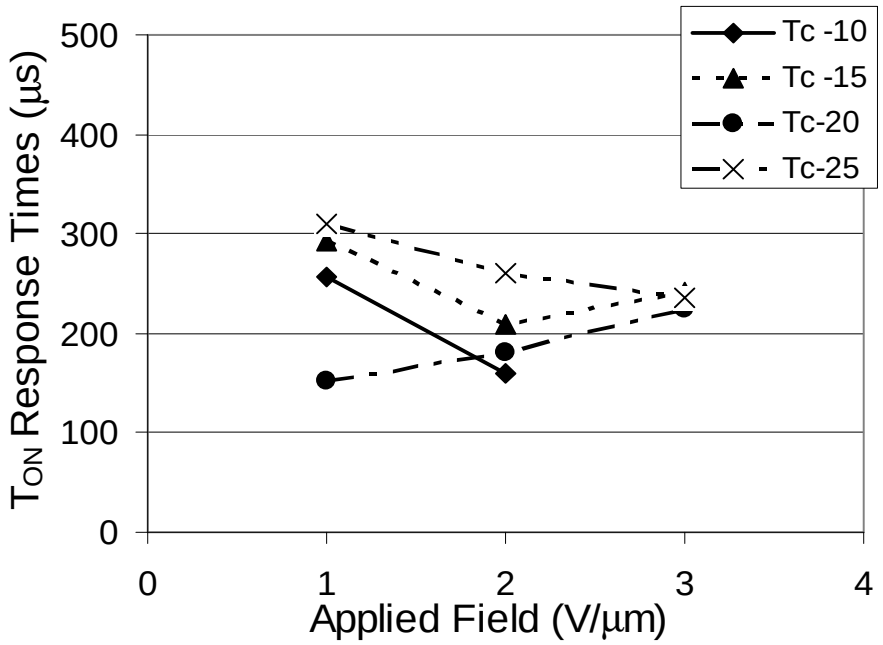

Figure 3.14: *The 10-90% (T_{ON}) response times of the chiral 7OCB sample as a function of applied field, at a range of temperatures below T_C.*

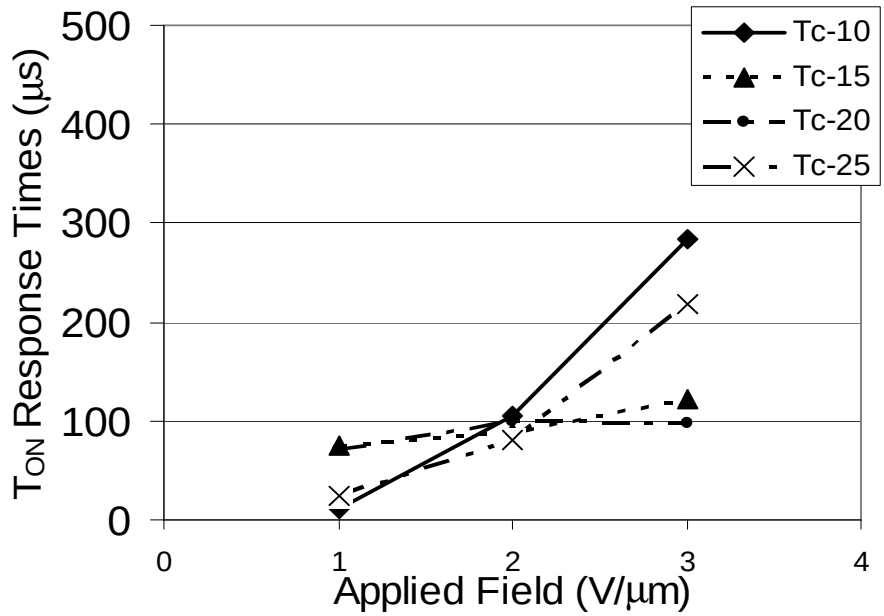

Figure 3.15: *The 90-10% (T_{OFF}) response times of the chiral 7OCB sample as a function of applied field, at a range of temperatures below T_C.*

What the trace in Figure 3.13 does reveal, though, is the first clear sign that dielectric coupling causes the applied field to partially unwind the director helix, adding to the birefringence. This manifests itself in the failure of the response to return to zero transmission at the point where the field changes polarity and the optic axis switches from $+\phi$ to $-\phi$, going through the vertical neutral position. Whether dielectric coupling can entirely account for this anomaly requires the application of a.c. fields of varying frequency over periods much longer than their frequency. This was not possible in these samples due to destruction of the texture, but is discussed further in the following Chapter where the textures are stabilised with polymers. Also, the response can be seen to be slightly asymmetric with respect to the different pulse polarities. This is probably due to a pre-tilt effect in the surface alignment giving a pre-disposition to the tilt deformation in one direction over the other.

The response times can be seen to be slightly faster than those of the FF09OCB sample, which again correlates with the measurements of these materials flexoelectro-optic properties in the ULH texture, 7OCB having a lower effective viscosity for the deformation. It is unexpected, however, that the response times should remain low despite the large degree of dielectric coupling which appears to be contributing to the overall optical response.

As a final investigation into the nature of the effect, this large switching sample was tested between parallel polarisers. If the effect is due purely to a straightforward induced birefringence as thought, an inverse effect ought to be visible in this situation, whereby the field causes an initially transmissive system to become attenuating. The observed response is given below, and can be seen to be an almost exact reflection of the crossed polariser response.

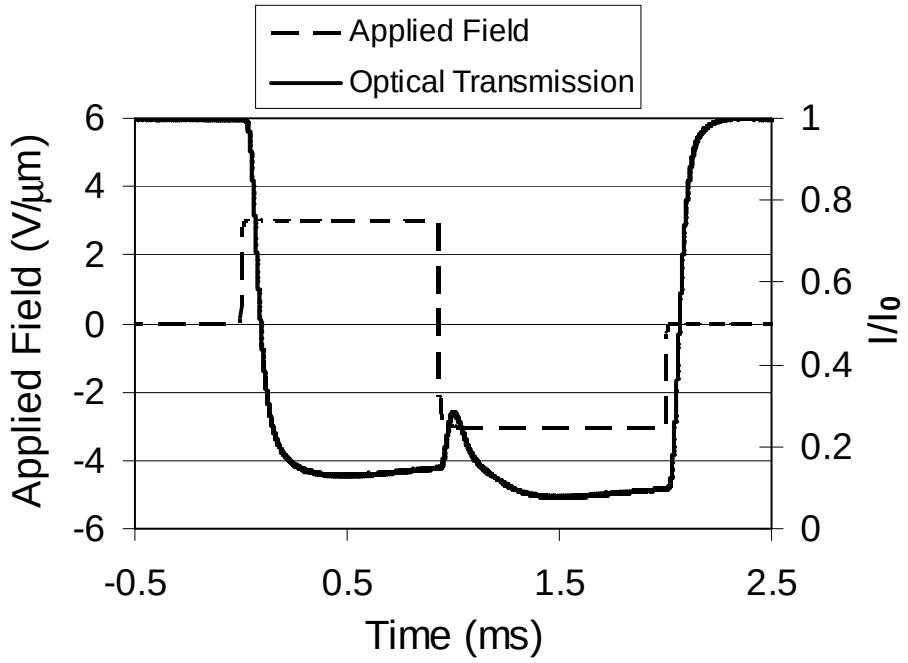

Figure 3.16: *The electro-optic response of the chiral 7OCB cell, between parallel polarisers, at T_C-10℃ to a +/-3V/μm 2ms duration bipolar square pulse.*

4.4. CONCLUSIONS

The results outlined in this Chapter clearly show the presence for the first time of a fast electro-optic effect at 1550nm in Grandjean textured chiral nematic liquid crystals with in-plane electric fields. These initial experiments have therefore successfully achieved their purpose. The observed response agrees well in both shape and magnitude to that predicted for a flexoelectro-optic effect operating in this geometry, which has the helical axis rotated by 90º with respect to the ULH geometry. The measurements of the electric field angle dependency of the magnitude of the induced birefringence, and the response exhibited by the sample between parallel polarisers give confidence that flexoelectro-optic switching is the correct description of the switching mechanism which is taking place in the sample.

The measured magnitude of the electro-optic response and characteristic response times are very encouraging for the development of a useful flexoelectric device. The retardations induced in the samples by applied square electrical pulses exceed expectations, mainly due to the cells constructed being several times thicker than first thought. This is no impediment to a useful device however, and serves to illustrate that simply increasing the optical path length of the device is a viable method of increasing the retardation available. The approximately 40µm thick 7OCB cell in particular was effectively a switchable half waveplate.

The characteristic response times which are observed, of the order 300-900 µs for the response to an applied field, and 200-400 µs for relaxation on removal of the field, are an order of magnitude faster than typical nematic devices, justifying the decision to investigate the flexoelectro-optic effect in this novel geometry as a way of improving the speed of dielectrically coupled nematic based cartwheel cell devices. The fact the T_{OFF} times are consistently shorter than the T_{ON} times is unusual, but is if anything an unforeseen advantage in any potential device. For the flexoelectro-optic effect, under the assumption of small angle switching, T_{ON} and T_{OFF} should be independent of field.

Several improvements need to be made however in order for the effect to be made viable for photonic device applications. The most serious concern is the inability of the liquid crystal texture to withstand continuous applied a.c. fields. While pulsed operation has proved useful here for characterising the effect, it would be severely limiting for any real-world device. One possible approach for preventing this texture breakdown is polymer stabilisation of the liquid crystal, which is discussed in the next Chapter.

The influence of dielectric coupling causing helix unwinding also needs to be investigated, as the 7OCB response indicates this may be a significant factor. This may not be a problem for device operation, as the 7OCB trace still exhibits comfortably sub-millisecond response times despite the suspected presence of this type of deformation, but for understanding and development of the effect the contribution from dielectric coupling needs to be quantified. Finally, an accurate, non destructive cell thickness measurement needs to be achieved in the cartwheel cells to allow conversion of the measured sample retardance into material birefringence. This will allow direct comparison of the magnitude of the response from different mixtures. These issues are also addressed in the following Chapter.

Overall however, the results outlined here can be said to show good proof of concept of the flexoelectro-optic phase modulator effect, and are encouraging for future device possibilities.

4.5. REFERENCES

[1]J. S. Patel and R. B. Meyer, *Phys. Rev. Lett.*, **58**, (15), 1538, (1987).

[2]J. S. Patel and S. D. Lee, *J. Appl. Phys.*, **66**, (4), 1879-81, (1989).

[3]P. Rudquist, M. Buivydas, L. Komitov and S. T. Lagerwall, *J. Appl. Phys.*, **76**, (12), 7778, (1994).

[4]J. S. Patel and R. B. Meyer, Patent: *EP0281341*, (1988).

[5]L. Komitov, G. P. Bryan-Brown, E. L. Wood and A. B. J. Smout, *J. Appl. Phys.*, **86**, (7), 3508, (1999).

[6]S. D. Lee and J. S. Patel, *Phys. Rev. A*, **42**, (2), 997-1000, (1990).

[7]H. J. Coles, M. J. Coles, S. P. Perkins, B. M. Musgrave and D. Coates, Patent: *GB2356629.*, (2001).

[8]Y. Ohtera, T. Chiba and S. Kawakami, *Ieee Photonics Technology Letters*, **8**, (3), 390, (1996).

[9]S. H. Rumbaugh, M. D. Jones and L. W. Casperson, *Journal of Lightwave Technology*, **8**, (3), 459, (1990).

[10]H. L. de Vries, *Acta Cryst.*, **4**, 219-26, (1951).

[11]H. J. Coles, *Chiral Nematic Liquid Crystals*, in *Handboook of Liquid Crystals*,**2a**, D. Demus, J. W. Goodby and G. W. Gray, Wiley-VCH, (1998).

[12]A. E. Blatch, M. J. Coles, B. Musgrave and H. J. Coles, *Mol. Cryst. Liq. Cryst.*, **401**, 161-9, (2003).

[13]M. J. Clarke, PhD Thesis, University of Southampton, (2004).

[14]B. Musgrave, PhD, University of Southampton, (2000).

[15]H. J. Coles, B. Musgrave, M. J. Coles and J. Willmott, *J. Mater. Chem.*, **11**, (11), 2709-16, (2001).

Chapter Five

Polymer Stabilised Grandjean Flexoelectro-optic Switching

7.1. INTRODUCTION

In Chapter 4, the ability to induce an electric field dependent birefringence in Grandjean textured chiral nematic liquid crystals, via the flexoelectro-optic effect, was demonstrated. Triangular electric waveforms were applied to cartwheel cells to demonstrate proof of concept of the effect, and millisecond duration bipolar square pulses were utilised to characterise the magnitude and speed of the effect and compare the response in different liquid crystal mixtures.

Unfortunately, it was found that applying an a.c. field over a certain time resulted in an irreversible degradation of the Grandjean texture required for the effect. This is believed to be due to non-uniformity of the field over the area of the cell causing dielectrophoretic flow effects, the result of which was the scrambling of the aligned, monodomain texture into a scattering focal conic state with small domain size. In order for any useful device to be developed which operates on the basis of the Grandjean flexoelectro-optic effect, the liquid crystal would have to withstand a.c fields over long periods. One method of making this feasible is the introduction of a polymer network into the bulk of the liquid crystal layer. This may provide sufficient stability and ruggedness of the texture to prevent the flow of the material, without hindering the electro-optic switch.

The combination of liquid crystals with polymer networks is a research topic in its own right.[1] Two principal liquid crystal/polymer configurations have been developed: the polymer dispersed liquid crystal (PDLC),[2] and the polymer stabilised liquid crystal (PSLC).[3] The morphology employed in this work is the latter, whereby the polymer concentration is sufficient to provide a stabilising influence on the liquid crystal texture, but not so much as to encapsulate the liquid crystal to form microdroplets.

In this work a photocurable monomer is used to provide the polymer network. The monomer itself was liquid crystalline, as this provides advantages over standard UV curing polymers in terms of miscibility with the liquid crystal host, adoption of the host director configuration, and stabilisation of the texture present at polymerisation.[4,5] The particular reactive mesogen used was RM257, supplied by Merck NB-C.[6] This was mixed in proportions of 3-5% (w/w) with the chiral nematic host and kept in the isotropic phase for 48 hours in a dark bottle to allow full dissolution in the host. A photoinitiator Irgacure 819, also provided by Merck, was used also in proportions of less than 1% of the mixture weight.

7.2. INCREASED RUGGEDNESS DUE TO POLYMER STABILISATION

A test mixture was made to examine the effectiveness of the polymer in preserving the texture. A cartwheel cell was filled with a mixture of the photocurable monomer and chiral 7OCB, examined under the microscope with a red filter to confirm the presence of the Grandjean texture without prematurely polymerising the sample, and then polymerised using the UV lamp. The resultant texture can be seen in Figure 5.1.

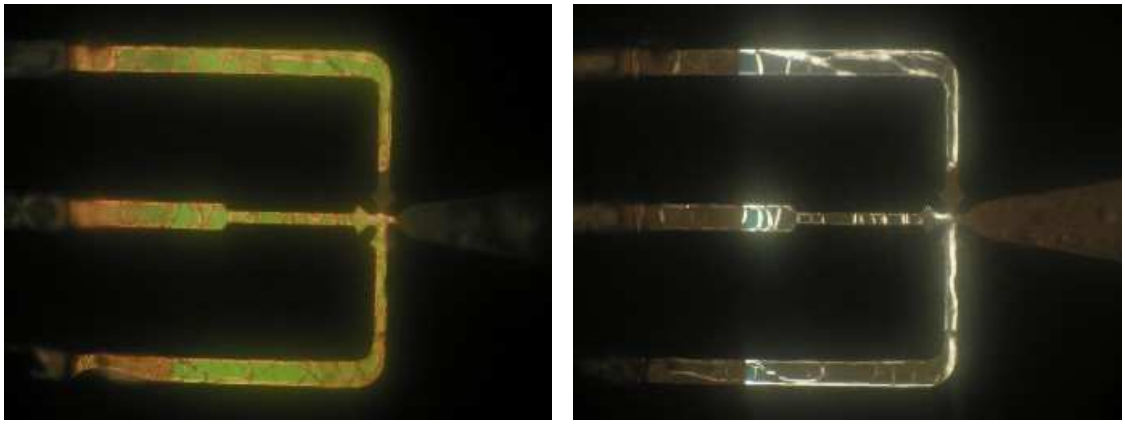

Figure 5.1: *Polarising microscopy images of the polymerised chiral 7OCB sample in the N* phase (left) and the isotropic (right).*

The polymerisation process did not alter the appearance of the sample under the polarising microscope at all, the texture remained unchanged. However, the texture was visibly more resistant to flow produced by prodding the sample with tweezers. The disclination lines "bulged" and returned with each prod, rather than genuine flow occurring, which was the case pre-exposure. Also, on heating into the isotropic phase, the disclination lines remained anisotropic, as visible in the right hand image of Figure 5.1. This is believed to be due to a tendency for the polymer to concentrate itself in the disclinations, resulting in anisotropic polymer strands forming upon exposure. This effect has been observed previously and utilised in the preservation of otherwise transitory blue phases.[7] With the disclination lines thus preserved, the sample recovered its texture identically on returning to the N* phase. As the areas of Grandjean texture also returned immediately, this suggests the polymer is also present in the areas of uniform texture and is

providing stabilisation, only in a much finer mesh which is not anisotropic in sufficiently large strands to be visible under the microscope in the isotropic phase.

Having successfully polymerised the sample, a continuous a.c. square wave of 80Hz frequency and up to 6V/μm field strength was applied across the cell. Unlike in the non-polymerised samples described in Chapter 4, neither flow effects nor degradation of the texture were visible under the microscope. The same material was also tested in a "lucid cell" in the ULH texture, and was found also to return to the same texture after temperature cycling into the isotropic phase, and also upon unwinding of the chiral nematic helix by high fields. This and other ruggedised liquid crystal/polymer mixtures are therefore potentially suitable for telecoms applications. In the remainder of this Chapter, the electro-optic properties of these mixtures will be investigated.

7.3. INDUCED BIREFRINGENCE

7.3.1. 7OCB

The mesogenic compound 7OCB was chosen for the initial tests as its flexoelectro-optic properties are well known,[8] and it produced a large response in the unpolymerised mixture examined in Chapter 4. The mixture was made up according to the following proportions: 90.57% 7OCB, 3.43% BDH1281, 5.1% RM257, 0.9% Irgacure 819. After polymerisation, the clearing point T_C of the mixture was found to be 85°C, in the probe station rig. The cell thickness was 11.7μm. The electro-optic response of the Grandjean textured sample to a +/-6V/μm bipolar square pulse in the cartwheel cell can be seen in Figure 5.2.

Tc	Δε	Δn
85˚C	8.8	1.44

Table 5-I: *Material parameters of the 7OCB mixture*

Comparison of the shape and magnitude of the trace with that of the un-polymerised chiral 7OCB mixture examined in Chapter 4 shows a very similar response. One small difference in the trace shown here is the tendency for the transmission to rise slightly after reaching extinction on removal of the field. This is due to a small texture defect in the active area causing a birefringence at zero voltage, which the field induced birefringence initially cancels out before overwhelming. The feature is small, so the peak transmission values are unaffected, but the response times as

measured, are somewhat reduced for this sample, as shown in Figure 5.3, compared with results shown in Chapter 4.

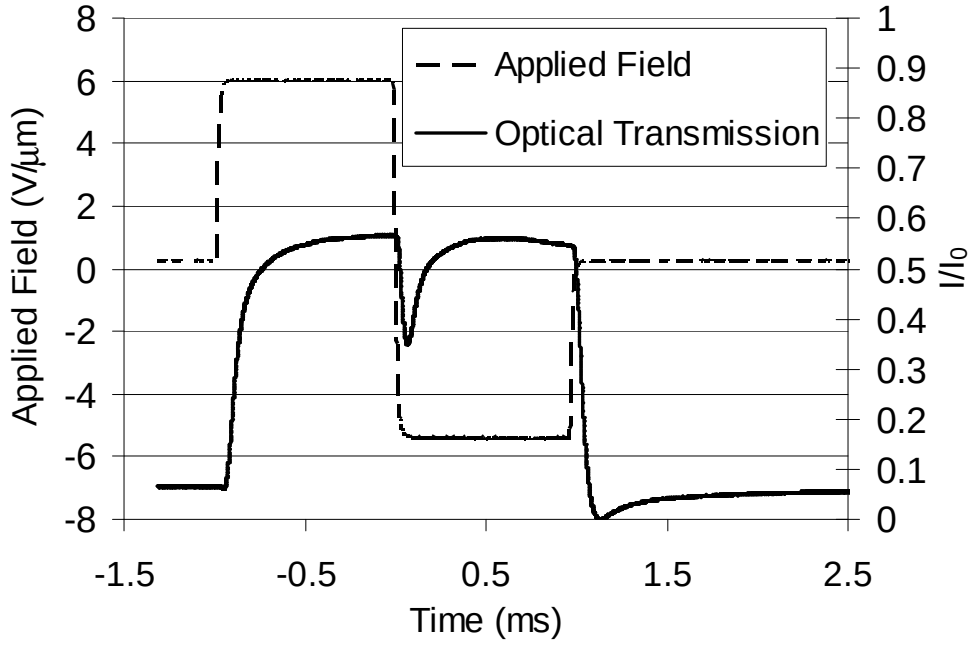

Figure 5.2: *The electro-optic response of the polymerised chiral 7OCB cell at T_C-10℃ to a +/- 6V/µm 2ms duration bipolar square pulse.*

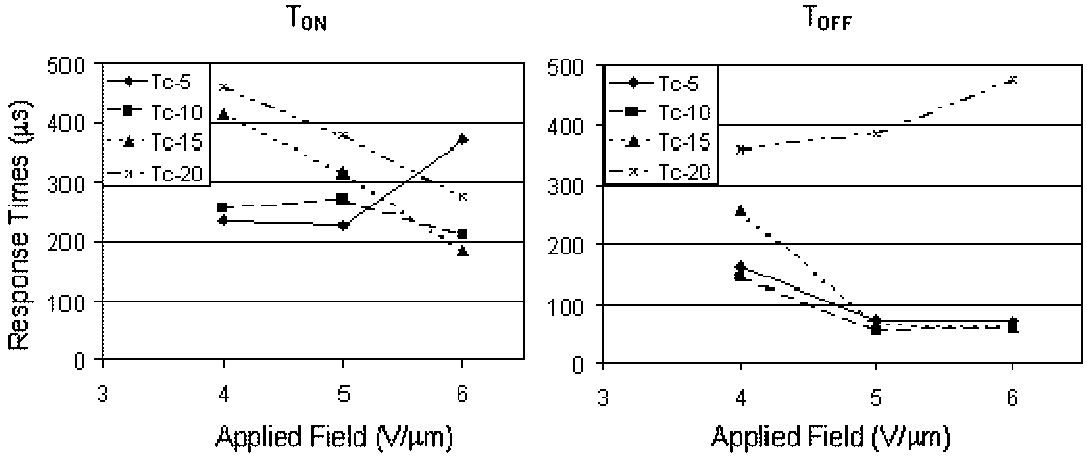

Figure 5.3: *The T_{ON}(10-90%) (left) and T_{OFF} (90-10%) (right) response times for the chiral 7OCB mixture in the cartwheel cell.*

The response times shown in the figure above are for order of magnitude demonstration only, due to the texture defect affecting the 10% and 90% level point for the switch. The responses are all below 500µs though, which is in the fast region desired and which it was hoped the flexoelectro-

optic response would deliver. The optical response is also certainly large, with a peak transmission of $0.56I_0$, corresponding to an induced birefringence of 0.036.

These flexoelectric and dielectric effects can now be separated in the polymerised cell, which is able to withstand continuous high strength fields. This is achieved as follows: a square wave a.c. waveform is applied to the cell and the birefringence monitored, the dielectric contribution, being dependent on the quadratic of the applied field, is constant, whereas the flexoelectric deformation, being dependent on the absolute field value, will reverse with the changing field polarity. In fact, as the birefringence resulting from the flexoelectro-optic deformation is identical for both positive and negative tilt angles, the only indicator of the flexoelectro-optic contribution is a brief drop in birefringence when the field changes polarity, as the optic axis tilt angle passes through the vertical neutral point on its way from $+\phi$ to $-\phi$. As the dielectric deformation remains during this transition, being dependent on the square of the applied field and therefore independent of polarity, any residual birefringence at the transition points can be attributed to helix unwinding, and subtracted from the optical response to leave the contribution from the flexoelectro-optic effect.

Figure 5.4 shows the electro-optic response of the cell to fields of up to 6V/μm R.M.S. at 500Hz and 10kHz. As can be seen, the magnitude of the induced birefringence (Δn=0.037 maximum) is comparable to the bipolar pulse response. The field-following (flexoelectric) fraction of the response is greatly reduced by increasing the drive frequency. At 10kHZ, the polarity dependent transmission modulation is reduced to an insignificant level ($<0.02\ I/I_0$) and an almost constant "baseline" birefringence remains.

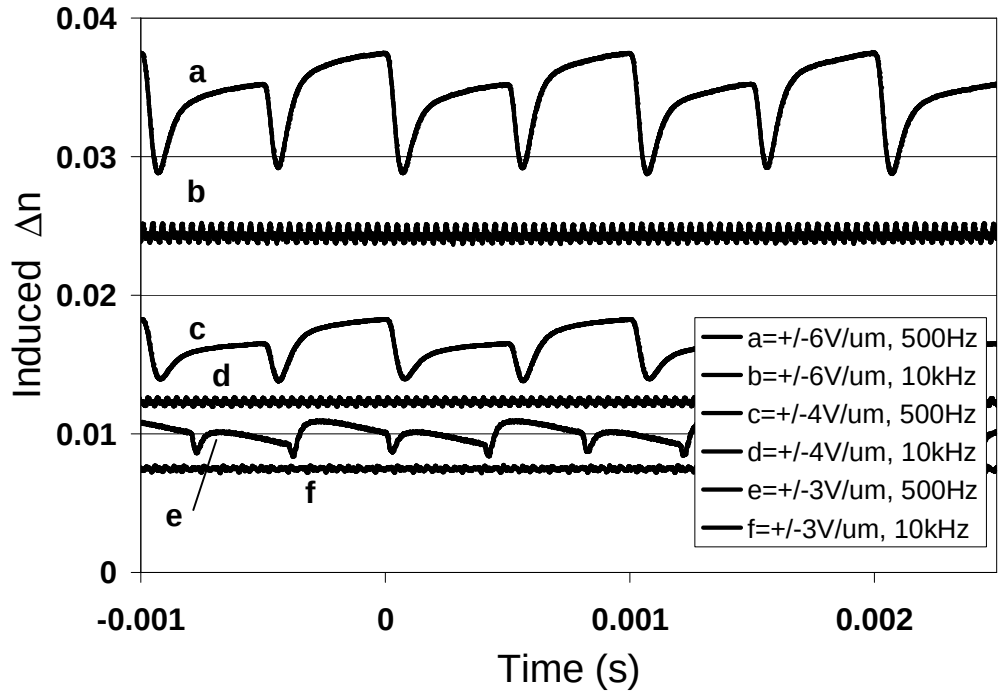

Figure 5.4*: The electro-optic response of the polymerised chiral 7OCB cell at T_C-10 ℃ to applied fields of 3, 4 and 6 V/μm at 500Hz and 10kHz.*

This "baseline" is the contribution from dielectric coupling to the field, which causes the director helix to partially unwind. The director deformation from the two effects are illustrated in Section 2.4.3, Figure 2.12., from which it can be seen that the two deformations are complementary in that they both contribute to a birefringence with equivalent optic axis direction.

It can be seen from Figure 5.4 that the base level birefringence does not fully account for the residual birefringence at lower frequencies during the field polarity transition, i.e. the 500Hz response does not drop all the way to the value of the 10kHz response in the dips as the field changes sign. This is partially because the amplifier used has a limited slew rate and cannot exactly replicate the input square wave at high frequencies, instead producing a slightly sloped transition edge, resulting in a reduced effective r.m.s. field value. The result is sufficient however, to demonstrate the significance of the dielectric mechanism in the overall response. If the minimum values at the field transition point are assumed to represent the true extent of the dielectric influence, then the field dependence of the two effects can be seen with a plot of the maximum and minimum points of the 500Hz response at a range of R.M.S. field values, as in Figure 5.5.

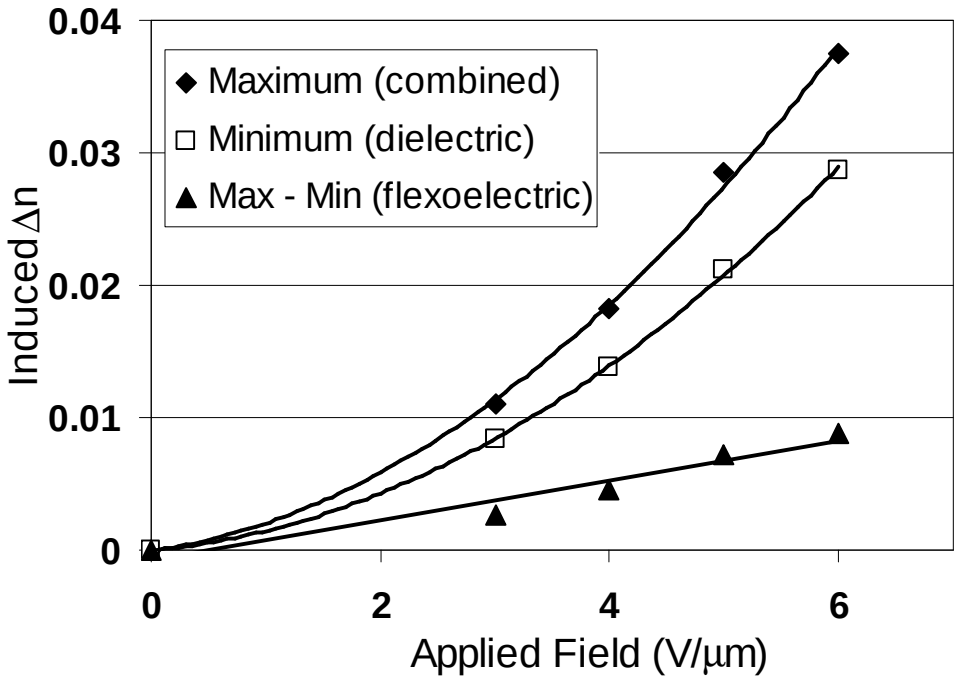

Figure 5.5: *The R.M.S field dependence of the maximum and minimum birefringence induced in the polymerised chiral 7OCB cell by a 500Hz applied field at T_C-10 ℃ .*

The above plot shows that, if the minimum of the field following response at 500Hz is taken as the total of the dielectric contribution to the induced birefringence, the dielectric contribution increases at an above linear rate with the applied field strength. The flexoelectrically-induced birefringence is then taken as the difference between the maximum and minimum induced birefringences of the 500HZ plots, i.e. the amplitude of the trace modulation. This can be seen to increase roughly linearly with the applied field strength. According to the theory outlined in Chapter 2, dielectric effects couple to the square of the applied field, while the flexoelectro-optic deformation ought to be proportional to the absolute field value.[9]

The curves in Figure 5.5. are a quadratic and linear fit to the data for the dielectric and flexoelectric portions of the response respectively, and show a reasonable agreement. The slight deviation from the fits is due to the fact that the coupling factors relate the applied field to the director deformation, and as discussed in Chapters 2 and 4, the induced birefringence does not depend linearly on the director deformation except in the region close to $\frac{\Delta nd}{\lambda} = \frac{1}{4}$, i.e. the 50% transmission point.

Overall, the performance obtained from the chiral 7OCB mixture in the cartwheel cell was very encouraging. The cell was comfortably able to withstand a.c. fields of high strength over long periods. A birefringence of $\Delta n = 0.0375$ was induced by a 6V/μm applied field and the switch both fully responded and relaxed, upon the application and removal of the field, in timescales of approximately 300μs. This is considerably faster than a typical nematic device, and a significant enough effect to produce a quarter waveplate effect in the cell used,[10] and would produce a half waveplate in a 21μm thick cell. The speed of the response is surprising, given the significant proportion (≈75%) of the induced birefringence resulting from dielectric helix unwinding. Dielectric effects are generally regarded as much slower than the flexoelectric effect, with typical response times of the order 10ms, rather than the sub millisecond switching observed here.

7.4. MIXTURE DEVELOPMENT

Despite the far quicker than expected response times of the 7OCB sample, for purposes of definite characterisation, a purely flexoelectric response was desirable. It has been shown that bimesogenic liquid crystals offer dramatically improved flexoelectric coefficients and only small dielectric coupling effects, two factors important in flexoelectro-optic switching in the ULH texture to maximise the tilt angle and eliminate helix unwinding.[11-13] These properties ought to be equally beneficial to a device based on the Grandjean texture, so the following sections detail the development and characterisation of such bimesogenic mixtures and the results they produced in the cartwheel cell.

The investigated mixtures were based on a non-symmetric bimesogen containing a cyanobiphenyl (CB) and a difluorobiphenyl (FF) end group, two homologues of symmetric bimesogens, in which the CB group is replaced by another FF group, and a mixture of these symmetric bimesogens with the equivalent ester linked molecules.

7.4.1. FFO11OCB

The non-symmetric bimesogen (so called because the mesogenic end units are chemically different, one side being double fluorinated) was α-(2',4-difluorobiphenyl-4'-yloxy)-ω-(4-

cyanobiphenyl-4’-yloxy)undecane, known by the acronym FFO11OCB. Its chemical structure is shown in Figure 5.6.

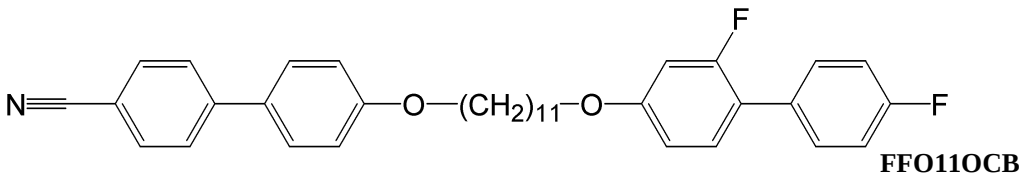

FFO11OCB

Figure 5.6: *The chemical structure of the non-symmetric bimesogen FFO11OCB.*

The proportions of the mixture examined were: 89.66% FFO11OCB, 3.48% BDH1281, 5.84% RM257, 1.02% Irgacure819. A 19.15μm thick cartwheel cell, measured via the etalon technique, was filled with this mixture, cooled into the N* phase, a Grandjean texture obtained and polymerised. The sample was found to undergo the I→N* transition at 128°C in the probe station.

Tc	Δε	Δn
128˚C	3.7	≈0.16

Table 5-II: *Material parameters of the FFO11OCB mixture*

The electro-optic response of the cell to a +/-6.7 V/μm 2ms duration bipolar pulse is shown in Figure 5.7.

The response can be seen to be considerably smaller in magnitude than the 7OCB response, and also slightly asymmetric in the response to the positive and –negative pulses. This is believed to be due to a slight pre-tilt effect in the surface alignment allowing for a preferential tilt of the optic axis in one direction compared to the other.

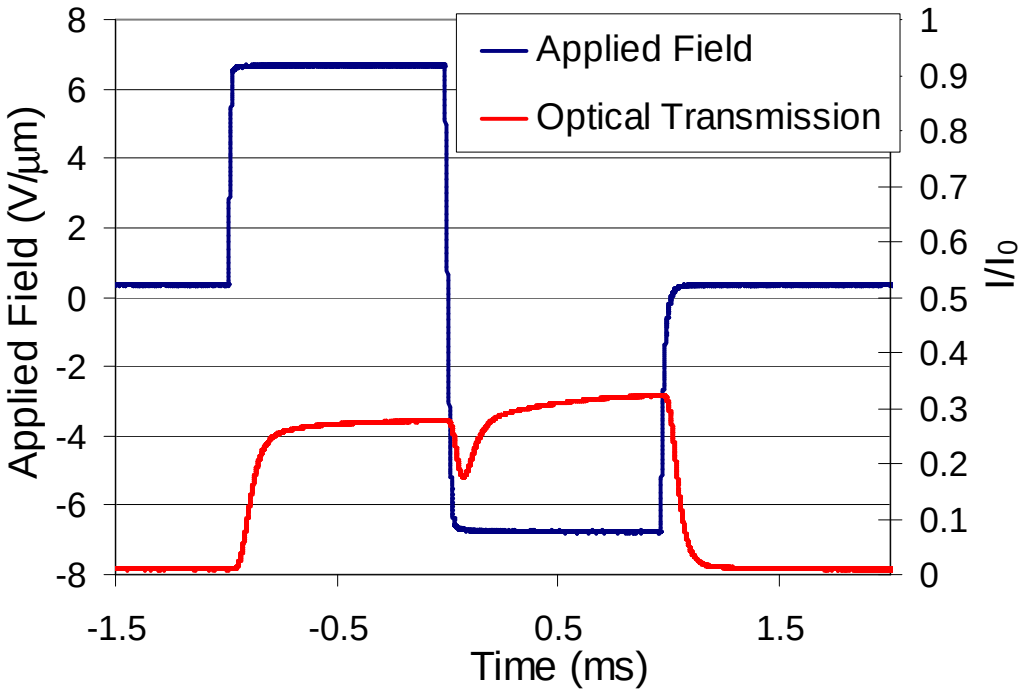

Figure 5.7: *The electro-optic response of the chiral FFO11OCB cell at T_C-10℃ to a +/-6.8 V/µm, 2ms duration bipolar square pulse.*

The response times for the effect in the chiral FFO11OCB mixture are shown in Figure 5.8.

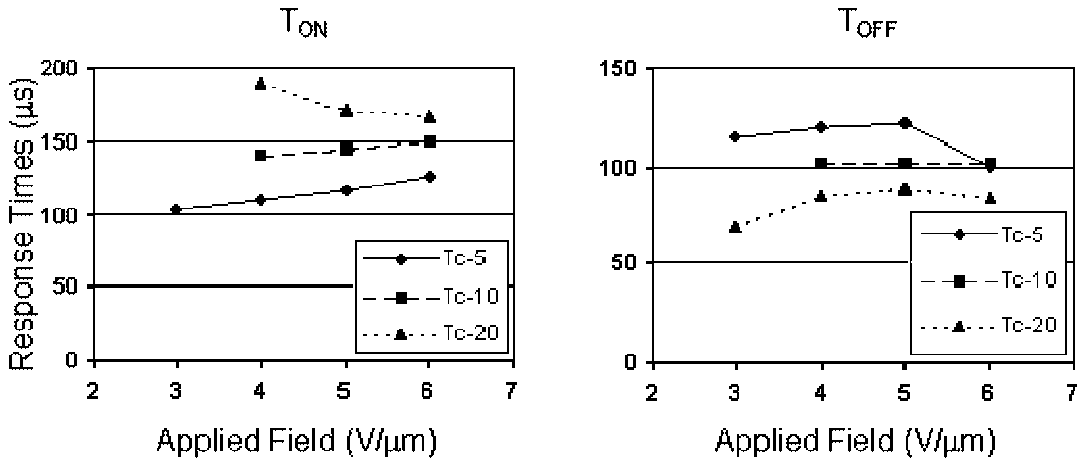

Figure 5.8: *The T_{ON}(10-90%) (left) and T_{OFF} (90-10%) (right) response times for the chiral FFO11OCB mixture in the cartwheel cell.*

The response times are below 200μs, which is faster than T_{ON} and similar to T_{OFF} of the polymerised 7OCB sample. This faster than expected response can be seen even at 20°C below the isotropic to chiral nematic transition point, where T_{OFF} times as fast as 70μs were observed. At T_C-10ºC, the response times are independent of the applied field strength. The overall temperature and field dependence of the response time is significantly smaller than for the polymerised 7OCB sample. The magnitude of the switch is only half that of the 7OCB sample. The added thickness of this cell in comparison to the 7OCB mixture cell means that the induced birefringence is just Δn = 0.016, approximately half that observed in the previous mixture.

The proportion of the induced birefringence which is derived from the flexoelectro-optic effect is again discernible from the response to variable frequency a.c. fields, as shown in Figure 5.9.

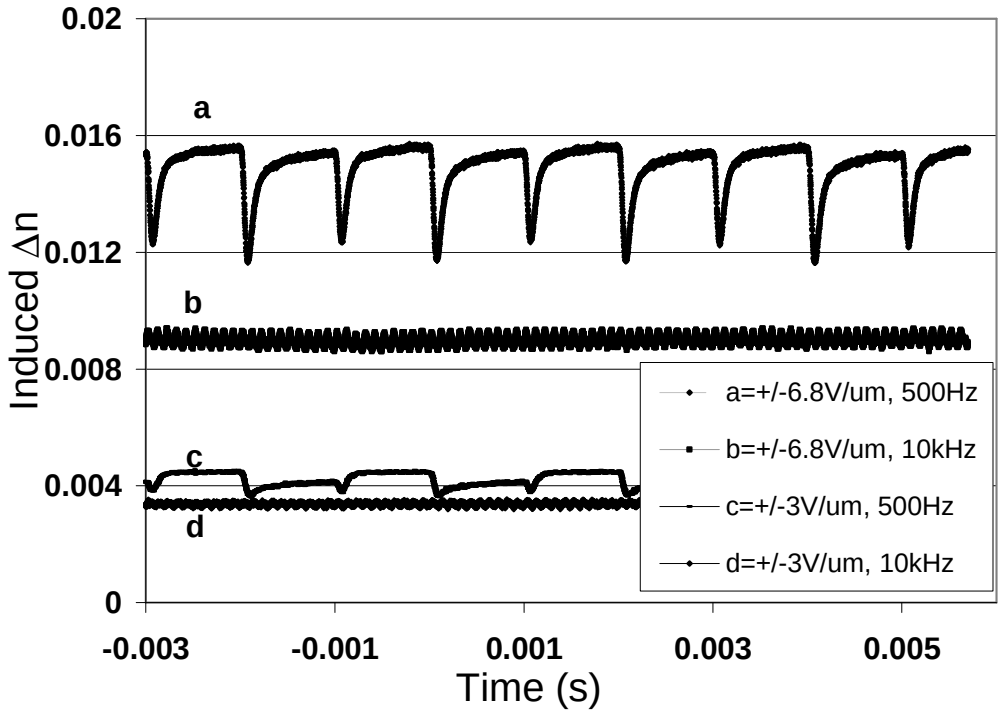

Figure 5.9: *The electro-optic response of the chiral FFO11OCB cell at T_C-10℃ to applied fields of 3 and 6.8 V/μm at 500Hz and 10kHz.*

The maximum and minimum values of the 500Hz traces are shown as a function of applied field strength in Figure 5.10.

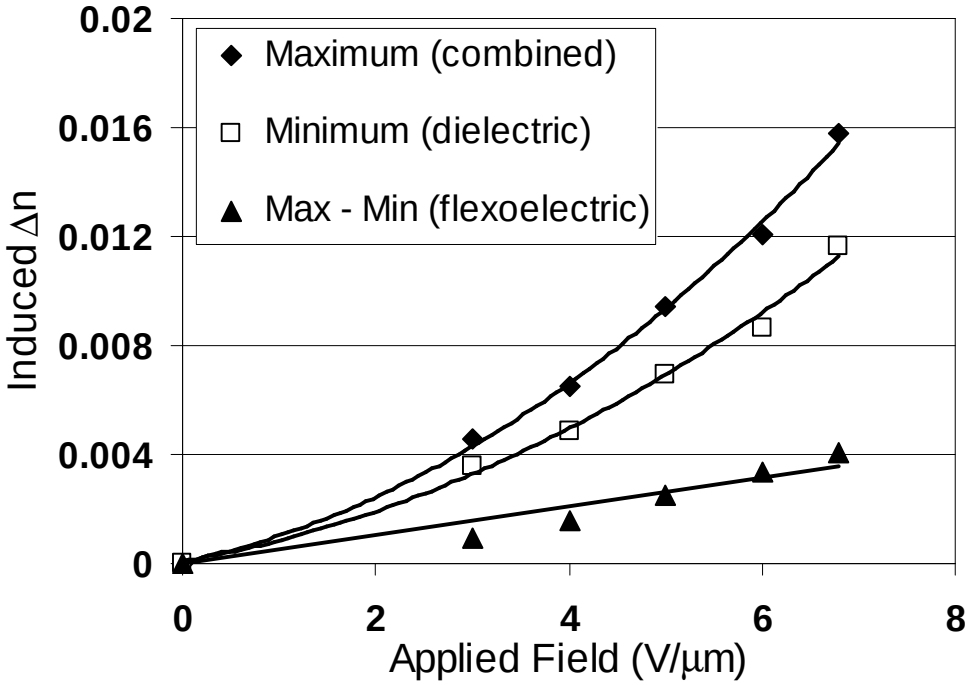

Figure 5.10: *The R.M.S field dependence of the maximum and minimum birefringence induced in the chiral FFO11OCB cell at 500Hz.*

Figures 5.9 and 5.10 show that the magnitude of the optical response is much reduced in the FFO11OCB mixture, in comparison to the 7OCB mixture. This is initially unexpected as, although the reduced dielectric anisotropy of the bimesogens produces the expected reduction in dielectrically induced birefringence, the larger flexoelectro-optic tilt angle of the FFO11OCB mixture as measured in the ULH texture should produce a larger flexoelectrically induced birefringence.

There are two possible explanations for this anomaly. As will be described in Chapter 6, increasing the proportion of polymer in the mixture beyond 3% (w/w) dramatically reduces the flexoelectro-optic tilt angle of the mixture. This mixture had an RM257 percentage of 5.84%, and although the tilt angles were measured in the ULH for these polymerised mixtures of 7OCB and FFO11OCB, the latter had the larger switch despite the high polymer content. It is possible however that the sample investigated here was not entirely evenly mixed and a higher than average polymer concentration entered the cell, restricting the tilt. The other possibility is that the flexoelectro-optic response is enhanced by the presence of the dielectric deformation in the sample. Some theoretical calculations carried out by A. Davidson at the University of Oxford on the chiral cartwheel cells

have suggested this might be a possibility.[14,15] This seems more likely, as investigation of further mixtures, which results in the overall plot shown in Figure 5.28, indicates that is the flexoelectric response of the 7OCB mixture which is unexpectedly large, rather than the response of this mixture which is excessively small.

7.4.2. FFO9/11OFF

Despite its reduced dielectric anisotropy, the non-symmetric bimesogen examined in the previous section still has a significant dielectric response. It is shown from previous work in the group that the dielectric anisotropy can be reduced further in bimesogenic materials without adversely affecting the flexoelectric characteristics by synthesising the material with symmetrical mesogenic units either side of the alkyl chain spacer.[12] The symmetric difluorinated bimesogens, synthesised by Andrew Blatch, were still available to compare their flexoelectro-optic properties with the non-symmetric bimesogen.

Since the spacer length has also been found to have an odd-even effect on these properties due to the degree of parallel alignment of the dipoles of each end unit dictated by the chain length,[16] the 9 and 11 spacer length homologues, α-(2',4-difluorobiphenyl-4'-yloxy)-ω-(2',4-difluorobiphenyl-4'-yloxy)nonane (FFO9OFF) and α-(2',4-difluorobiphenyl-4'-yloxy)-ω-(2',4-difluorobiphenyl-4'-yloxy)undecane (FFO11OFF), shown in Figure 5.11 were used in this work. These materials are largely monotropic (the 11 spacer material exhibits a nematic phase of a few degrees on heating) but mixtures of these materials have been found to exhibit wide nematic phases in a supercooled regime down to room temperature.[17]

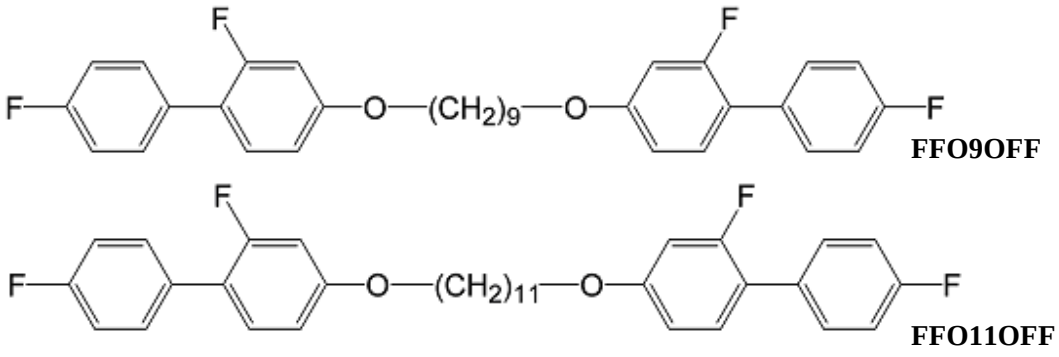

Figure 5.11: *The chemical structures of the symmetric difluorinated bimesogens FFO9OFF and FFO11OFF.*

The proportions of the mixture examined here were: 47.0% FFO9OFF, 47.26% FFO11OFF, 2.01% BDH1281, 3.26% RM257 and 0.47% Irgacure 819. As the concentrations of the 9 and 11 spacer homologue are approximately equal, this mixture will be referred to as FFO9/11OFF. This mixture cooled from the isotropic to the chiral nematic phase at 66°C in a cartwheel cell 11.5μm thick.

Tc	Δε	Δn
66˚C	0.9	≈0.16

Table 5-III: *Material parameters of the FFO9/11OFF mixture*

The electro-optic response to positive and negative millisecond duration pulses of 6.8V/μm field strength is shown in Figure 5.12. The positive and negative polarity pulse sections have been separated in this trace, in comparison to the previous two sets of results. This is simply for greater clarity in the relaxation portion of the traces to the two field polarities. The amplitude and response time measurements remain unaffected.

The magnitude of the switch is slightly smaller in this cell than the previous sample; however, the cell thickness is almost halved in this example. Therefore, the a material birefringence of this FFO9/11OFF mixture is $\Delta n = 0.023$, a significant improvement over FFO11OCB with $\Delta n = 0.016$

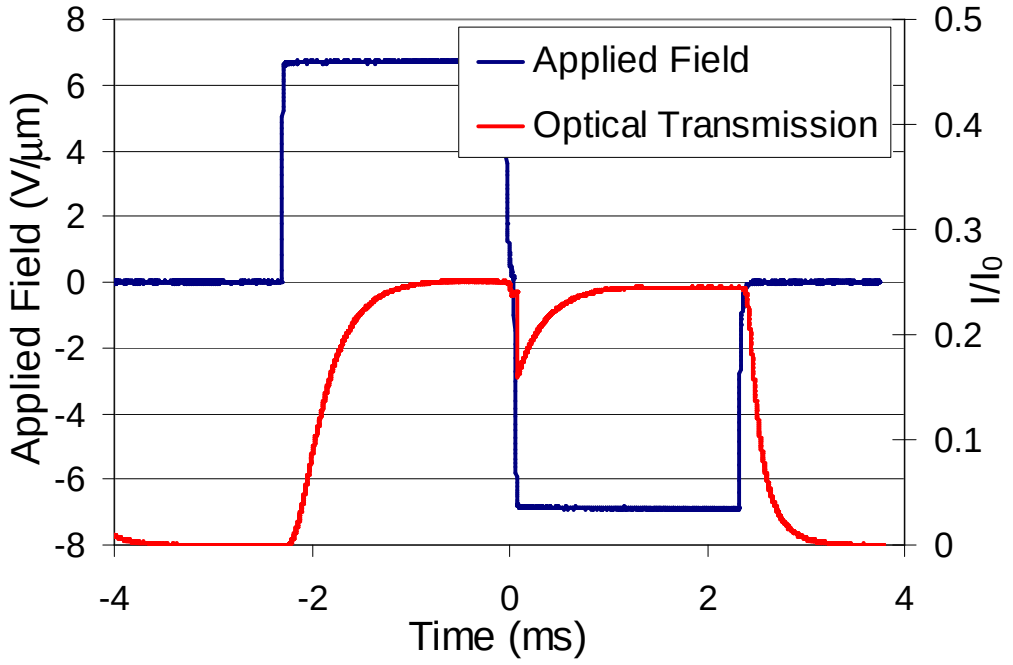

Figure 5.12: *The electro-optic response of the chiral FFO9/11OFF cell at T_C-10 ℃ to a +/-6.8 V/µm, 4ms duration bipolar square pulse.*

The response times for the switch in this mixture can be seen in Figure 5.13. Comparison of these times reveals the switch is considerably slower in this mixture than in the previous two, the low temperature response taking over 3ms to react fully to the applied field. This is likely to be a result of the fact that the flexoelectro-optic switch is larger in this material, and that the sample is a mixture of roughly equal parts of two bimesogens of differing alkyl chain length. This will disrupt the packing arrangement for the molecules and could adversely affect the viscosity.

The response being slower, however, appears to improve the inconclusive nature of the trends seen in the 7OCB and FFO11OCB mixtures. Genuine dependencies can now be seen, the response times getting significantly slower with lower temperature as would be expected from the increase in viscosity with cooling. Also, at all temperatures, the T_{ON} switching times decrease with increasing field strength, despite the angle of rotation of the optic axis being larger.

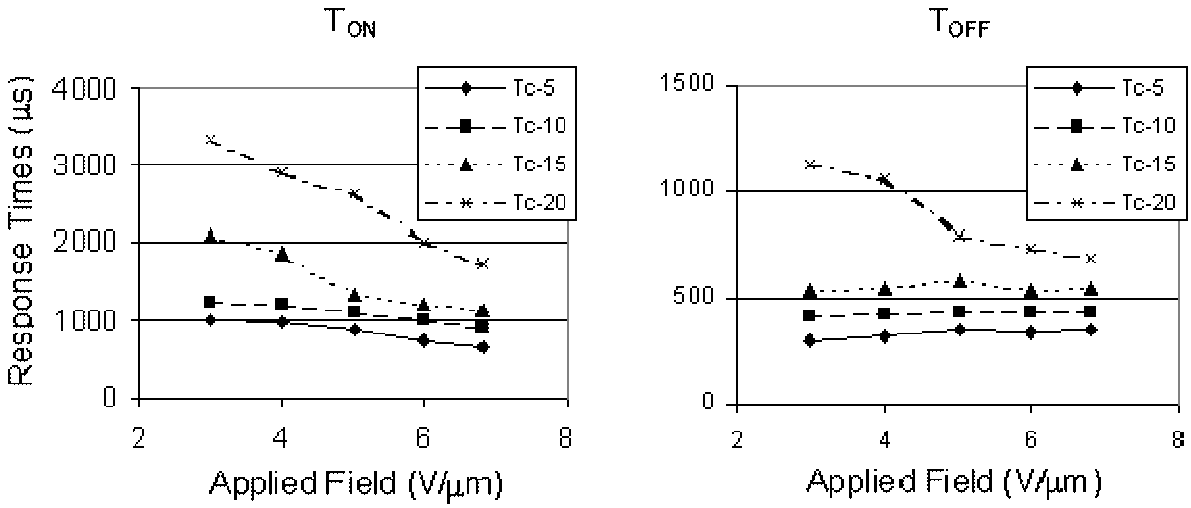

Figure 5.13: *The T_{ON}(10-90%) (left) and T_{OFF} (90-10%) (right) response times for the chiral FFO9/11OFF mixture in the cartwheel cell.*

The response of the sample to continuous a.c. waveforms of varying field strengths and frequencies is shown in Figure 5.14. As shown on the trace, the drive frequency for the low frequency trace in this plot has been be lowered from 500 to 250Hz, due to the slower nature of the response.

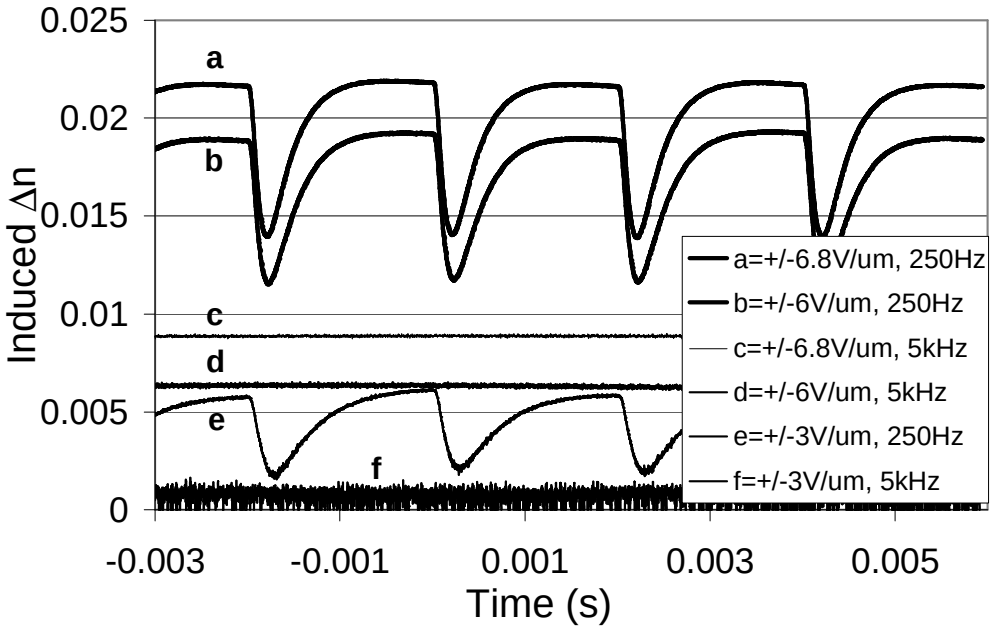

Figure 5.14: *The electro-optic response of the chiral FFO9/11OFF cell at T_C-10 ℃ to applied fields of 3 and 6.8 V/µm at 500Hz and 10kHz.*

The main feature of the traces shown above is the increase in the modulation amplitude of the low frequency traces, i.e. the flexoelectric contribution to the induced birefringence. The dielectric "baseline" for this sample is approximately equivalent to that of the previous sample, based on FFO11OCB, at $\Delta n \approx 0.01$. In this sample, however, the flexoelectro-optic effect doubles the birefringence during the periods of d.c. field. This equal contribution from dielectric and flexoelectric coupling to the applied field is a marked improvement on the last sample, the response of which was only roughly ¼ flexoelectric in origin.

This improved proportion is illustrated by the plot of the maximum and minimum induced birefringences for the low frequency response at various field amplitudes: Figure 5.15.

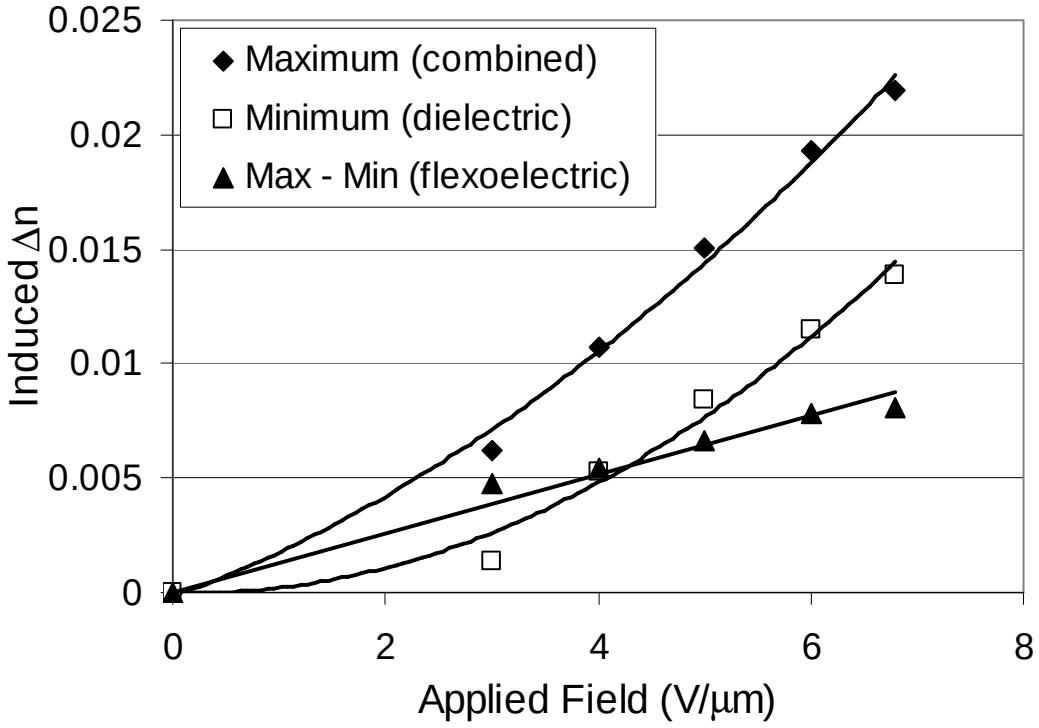

Figure 5.15: *The R.M.S field dependence of the maximum and minimum birefringence induced in the chiral FFO9/11OFF cell at 250Hz.*

The separation of the maximum and minimum lines in the above trace illustrates the increase in flexoelectro-optic response in this sample compared to the previous one, as shown in the Max – Min trace. In fact, this is the first sample in which the flexoelectric contribution to the birefringence is greater than the dielectric contribution at lower applied field strengths. It is only

for fields greater than 4 V/μm that the dielectric couplings dependency on the square of the applied field causes it to supersede the flexoelectro-optic response, which remains linear in the applied field.

The overall birefringence is still only slightly more than half that seen in the chiral 7OCB cell though, and that is despite a still considerable, though much reduced dielectric contribution. The challenge remained therefore, to develop a mixture which addressed this issue, and remove the dielectric contribution from the optical response, while still leaving a sufficiently significant overall response to enable a useful phase device.

7.4.3. FFE9/11EFF

Simultaneously to the progress of this work, it was found in another project in the group that the addition of an ester linkage to the symmetric bimesogenic materials improved the flexoelectro-optic performance significantly.[13,18] The ester linked difluorinated bimesogenic materials with alkyl chain lengths of 9 and 11 CH_2 groups were made available to the project. These materials, α-(2',4-difluorobiphenyl-4'-ester)-ω-(2',4-difluorobiphenyl-4'-ester)nonane (FFE9EFF) and α-(2',4-difluorobiphenyl-4'-ester)-ω-(2',4-difluorobiphenyl-4'-ester)undecane (FFE11EFF), exhibit only very small temperature width, monotropic nematic phases. When mixed together however, they gave a respectable 22°C wide nematic phase, and with further mixing with non-ester linked bimesogens this could be further extended and very dramatic flexoelectro-optic switching achieved.

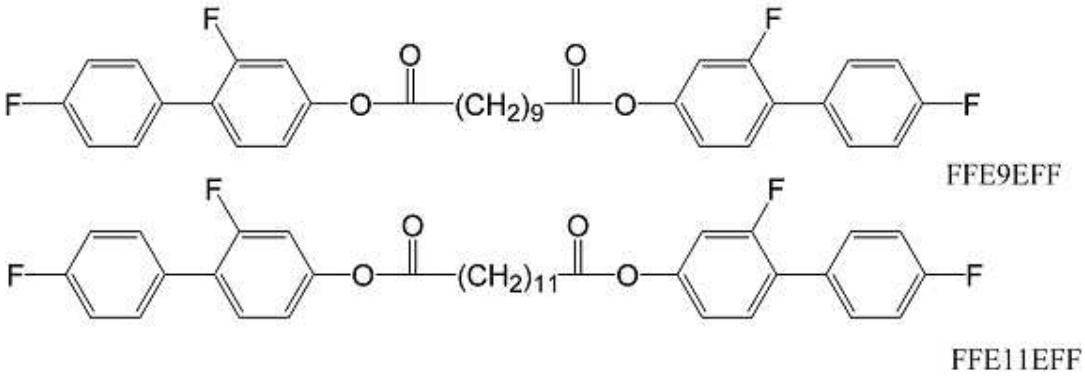

Figure 5.16: *The chemical structure of the ester linked bimesogens FFE9EFF and FFE11EFF.*

The exact mixture examined here was: 23.58% FFE9EFF, 23.7% FFE11EFF, 25.11% FFO9OFF, 21.5% FFO11OFF, 4.28% RM257 and 1.78% BDH1281. Due to the approximately equal proportions of all four bimesogens, this mixture was known as FFE9/11EFF-FFO9/11OFF.

Tc	Δε	Δn
64˚C	<0.9	≈0.16

Table 5-IV: *Material parameters of the FFE9/11EFF mixture*

This mixture was polymerised in situ, in a cartwheel cell measuring 12.55μm, and was found to cool into the chiral nematic phase at T_C = 64°C. The electro-optic response of the cell to 3 and 6.8 V/μm field strength waveforms at 100Hz is shown in Figure 5.17. The high frequency applied field responses for this cell are not shown in the figure as they produced a negligible birefringence. This indicates that the dielectric coupling response has been eliminated in this sample, one of the principle aims of the development of this effect with bimesogenic materials.

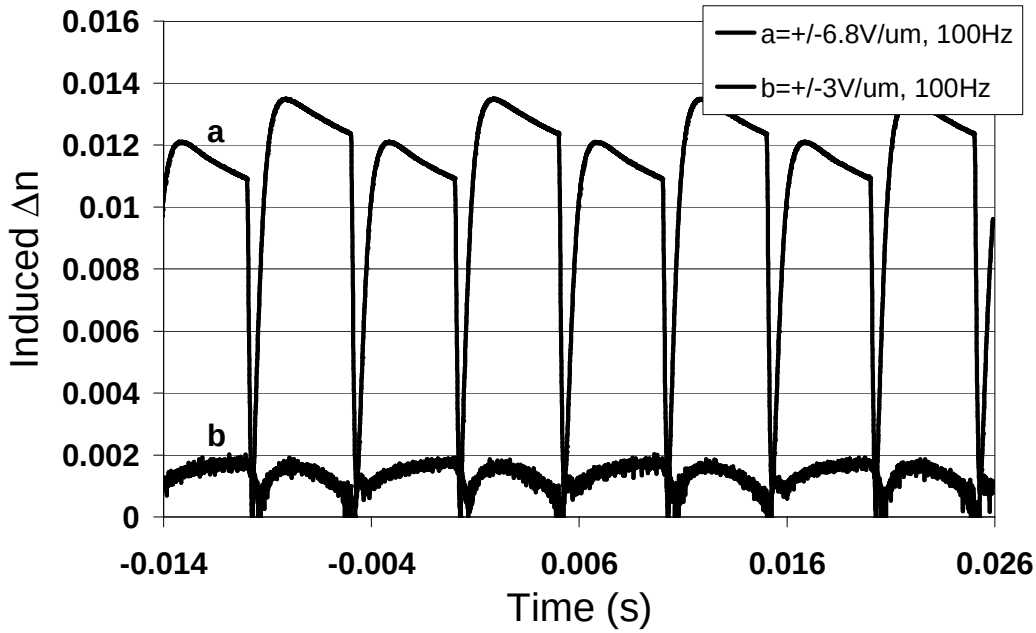

Figure 5.17: *The electro-optic response of the cell at T_C-10 ℃ to applied fields of 3 and 6.8 V/μm at 100Hz.*

The flexoelectric portion of the response, which remains, is also of significant magnitude. The overall response is not as large as has been measured in the previous mixtures, but as this response is flexoelectric in origin in its entirety, the measured maximum induced birefringence of Δn =

0.0121 is the largest response yet measured when compared to the previous traces with their dielectric contributions removed.

The difference in nature in the response of this sample and the previously examined samples is shown in the plot of the maximum and minimum induced birefringence values for the 100Hz applied waveforms at a range of field strength. This is shown in Figure 5.18.

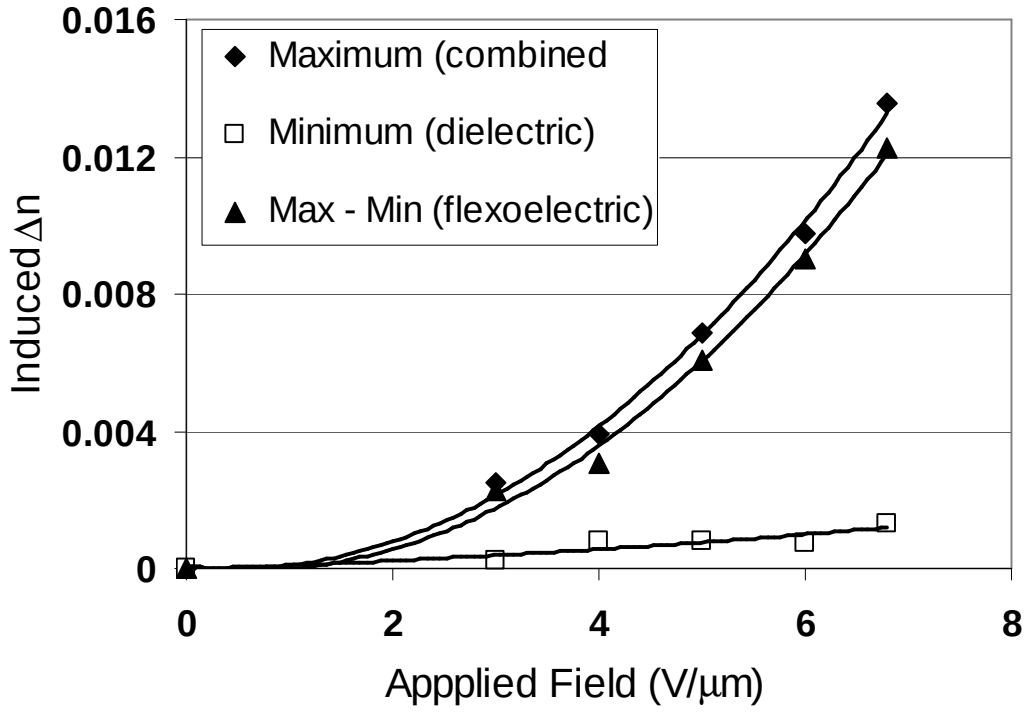

Figure 5.18: *The R.M.S field dependence of the maximum and minimum birefringence induced in the cell at 100Hz.*

The increase in separation between the maximum and minimum induced Δn traces shown in the last sample has now been maximised with the contribution from dielectric coupling to the birefringence reduced to practically zero. The flexoelectric contribution now makes up almost all of the total optical response.

The response times for this material continue the trend towards slower responses in the materials composed of more mesogenic compounds with a larger flexoelectrically induced birefringence. The response times are shown in Figure 5.19.

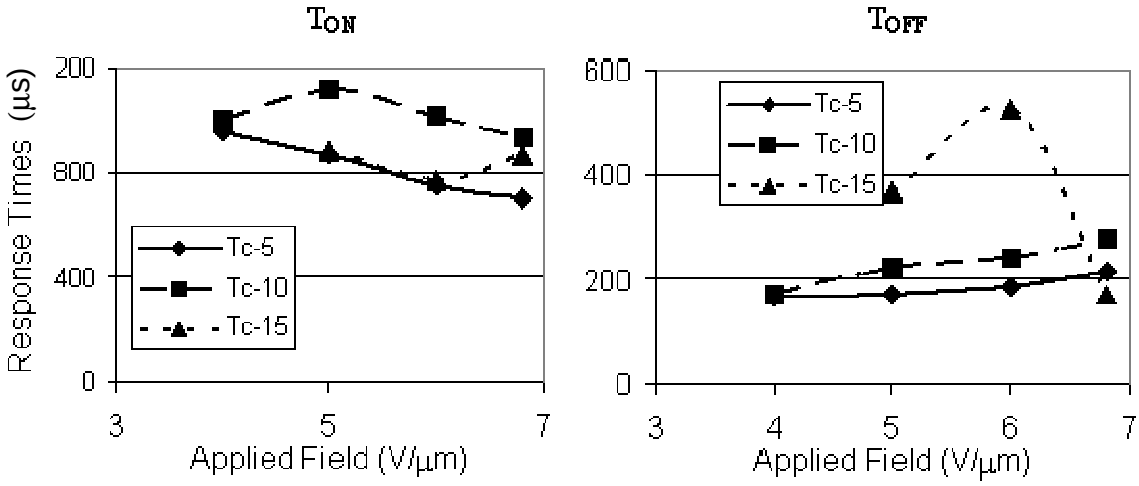

Figure 5.19: *The T_{ON}(10-90%) (left) and T_{OFF} (90-10%) (right) response times for the chiral FFE9/11EFF-FFO9/11OFF mixture in the cartwheel cell.*

Although the response times shown above do not form trends as identifiable as the previous sample, and the T_{OFF} times appear to be shorter then expected due to the slight residual birefringence at zero field, as in the FFO11OCB sample, the response can be seen to be faster than the previous sample. This indicates that the development towards a flexoelectric only response will provide a faster switching mechanism. The single mesogenic compound mixtures are still faster switching however, so in a working device, the priority judgement may have to be made between the fastest possible response and the elimination of dielectric effects.

For the purposes of characterisation of the switching effect, however, this material development has served to demonstrate the possibility of a significant response based solely on the flexoelectro-optic effect. It has also been shown that the bimesogenic materials now available provide a means of controlling the relative contributions from the two coupling mechanisms for tailoring to an intended device specification.

7.5. **ULH TILT ANGLES**

Having observed the electro-optic response of the series of mixtures outlined above in the Grandjean texture at 1550nm, it was important to analyse the purely flexoelectro-optic responses

of the mixtures in order to confirm that is it indeed the differing flexoelectric properties of the mixtures that account for the differing natures of the electro-optic responses seen.

When the flexoelectro-optic switch is observed in the uniform lying helix (ULH) texture in cells with transparent electrodes on the cell surfaces, direct measurement of the flexoelectro-optic tilt angles and response times are possible. Although dielectric helix unwinding may be present it does not effect the position of the optic axis of the material in the plane of the cell, so does not affect the measurements taken. For this reason, all the materials analysed in the previous section were tested for their flexoelectro-optic properties in this texture. This was performed according to the method described in Section 3.4.1. The results for these measurements on each of the above mixtures is outlined in the following sections.

7.5.1. 7OCB

The chiral 7OCB sample was placed into a "Lucid" cell measuring 5.01µm in thickness. The ULH texture was obtained by cooling from the isotropic phase into the N* under a 3V/µm R.M.S., 80Hz frequency applied field[19]. Once confirmed under the microscope, this texture was stabilised by UV exposure of the reactive mesogen containing mixture. The flexoelectro-optic tilt angles and response times were then measured at a range of applied field strengths.

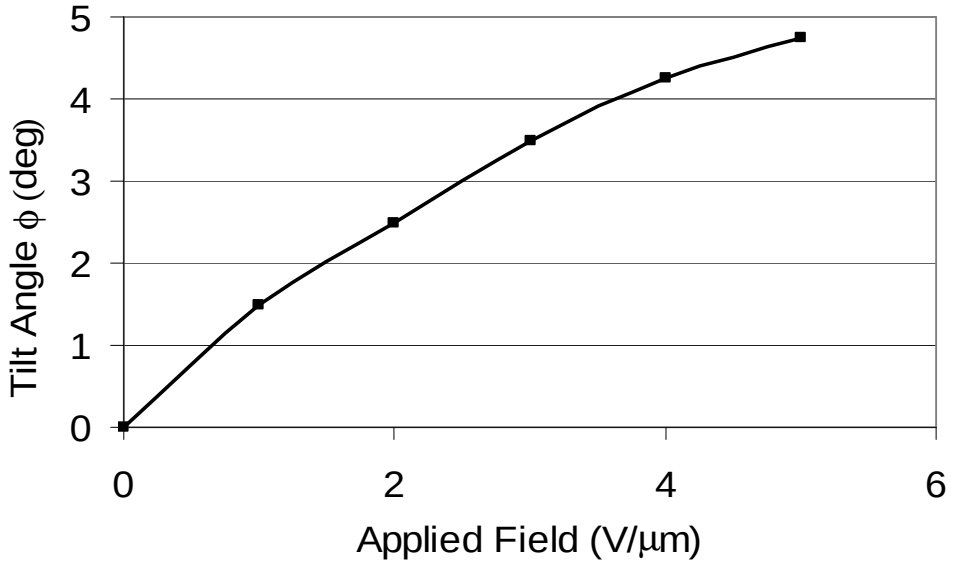

Figure 5.20: *The flexoelectro-optic tilt angle ϕ of the polymerised chiral 7OCB sample as a function of applied field strength, at T_C-10ºC.*

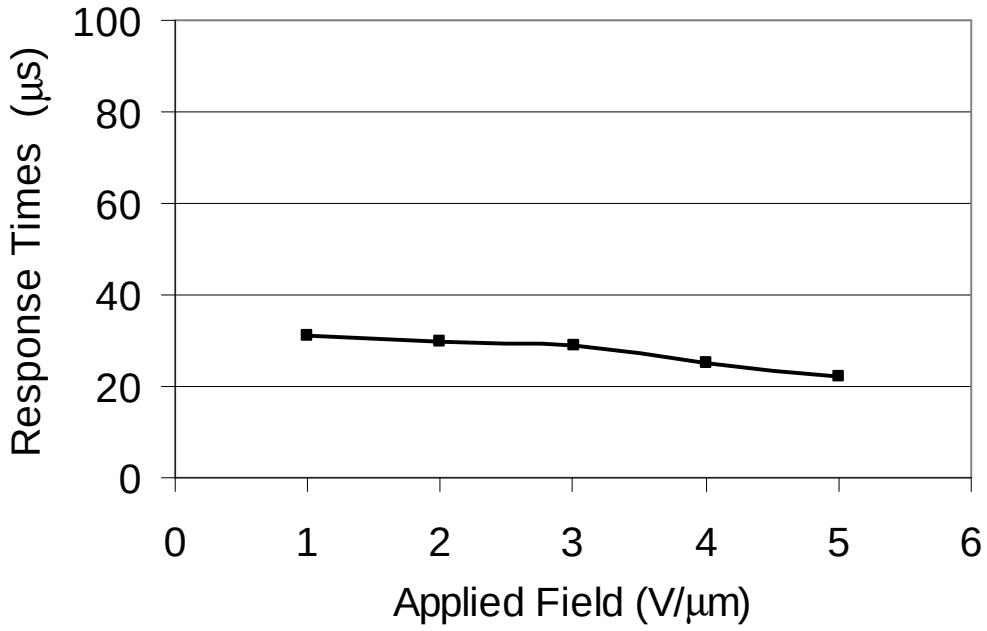

Figure 5.21: *The average of the 10-90% and 90-10% response times of the polymerised chiral 7OCB sample as a function of applied fields, at T_C-10ºC.*

The chiral 7OCB sample has a very limited tilt angle, less than 5 degrees, mainly due to the material's large dielectric anisotropy causing helix unwinding effects above an applied field of just 5 V/µm. The response can be seen to be very fast, however. This is characteristic of the flexoelectro-optic effect, but these times are particularly short (less than 100 µs) as a result of the very limited magnitude of the switch.

7.5.2. FFO11OCB

The chiral FFO11OCB sample was induced into the ULH texture in a "Lucid" cell measuring 4.98µm in thickness as before. The flexoelectro-optic response of the sample was characterised at a range of temperatures, and the relevant results are displayed below.

In the tilt angle plots (Figure 5.22), the lower temperature trace is extended to higher field values as the ULH texture becomes more resistant to higher fields at lower temperatures. The response times are only measured for applied fields up to those which induce an optical axis rotation of up to of up to 22.5º, for the reasons discussed in Chapter 3.4.1.

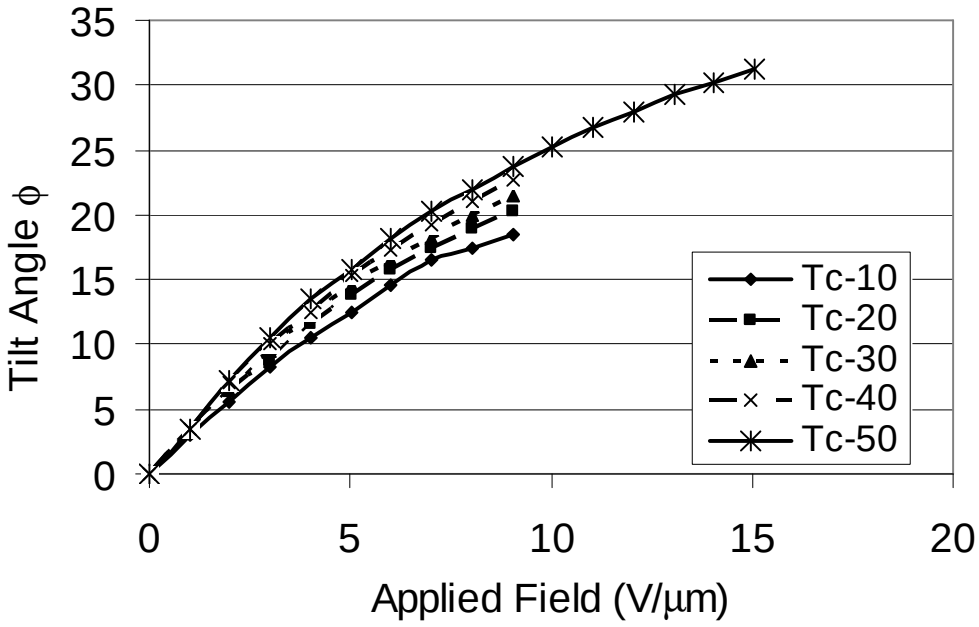

Figure 5.22: *The flexoelectro-optic tilt angle ϕ of the polymerised chiral FFO11OCB sample as a function of applied field strength, at a range of temperatures below T_C.*

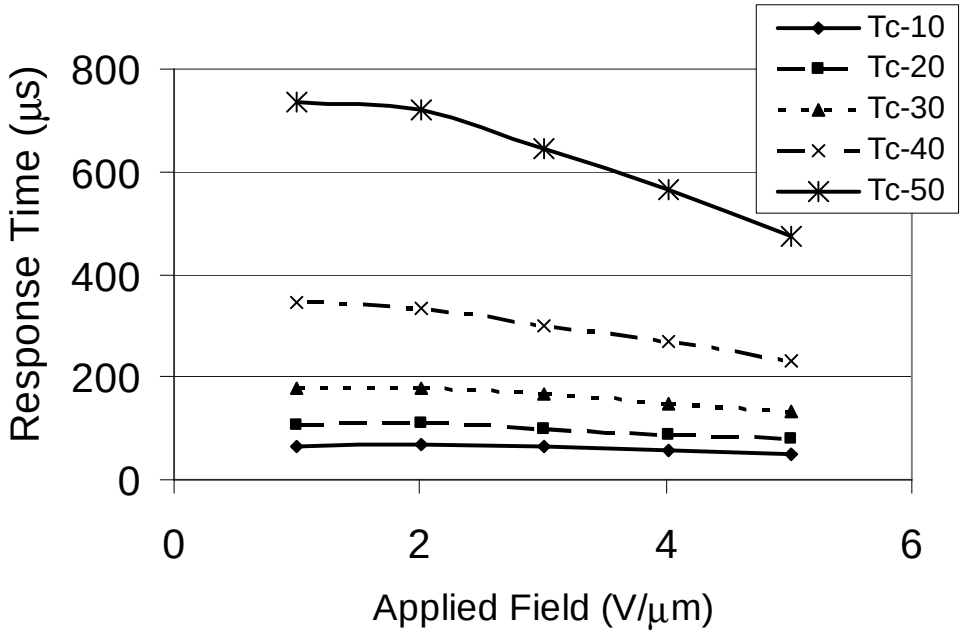

Figure 5.23: *The average of the 10-90% and 90-10% response times of the polymerised chiral FFO11OCB sample as a function of applied field, at a range of temperatures below T_C.*

These results show the dramatic increase in tilt angle achievable with the bimesogenic materials in comparison to 7OCB. This also demonstrates the limitations imposed by the amplifier used to

apply the field to the Grandjean textured samples in the cartwheel cells. As the electrode separation in these cells is 50µm, the maximum available field is 6.8V/µm, whereas this material will reliably tilt at fields of up to 10V/µm at lower temperatures. A superior amplifier would therefore allow larger tilts to be induced in the cartwheel cells with these materials, and therefore larger induced birefringences.

7.5.3. FFO9/11OFF

The chiral FFO9/11OCB sample was induced into the ULH texture in a "Lucid" cell measuring 4.91µm in thickness as before. The flexoelectro-optic response of the sample was characterised at a range of temperatures, and the results are displayed below.

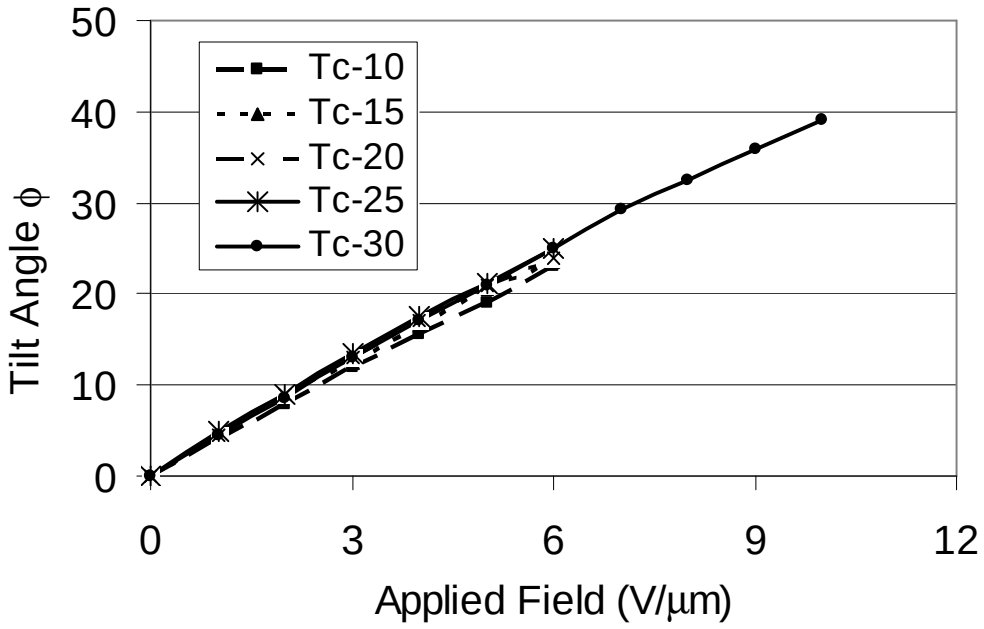

Figure 5.24: *The flexoelectro-optic tilt angle ϕ of the polymerised chiral FFO9/11OFF sample as a function of applied field strength, at a range of temperatures below T_C.*

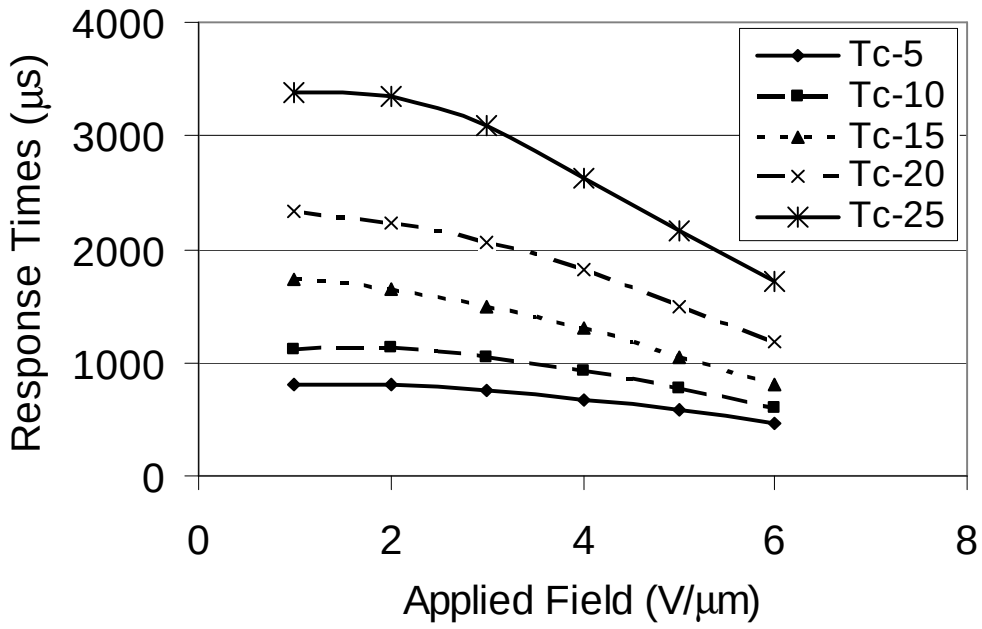

Figure 5.25: *The average of the 10-90% and 90-10% response times of the polymerised chiral FFO9/11OFF sample as a function of applied field strength, at a range of temperatures below* T_C.

As expected from their electro-optics in the cartwheel cell, this material shows a greater tilt angle for the same applied field than the previous sample, but with a slower response.

7.5.4. FFE9/11EFF

The flexoelectro-optic characteristics of the chiral FFE9/11EFF-FFO9/11OFF sample once polymerised in the stabilised ULH texture are shown below in Figure 5.26 and Figure 5.27.

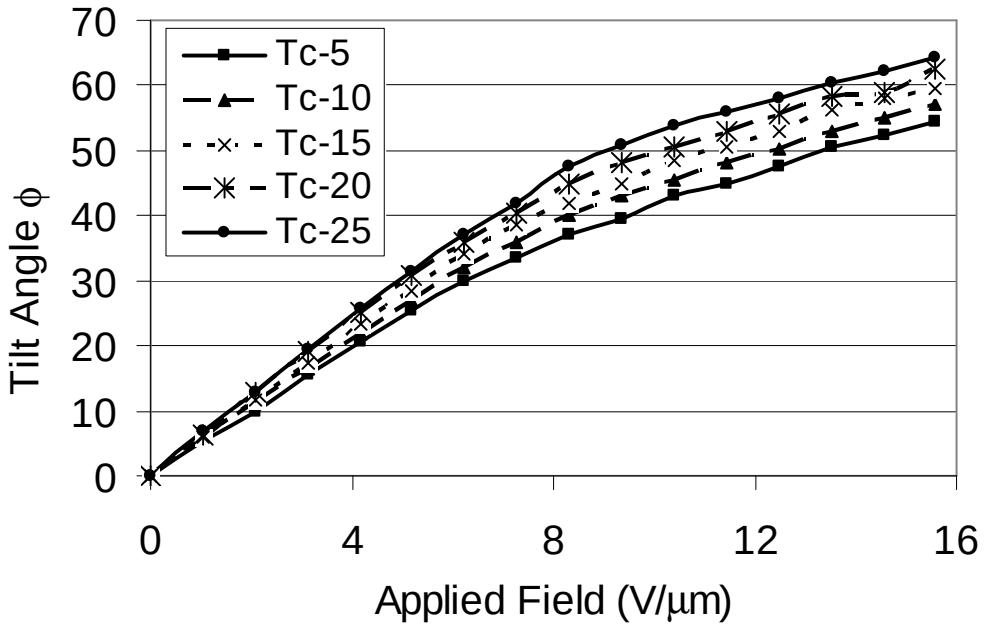

Figure 5.26: *The flexoelectro-optic tilt angle ϕ of the polymerised chiral FFE9/11EFF-FFO9/11OFF sample as a function of applied field strength, at a range of temperature below T_C.*

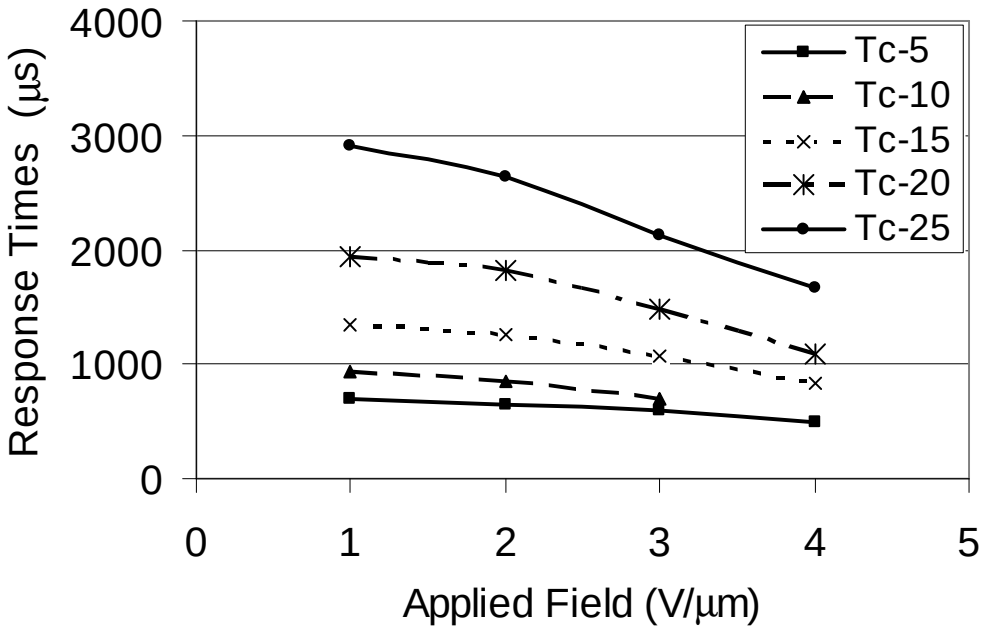

Figure 5.27: *The average of the 10-90% and 90-10% response times of the polymerised chiral FFE9/11EFF-FFO9/11OFF sample as a function of applied field strength, at a range of temperatures below T_C.*

This mixture can be seen to exhibit extremely large tilt angles, up to 65º, and its resistance to dielectric helix unwinding allows relatively large fields of up to 15.5 V/µm to be applied to the sample. The maximum tilt of approximately ϕ = 65º is one of the largest tilt angle materials recorded to date.[13,18] This corroborates very well the observed strong flexoelectric behaviour and very weak dielectric coupling observed in this material in the Grandjean texture. The response times are relatively slow for a flexoelectro-optic device however, as was also observed in the Grandjean texture, and this probably a result of the mixture having four separate nematic constituents increasing the viscosity, and the large deformation being induced taking more time to manifest itself.

In fact, if the flexoelectric portion of the induced birefringence of each of the samples in the Grandjean texture (taken as the difference between the maximum and minimum values of the induced Δn by the low frequency, maximum amplitude applied field) is plotted against the flexoelectro-optic tilt angle ϕ at 6V/µm of the same sample, an excellent correlation is observed for the bimesogenic samples. Increasing the tilt angle of a sample appears to increase the flexoelectrically induced birefringence proportionately. The 7OCB sample does not fit the trend, however, exhibiting a large flexoelectric response in the Grandjean texture, despite having a very small tilt angle. It is thought that this is probably due to an effect whereby the flexoelectro-optic deformation of the helix has an exaggerated effect on the induced Δn in the presence of the dielectric deformation, as discussed in Section 7.4.1.

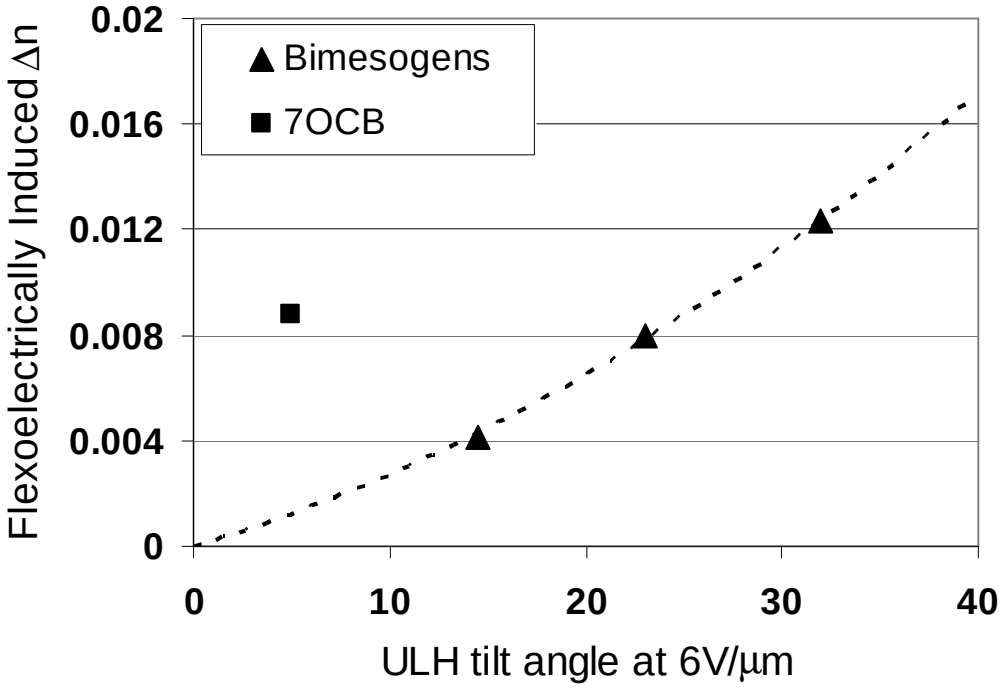

Figure 5.28: *The flexoelectrically induced birefringence of the samples at 1550nm in the Grandjean texture as a function of their flexoelectro-optic tilt angle in the ULH texture, all at T_C-10ºC.*

The slightly anomalous 7OCB result aside however, the correlation shown in the above graph confirms that the same flexoelectro-optic deformation of the director helix is responsible for both the field-following response of the samples in the Grandjean texture and the optic axis rotation in the ULH. The trend shown in the figure can be seen to tend to zero induced birefringence for tilt angles of approximately 5 degrees or less. This can be thought of as a "threshold" tilt angle for an observable effect. The ellipsoid nature of the refractive indicatrix of the nematic medium means that a minimum rotation of the director has to occur before the refractive index in the direction of light polarisation is significantly changed.

7.6. **CONCLUSIONS**

In conclusion, the addition of a small percentage (3-5%) of reactive mesogen to the chiral nematic mixtures used to observe the flexoelectro-optic effect in Grandjean textured liquid crystals proved

extremely successful in eliminating the flow and consequent texture degradation observed in non-polymer samples subject to continuous a.c. applied fields in Chapter 4.

The ability of the samples to withstand continuous fields of high amplitude and varying frequency provided a method of distinguishing the contributions from dielectric and flexoelectric coupling in the induced birefringence via variation of the frequency of the applied square wave a.c. field.

This field-frequency dependent response was observed in a succession of samples, starting with chiral mixtures based on the basic monomesogen 7OCB and developing into multi-component bimesogenic mixtures in order to maximise the contribution from the flexoelectro-optic effect and minimise dielectric coupling. This was achieved with the final sample examined, a mixture of equal parts of the bimesogenic compounds FFO9OFF, FFO11OFF, FFE9EFF and FFE11EFF, with small percentages chiral dopant and reactive mesogen added. This material exhibited an induced birefringence at 1550nm of $\Delta n = 0.012$ at 6.8V/µm, originating solely from flexoelectric coupling. The birefringence resulting from flexoelectric coupling in the bimesogenic samples was shown to have a proportional dependence on the flexoelectro-optic tilt angle of each mixture, as measured in the uniform lying helix texture, providing confirmation of the common origin of these two effects.

The largest induced birefringence, resulting from both dielectric and flexoelectric coupling, was observed in the chiral 7OCB sample, which produced $\Delta n = 0.037$. This is sufficient to generate a switchable half waveplate in a 21µm thick cell. The response times for all the mixtures were sub-millisecond at the higher end of their respective chiral nematic temperature ranges. This effect therefore shows considerable promise for a fast response, continuously variable phase retarder for operation at telecommunications wavelengths.[20]

7.7. **REFERENCES**

[1]G. P. Crawford and S. Zumer, *Liquid Crystals in Complex Geometries*, Taylor and Francis Ltd., (1996).

[2]J. W. Doane, N. A. Vaz, B. G. Wu and S. Zumer, *Applied Physics Letters*, **48**, (4), 269-71, (1986).

[3]D. K. Yang, L. C. Chien and J. W. Doane, *Applied Physics Letters*, **60**, (25), 3102-4, (1992).

[4]D. J. Broer, R. G. Gossink and R. A. M. Hikmet, *Angewandte Makromolekulare Chemie*, **183**, 45-66, (1990).

[5]R. A. M. Hikmet, *Liquid Crystals*, **9**, (3), 405-16, (1991).

[6]Merck-NB-C, Chilworth Science Park, Southampton, SO16 7NP,

[7]H. Kikuchi, M. Yokota, Y. Hisakado, H. Yang and T. Kajiyama, *Nature Materials*, **1**, (1), 64-8, (2002).

[8]H. J. Coles, B. Musgrave, M. J. Coles and J. Willmott, *Journal of Materials Chemistry*, **11**, (11), 2709, (2001).

[9]J. S. Patel and S. D. Lee, *J. Appl. Phys.*, **66**, (4), 1879-81, (1989).

[10]B. J. Broughton, M. J. Clarke, R. A. Betts, T. Bricheno and H. J. Coles, *Proceedings of the Society of Photo-Optical Instrumentation Engineers (Spie)*, **5741**, 190-6, (2005).

[11]H. J. Coles, M. J. Coles, S. P. Perkins, B. M. Musgrave and D. Coates, Patent: *GB2356629.*, (2001).

[12]B. Musgrave, M. J. Coles, S. P. Perkins and H. J. Coles, *Molecular Crystals and Liquid Crystals*, **366**, 2587-94, (2001).

[13]H. J. Coles, M. J. Clarke, S. M. Morris, B. J. Broughton and A. E. Blatch, *Journal of Applied Physics*, **99**, 034104 (2006).

[14]A. J. Davidson, *Private Communication*, (2005).

[15]A. J. Davidson, S. J. Elston and E. P. Raynes, *Journal of Physics D-Applied Physics*, **38**, (9), 1470-7, (2005).

[16]S. M. Morris, Phd Thesis, University of Cambridge, (2005).

[17]A. E. Blatch, M. J. Coles, B. Musgrave and H. J. Coles, *Molecular Crystals and Liquid Crystals*, **401**, 161-9, (2003).

[18]M. J. Clarke, PhD Thesis, University of Southampton, (2004).

[19]S. D. Lee and J. S. Patel, *Phys. Rev. A*, **42**, (2), 997-1000, (1990).

[20]B. J. Broughton, M. J. Clarke, A. E. Blatch and H. J. Coles, *J. Appl. Phys.*, **98**, 034109, (2005).

Chapter Six

The Effect of Polymer Concentration on Flexoelectro-optic Switching in the Stabilised ULH Texture

7.8. INTRODUCTION

In Chapter 5, the addition of a polymer network to the Grandjean textured chiral nematic material was found to be of great benefit for the stability of the device. The polymer stabilization by the addition, and curing in-situ, of a small amount of UV reactive mesogen, was found to significantly increase the texture ruggedness and ability to withstand the continuous application of a.c. square waveforms of high voltage amplitude. It also allowed heating of the material into the isotropic phase and subsequent cooling back into the chiral nematic with reliable reproduction of the desired Grandjean texture. Having demonstrated these benefits, it was important to gauge the effect of such a polymer network on the flexoelectro-optic behaviour of the chiral nematic materials investigated.

The uniform lying helix (ULH) liquid crystal texture is not straightforward to obtain and tends to degrade to the lower energy Grandjean (standing helix) configuration over time. For this reason, stabilization of the texture has been previously investigated elsewhere. The ULH texture has been made stable over time by the use of periodic surface alignment patterning,[1] but the only method so far found to stabilize the ULH texture to thermal cycling out of the chiral nematic (N*) phase, and the effects of dielectric unwinding of the director helix by applied electric fields, has been the introduction of a polymer network in the texture by UV curing approximately 10% of dissolved photoreactive monomer whilst in the ULH texture.[2]

Due to these concerns over the restrictive effect such volume stabilization may have on the already small angle switching capabilities of the materials reported in the literature,[2] methods of selectively polymerizing only the surface regions of the device, thereby providing sufficient stabilization but leaving the bulk free to switch have been developed.[3] These have also been shown to reduce the residual birefringence introduced by the anisotropic polymer network through the bulk of the material.

Although the texture has been successfully stabilized previously, and been shown to undergo flexoelectro-optic switching despite the presence of the polymer, no quantative study on the degree of restriction of the optic axis tilt angle induced by a given field caused by the polymer, or the effect of polymer concentration, has been carried out. The availability to this study of both reactive mesogens (RM257, Merck NB-C) which can provide polymer stabilization at relatively small

concentrations in the liquid crystal (≈ 3%), and bimesogenic liquid crystal compounds which exhibit extremely high flexoelectro-optic tilt angles,[4,5] provided an opportunity to examine the flexoelectro-optic switch and the impact the polymer has upon it in high resolution, and that is the purpose of this chapter.

7.9. POLYMER CONCENTRATION EFFECTS

A mixture was prepared of the following bimesogenic liquid crystals, in equal quantities: FFO9OFF, FFO11OFF, FFE9EFF, FFE11EFF. These materials were developed in-house specifically for their large flexoelectro-optic response and small dielectric constants ($\Delta\varepsilon\approx 0$),[6] and this specific mixture was shown, in chapter 5, to exhibit an extremely large tilt angle (>60º) in the unpolymerized sample.

To this was added 1.85% (w/w) BDH1281 high twisting power chiral dopant (Merck NB-C). This mixture was kept in the isotropic phase (I) overnight to allow complete mixing, at which point it was divided into four parts. The reactive mesogen RM257 (Merck NB-C) was added to three of these in the required quantities to provide a range of mixtures of the chiral nematic material with the following concentrations: 0%, 3.12%, 6.18% and 10.09% (weight/weight). Each of the three reactive mesogen containing mixtures was then supplied with approximately 1% weight of Irgacure 819 photoinitiator (Merck NB-C) before again allowing overnight mixing to ensure homogeneity.

The completed mixtures were then capillary filled into test cells of ITO coated glass with a 5µm cell gap and rubbed polyimide surface treatment ("Lucid cells") to provide planar alignment of the local nematic director. The ULH texture was obtained in these cells by cooling the mixtures from the isotropic into the chiral nematic phase under the influence of an applied electric field, and applying pressure to the cell to shear the mixture.

Once obtained, the ULH was stabilized by exposing the cell to a UV light source (Macam flexicure) at 5ºC below the isotropic-nematic transition point (T_C-5), cross-linking the reactive mesogen and creating a polymer network through the bulk of the cell. In the 0% reactive mesogen mixture, the a.c. field applied to the cell could be varied in amplitude for the electro-optic measurements, but had to remain present at all times to prevent relaxation into the Grandjean

texture. In the 10% reactive mesogen mixture, phase separation occurred between the nematic mixture and the monomer and no ULH texture could be obtained. In the remaining three cells, the flexoelectro-optic tilt angles and response times were measured for the mixtures, at a range of temperatures below $T_{I\rightarrow N^*}$, according to the method outlined in Chapter 3.

7.9.1. Tilt Angles and Response Times

The I→N* temperature transition point (T_C) was measured and found to be 61ºC for all mixtures, with no hysterisis on re-heating. Both the 3% and 6% reactive mesogen mixes were found to return spontaneously to the ULH texture on entry to the N* from either the isotropic or crystalline phases. The undoped mixture had to undergo the alignment procedure outlined above each time the mixture was heated into the isotropic phase. Figure 2.1 shows the ULH textures of the three mixtures without applied field. This is evidence of the stabilization of the texture as found previously using 10% (w/w) of UV curing monomer BAB.[1] The level of ruggedness of texture achieved can also be tested by applying a strong enough electric field to completely unwind the director helix and cause an N* to homeotropic nematic transition in the material, before removing the field again and observing the texture. This was not possible in these samples due to the very low dielectric anisotropy of the bimesogens preventing complete helix unwinding. The textures were also observed in the isotropic phase (right column in Figure 2.1), with both the 0% and 3% mixtures exhibiting a uniform black state between crossed polarizers, but the 6% mixture having a residual birefringence due to the greater mesogenic polymer density.

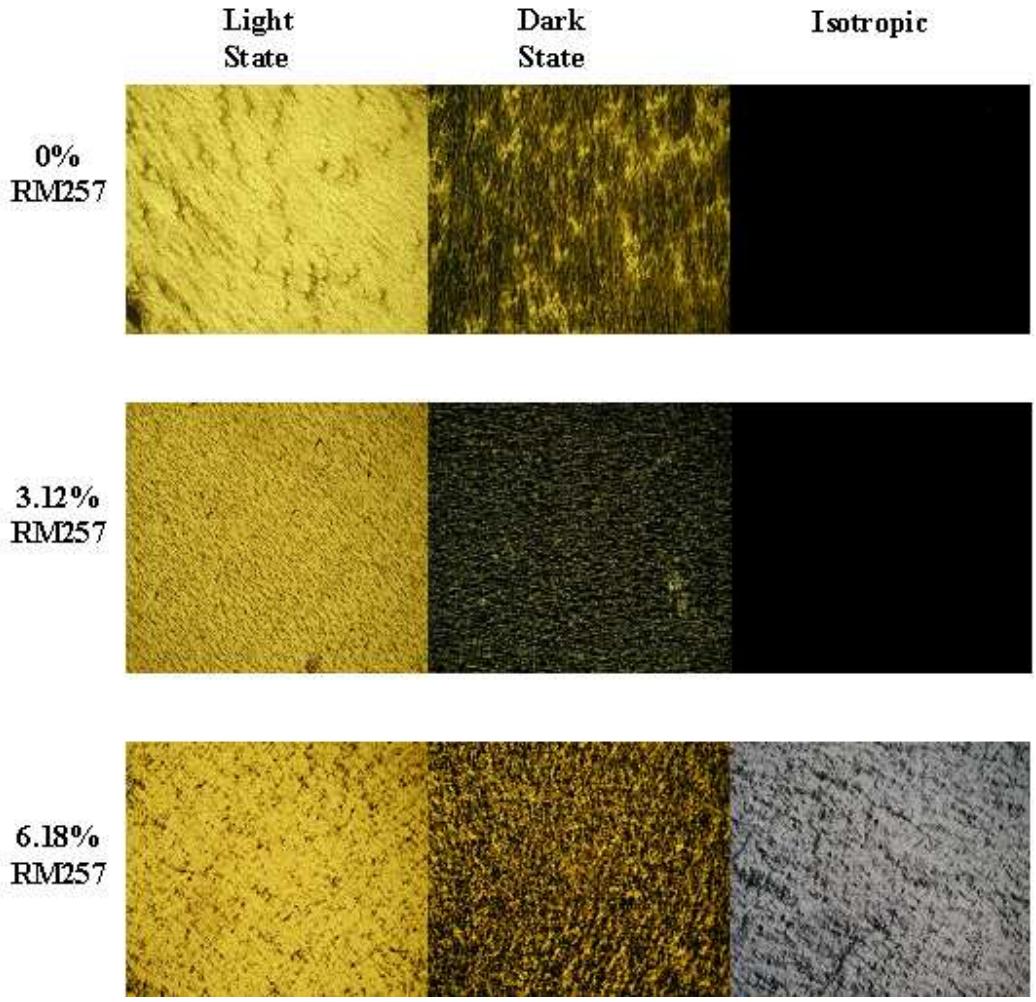

Figure 2.1: *Polarising microscopy images of the ULH textures obtained in the 0%, 3% and 6% RM257 mixtures at 50ºC and zero applied field, with the helical axis aligned parallel to the polariser transmission axis (dark state), at 45º (light state) and with the material heated to 70ºC to show any residual birefringence in the isotropic. Each image was observed using a 10X objective on the microscope, so corresponds to approximately 1mm^2 of sample area.*

Having obtained and stabilized the required textures, the flexoelectro-optic tilt angles were measured for the three mixtures at a range of temperatures from T_C to slightly above room temperature and found to exhibit the usual electric field and temperature dependence.[5,6] The measured tilt angles for each mixture at T_C-20ºC are plotted in Figure 2.2. The response times for the $+\phi$ to $-\phi$ switch were also measured for the same temperatures, and their field dependence at T_c-20ºC is shown in Figure 2.3. The maximum field strength was restricted to 4 V/μm to keep the induced tilt angles below 45˚.

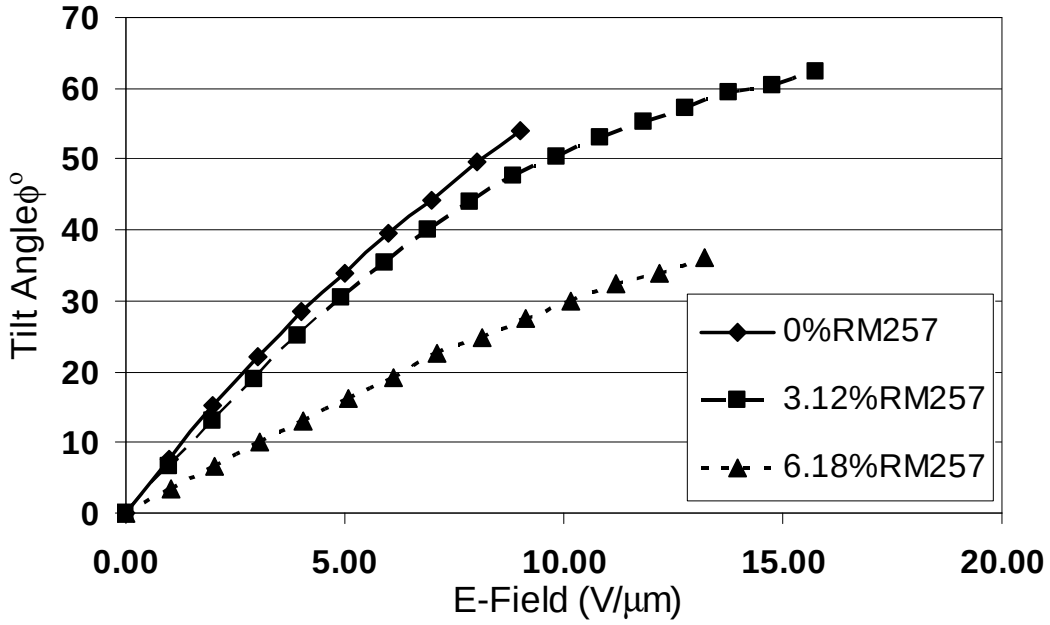

Figure 2.2: *The flexoelectro-optic tilt angles measured for the 0%, 3% and 6% RM257 mixtures as a function of the r.m.s. applied field value, at T_c-20ºC.*

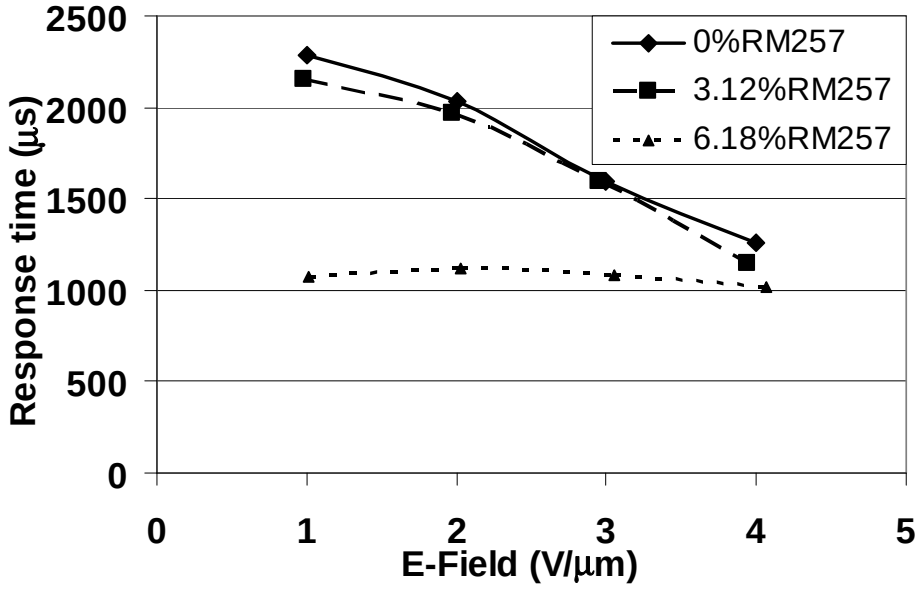

Figure 2.3: *The average of the 10-90% and 90-10% response times for the flexoelectro-optic switch in the 0%, 3% and 6% RM257 materials, at T_c-20ºC.*

Analysing the data from the figures above, the addition of 3% reactive mesogen restricts the optic axis tilt angle switch to an average of 88.4% of the unpolymerized switch over the applied E-field range. However, this negative effect can be compensated for by the fact that the 3% mixture can be

made to switch over larger angles than the pure chiral nematic mixture by the application of higher fields, which disrupted the response in the pure chiral nematic. The 6% (w/w) RM257 mixture, however, exhibited switching on average of only 47.8% of that of the undoped chiral nematic. This indicates considerable restriction at these levels of polymer concentration. The response times exhibited a similar level of monomer concentration dependency, switching at 95.6% and 62.8% of the pure chiral nematic response time in the 3% and 6% mixtures respectively. This result is unexpected, as the addition of a polymer network will generally increase the switching time. For practical purposes, the polymerization allows a trade-off between switching angle, of which these materials have an excess (most devices requiring only ϕ=22.5º for full intensity modulation), for a faster response.

7.9.2. Reduced Temperature Dependence

The addition of the polymer also enhances the temperature independence of the device characteristics. Figure 2.4 shows the flexoelectro-optic tilt angle measurements for the three differing polymer concentration mixtures over a range of temperatures below the isotropic-nematic transition point.

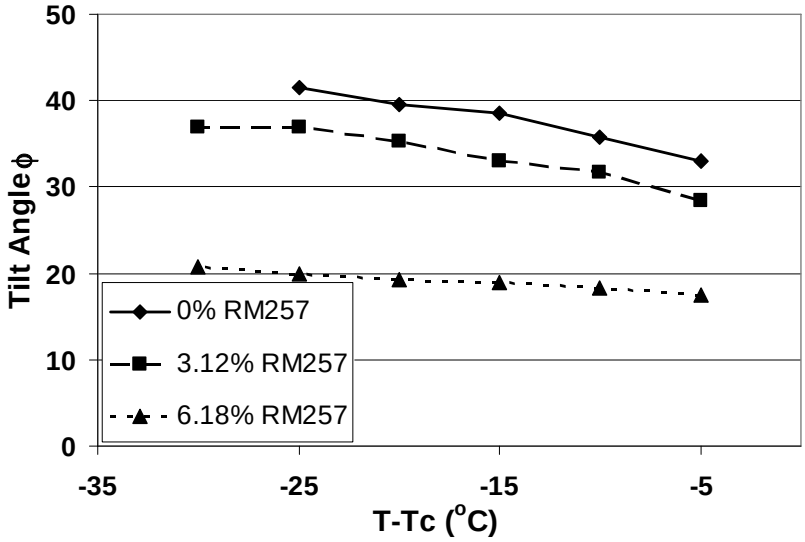

Figure 2.4: *The flexoelectro-optic tilt angle for the 0%, 3% and 6% RM257 mixtures at an applied field of 6V/μm, as a function of shifted temperature.*

The tilt angle is reduced by the addition of greater percentages of polymer as shown above for all temperatures, but the change of tilt angle over the temperature range is also reduced by the addition of a polymer network. For the undoped sample and the 3% reactive mesogen mixture, the tilt angle increases by approximately 25% upon reducing the temperature from 5°C to 25°C below the isotropic to chiral nematic transition point. However, this change is reduced to 14.3% in the mixture containing 6% crosslinked polymer.

The reduced temperature dependence of the electro-optics in the 6%RM257 sample can also be observed in the response time measurements. Here, a direct comparison of response times for a switch induced by a given field is not possible, as the different mixtures have different tilt angles for a given field and a larger switch will generally have a longer response time, but the temperature dependence for either switches induced by a constant field of 2V/μm (Figure 2.5), or for a constant 22.5º angle of switch (Figure 2.6), can be examined, and both comparisons show the reduction in observed temperature dependence.

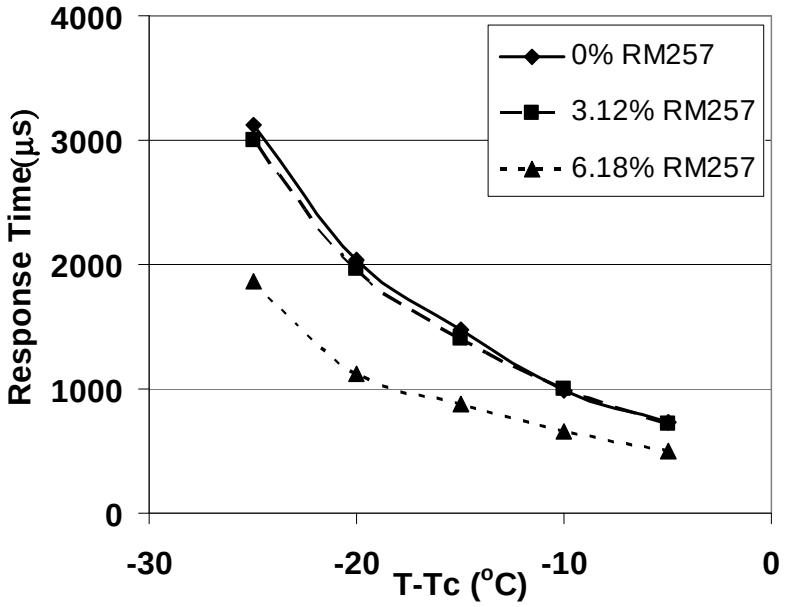

Figure 2.5: *The 10-90% response times for the 0%, 3% and 6% RM257 mixtures for a 2V/μm switch, as a function of shifted temperature.*

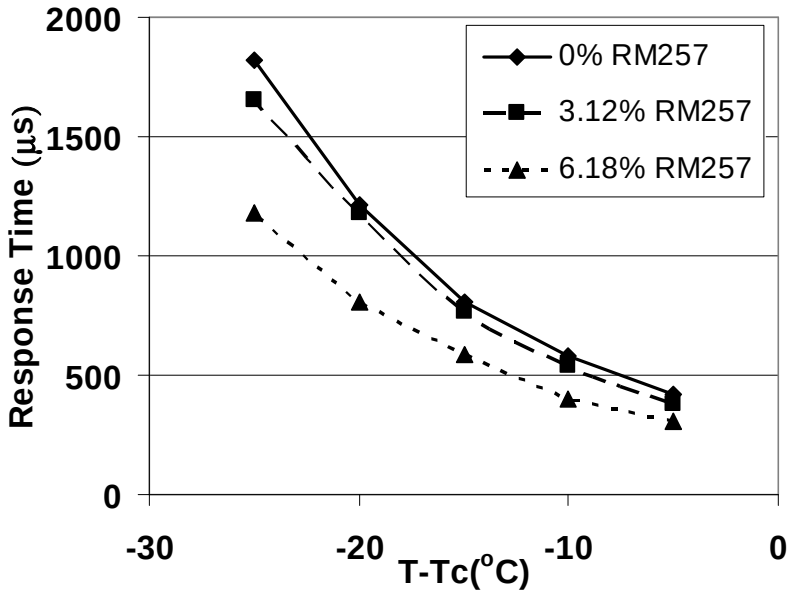

Figure 2.6: *The 10-90% response times for the 0%, 3% and 6% RM257 mixtures for a 22.5 ° switch, as a function of shifted temperature.*

On decreasing the temperature of the samples from 5°C to 25°C below the isotropic to chiral nematic transition, the unpolymerized mixture showed a three-fold increase in 10-90% response time for a 2V/µm switch. This was reduced to a factor of 2.8 change in the 6% polymer mixture. For a constant optic axis rotation of 22.5° over the same temperature range, the addition of the polymer again reduced the change in the response time from a 3.3 times change to 2.8, going from 0% to 6% polymer. These temperature dependencies are shown in Figure 2.5 and Figure 2.6.

It was suspected that the observed reduction in the temperature dependence of the flexoelectro-optic effect in polymer stabilized samples is principally due to restriction of the change in the chiral nematic pitch with temperature. The flexoelectro-optic tilt angle ϕ for a given applied field is shown in equation 2.34 (reproduced here as 6.1), where $\bar{e}$ is the average of the flexoelectric coefficients, E is the applied field, K is the average of the splay and bend elastic constants for the material, and $\tan\phi$ can be seen to be linearly proportional to the pitch, *P*.[7,8]

$$\tan\phi = \frac{\bar{e}EP}{K2\pi} \tag{6.1}$$

The response time, τ, of the switch is given by equation 2.37, where γ is the effective viscosity associated with the rotation, and τ can be seen to be proportional to the pitch squared.

$$\tau = \frac{\gamma P^2}{K 4\pi^2} \tag{6.2}$$

"Freezing" or "pinning" of the pitch and consequent reduction in its usual temperature variation by the presence of a polymer network would then account for this reduction in temperature dependence of the electro-optic response. "Freezing" of the chiral nematic pitch via polymerization has been observed previously in Grandjean textured chiral nematic liquid crystals in which the alignment layer on the glass also helps stabilize the pitch. This has been used to broaden the reflection band in chiral nematic samples by stabilizing an out-of-equilibrium condition pitch gradient caused by either photo induced diffusion[9] or curing over the period of a temperature ramp.[10]

The mixtures described above have too long a pitch for the characteristic chiral nematic reflection band to be measurable in a Grandjean aligned cell with a standard microscope mounted visible band spectrometer. For this reason, a second set of mixtures was made with the same mesogenic components, but a higher percentage of chiral dopant (2.5% BDH1281 (w/w). The pitch of these was estimated by measuring the position of the long wavelength band edge in the reflection spectra of Grandjean textured cells. In the 0% polymer sample, this band edge moved from 611nm to 689nm on cooling from T_c-5 to T_c-30. As the position of the long-wavelength band edge in a chiral nematic sample is given by[11]

$$\lambda_{long} = n_{\parallel} P \tag{6.3}$$

where $n_{\parallel}$ is the refractive index of the material parallel to the local nematic director and P is the pitch. As an estimate, we take $n_{\parallel}$ = 1.7, therefore the pitch change in this sample is from approximately 359 to 405 nm. In the 6% polymer sample, which was UV cured to crosslink the polymer at Tc-5, the long wavelength band edge remained pinned at 649 nm, corresponding to a pitch of approximately 382nm, over the temperature range from T_C-5 to T_C-30. The reflection spectra for the two samples of differing polymer concentration are shown below at a range of temperatures.

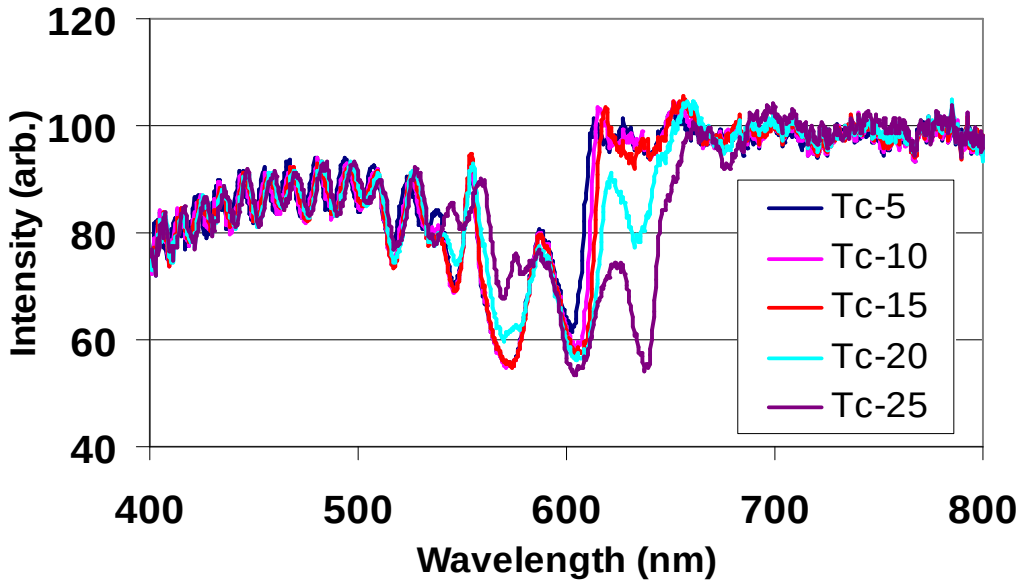

Figure 2.7: *The reflection spectrum of the 0% polymer mixture at a range of temperatures.*

Comparison of Figure 2.7 and Figure 2.8 shows this pitch restriction very clearly. The 6% polymer sample is seen to maintain an identical reflection spectrum over the whole nematic temperature range, whereas the undoped sample maintains a relatively steady reflection spectrum over the first ten degrees of cooling, but then rapidly shifts towards the red end of the spectrum.

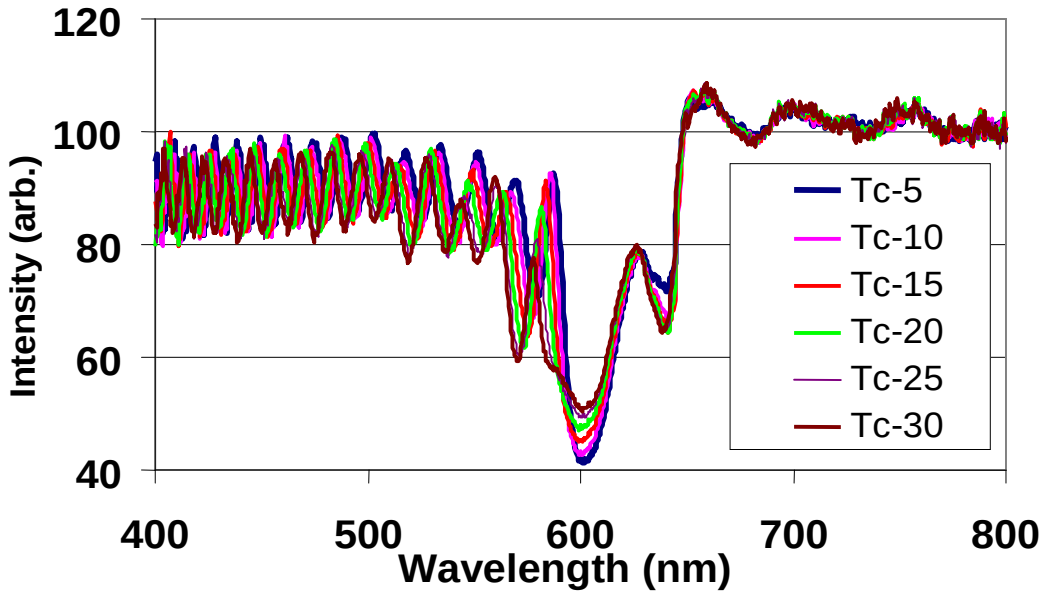

Figure 2.8: *The reflection spectrum of the 6% polymer sample at a range of temperatures.*

7.9.3. Polymerisation Temperature Effects

The freezing of the chiral nematic pitch by the polymerization of the small percentage of UV curing monomer, as well as reducing the temperature dependence of the flexoelectro-optic properties, allows selection of the optimum pitch, within the range exhibited by the undoped sample. This can be fixed over the entire chiral nematic range by UV curing at the temperature exhibiting the desired pitch.

In order to demonstrate this, a second cell was made with the 6% polymer mixture, in addition to the 382nm pitch sample described above, and UV cured to polymerise, but this time at T_c-30ºC. The cured sample exhibited a reflection spectrum from the Grandjean texture with a long wavelength band edge at 701nm (pitch approximately 412nm), which was pinned throughout the entire nematic range. In both these samples, polymerized at different temperatures and exhibiting pitches fixed at different values, the textures and pitches were unchanged by thermal cycling into the isotropic and back to the chiral nematic phase.

The results shown in the previous two figures, obtained in the Grandjean texture, raise the question whether the presence of the polymer is as effective in pinning the pitch of the material in the ULH texture, in which there are no additional glass boundary restrictions to the pitch. If so, it ought to allow selection of an optimum pitch for the desired flexoelectro-optic properties. It is not possible to measure the pitch of a chiral nematic sample aligned in the ULH texture via an equivalent reflection spectrum method as with the Grandjean texture, but if the pitch is frozen in by UV polymerization at a particular temperature, this ought to manifest itself in the flexoelectro-optics over the entire chiral nematic temperature range.

Two further cells were made and filled with the same 6% polymer chiral nematic mixture. The ULH texture was obtained and the cells UV cured to fix the texture and the pitch, one cell at T_c-10, and one at T_c-30. The portions of the cell outside the electrode area remained in the Grandjean configuration, and the pitch of these was measured to be 388nm and 405nm respectively. This was unchanged for both cells over the chiral nematic temperature range. The flexoelectro-optic tilt angles and response times were measured for each of these cells, as above, for a range of temperatures, and the results are shown in Figure 2.9 and Figure 2.10 respectively.

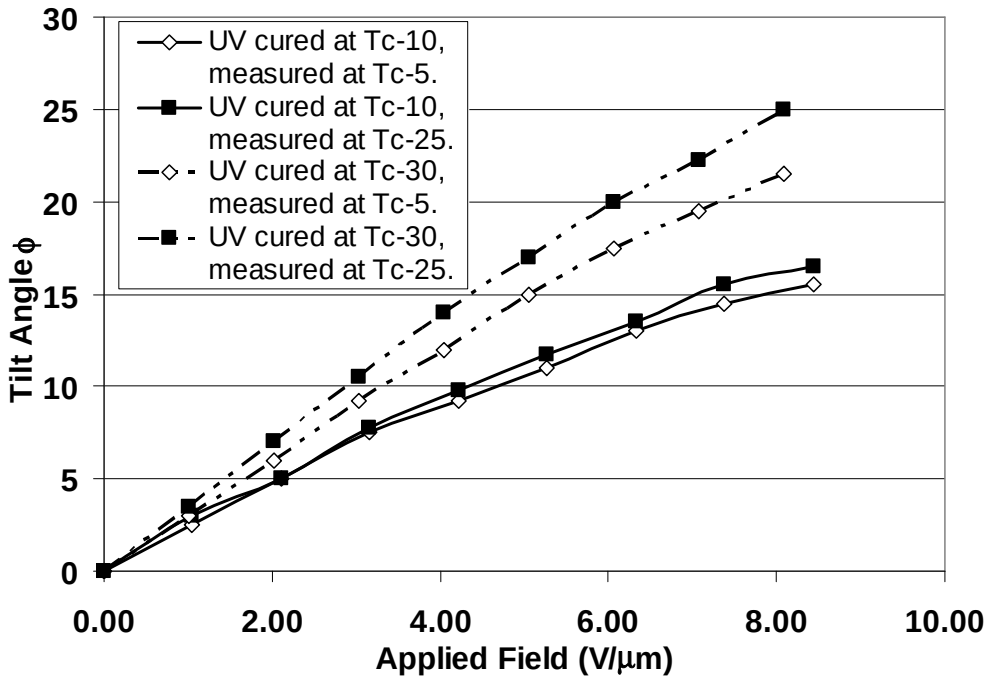

Figure 2.9: *The flexoelectro-optic tilt angles for the 6%RM257 material polymerized at two different temperatures, T_c-10 (solid line) and T_c-30 (dashed line), the operation of each shown at both T_c-5 (◊) and T_c-25 (■). The materials polymerised at the same temperature are depicted with the same joining line (solid or dashed), and those operated at the same temperature are depicted with the same point marker (diamond or square).*

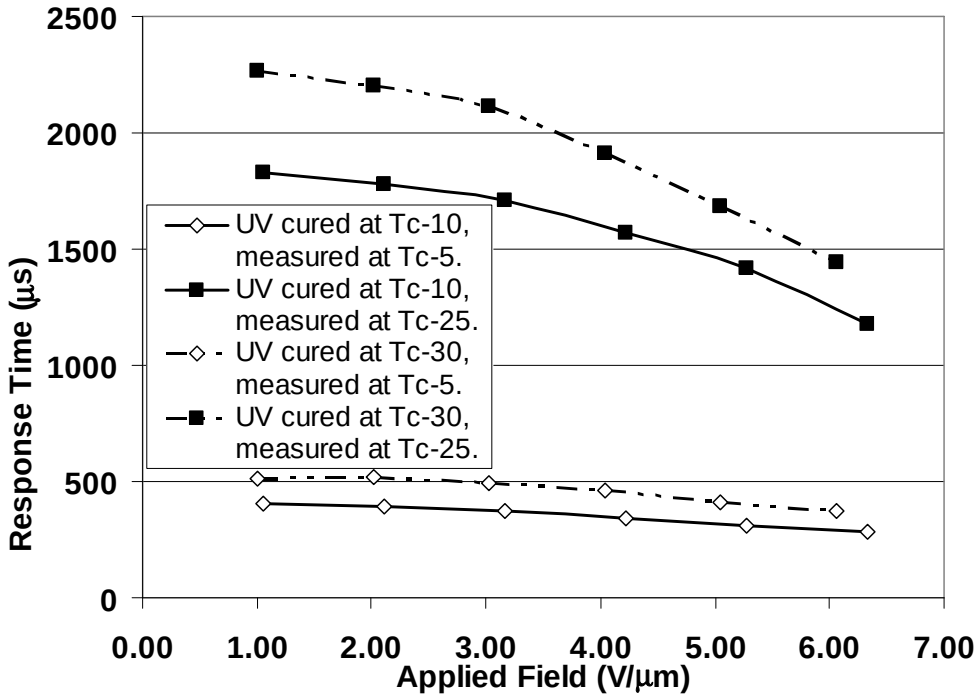

Figure 2.10: *The 10-90% response times the 6%RM257 material polymerized at two different temperatures, T_c-10 (solid line) and T_c-30 (dashed line), the operation of each shown at both T_c-5 (◊) and T_c-25 (■). The materials polymerised at the same temperature are depicted with the same joining line (solid or dashed), and those operated at the same temperature are depicted with the same point marker (diamond or square).*

These plots show conclusively that the polymerization of the samples does freeze the chiral nematic pitch in the ULH texture, and that this restriction of the pitch to its value at the time of polymerization has a significant effect on the flexoelectro-optic characteristics of the sample over the entire chiral nematic temperature range, as would be expected from equations 6.1 and 6.2. Indeed, Figure 2.9 shows that the temperature at which the sample is polymerized has a significantly greater effect on the observed tilt angles for a given field than the operating temperature. There is however still some change in the tilt angle with operating temperature, which suggests that, in spite of the thermally invariant pitch, the flexoelastic ratio, ē/K, must depend on temperature. The average of the splay and bend elastic constants,

$$K = \left(k_{11} + k_{33}\right)/2 \tag{6.4}$$

is believed to change with temperature as the square of the nematic order parameter, S. Previous reports have suggested that the sum of the splay and bend flexoelectric coefficients

$$\bar{e} = e_s + e_b \tag{6.5}$$

is also proportional to S^2.[12] If this is the case, then the flexoelastic ratio should be temperature independent overall. However, the results presented here contradict this hypothesis, and suggest that the flexoelastic ratio actually has a small temperature dependence. As a matter of fact, other reports have suggested that the flexoelectric constants have a linear dependence on S.[13,14]

Figure 2.10 shows that, although the UV curing temperature does have a significant effect on the response times, the operating temperature is still more important for this parameter, as it is the traces with the same point marker which are now closely aligned, not those with the same line type as was the case in Figure 2.9. This indicates that although the switching time is dependent on P^2, from equation 6.2, the temperature dependence of the viscosity, which follows an Arrhenius curve, outweighs this, and that this is not made temperature independent by the introduction of the polymer.

The practical significance of this result is that it allows the tilt angle to be maximised (normally by operating at low temperature) at the same time as the response time is minimised (normally at high temperature). Optimisation of both aspects of a device's performance simultaneously can now be achieved by UV curing the sample at low temperature, and operating at high temperature. Previously, in an unpolymerised sample, the operating temperature would have to be chosen to effect the best compromise between these two performance aspects, the temperature optimisation of which would be mutually exclusive.

7.10. CONCLUSIONS

Volume stabilization of the ULH texture in short-pitch chiral nematic liquid crystals, by UV curing of a small percentage of reactive mesogen, has been found to have a concentration dependent influence on the flexoelectro-optic characteristics of a large tilt-angle mixture. The polymer network restricts the electric field dependent rotation of the optic axis in the plane of the cell, and reduces the response time of the switch. A reactive mesogen concentration of approximately 3%, however, appears to offer sufficient texture stabilization with minimal impact on the electro-optic response of the device.

The introduction of a polymer network has also been shown to reduce the temperature dependence of the flexoelectro-optic tilt angles and response times measured in the sample over the chiral

nematic temperature range. This is believed to be principally due to restriction of the temperature variation of the pitch of the material, characteristic of chiral nematic liquid crystals.

The ability to UV cure the reactive mesogen within the sample at a temperature which exhibits optimal device performance ensures that this performance is maintained over the chiral nematic temperature range. The flexoelectro-optic tilt angle has been shown to be restricted to temperature variations to a far greater extent than the response time of the switch. This is due to the fact that the Arrhenius temperature dependency of the viscosity remains despite polymerization. This allows a device to be fabricated in which the material is UV cured at a temperature providing optimal tilt angle characteristics, and operated at a temperature providing optimal response times. These two, usually antagonistic, performance factors can therefore now be simultaneously optimised, providing increased potential for flexoelectro-optical devices.

7.11. REFERENCES

[1]L. Komitov, G. P. Bryan-Brown, E. L. Wood and A. B. J. Smout, *J. Appl. Phys.*, **86**, (7), 3508, (1999).

[2]P. Rudquist, L. Komitov and S. T. Lagerwall, *Liq. Cryst.*, **24**, (3), 329, (1998).

[3]S. H. Kim, L. C. Chien and L. Komitov, *Applied Physics Letters*, **86**, (16), 161118, (2005).

[4]H. J. Coles, M. J. Clarke, S. M. Morris, B. J. Broughton and A. E. Blatch, *Journal of Applied Physics*, **99,** 034104, (2006).

[5]M. J. Clarke, PhD Thesis, University of Southampton, (2004).

[6]C. Noot, M. J. Coles, B. Musgrave, S. P. Perkins and H. J. Coles, *Mol. Cryst. Liq. Cryst.*, **366**, 2577, (2001).

[7]J. S. Patel and R. B. Meyer, *Phys. Rev. Lett.*, **58**, (15), 1538, (1987).

[8]J. S. Patel and S. D. Lee, *J. Appl. Phys.*, **66**, (4), 1879-81, (1989).

[9]D. J. Broer, J. Lub and G. N. Mol, *Nature*, **378**, (6556), 467-9, (1995).

[10]C. Binet, M. Mitov and M. Mauzac, *Journal of Applied Physics*, **90**, (4), 1730-4, (2001).

[11]H. L. de Vries, *Acta Cryst.*, **4**, 219-26, (1951).

[12]P. R. M. Murthy, V. A. Raghunathan and N. V. Madhusudana, *Liq. Cryst.*, **14**, (2), 483-96, (1993).

[13]D. L. Cheung, S. J. Clark and M. R. Wilson, *J. Chem. Phys.*, **121**, (18), 9131-9, (2004).

[14]M. A. Osipov, *Journal de Physique (Paris) Lettres*, **45**, 823, (1984).

[15]B. J. Broughton, M. J. Clarke, S. M. Morris and H. J. Coles, *J. Appl. Phys*, **99**, 023511, (2006).

Chapter Seven

Tuning of Chiral Nematic Lasers by the Flexoelectro-optic Effect

7.12. INTRODUCTION

The development of high tilt angle flexoelectro-optic mixtures[1,2] poses some interesting questions as to the liquid crystal director structure in a material which is undergoing a deformation of up to ±80˚ in the orientation of its optic axis. Although the theoretical description of the flexoelectro-optic deformation, as shown in Figure 2.10, incorporates no change in the spacing of the nematic layers, and therefore no change in the chiral nematic pitch length as a result of the deformation, this theory was developed for small angle deformations, and may not be an entirely accurate description of the deformation in these higher tilt materials. It seems probable that with deformations of the magnitude that have been observed in the bimesogenic mixtures in this work and previously, some alteration to the pitch length is induced. This would not have been observable in the conventional ULH texture based observation of flexoelectro-optic switching, but the development of the Grandjean based effect outlined in Chapters 4 and 5 should allow a means of monitoring the chiral nematic pitch length throughout the flexoelectro-optic switch via the effect on the reflection spectrum. The effect in polymer stabilised samples under a.c. applied waveforms should also allow determination of the effect on the pitch of dielectric and flexoelectric coupling, as detailed in Chapter 5, perhaps providing some insight into the exact mechanism of dielectric helix unwinding, differing theories of which have been proposed. [3,4]

The edges of the reflection spectrum, which relate to the pitch of the material according to equations 2.22 and 2.23, are not always easy to measure accurately due to internal chromatic reflection from the cell walls and noise in the spectrometer plot, as can be seen in Figure 6.7. This poses a problem as, while the spectra are fine for estimating the pitch length of samples, the level of subjectivity in determining the actual band edge may be too great to allow detection of very small changes in the pitch, as may be induced by the flexoelectro-optic deformation. Also the spectrometer can take of the order of 100ms to obtain a reading, which may be too slow to detect any change resulting from the deformations in our samples. The output from a photonic band edge (PBE) chiral nematic laser, however, provides a very high resolution, entirely objective marker of the position of the band edge in a dye-doped sample. PBE lasing peaks typically have a full width at half maximum of less than a nanometer,[5] and the emission can be timed to coincide with the deformation resulting from an applied electric field pulse, as shown in Figure 3.5.

The purpose of the work presented in this Chapter was therefore to observe a change in the output wavelength of a PBE laser, consisting of a dye-doped, Grandjean textured chiral nematic sample, when subjected to a flexoelectro-optic deformation as a result of an electric field applied in the plane of the cell. It was hoped that this would demonstrate for the first time electric tuning of chiral nematic PBE laser, and provide an insight into the effect of the flexoelectro-optic effect on the pitch of the material in high-tilt samples.

7.13. FLEXOELECTRO-OPTIC TUNING

The first attempt to observe an electric laser tuning effect was a dye doped chiral nematic mixture based on the non-symmetric bimesogen FF0-8-OCB. Although the odd-spacer length bimesogens have been shown to have a greater flexoelastic ratio,[6] the FFO-8-OCB material had been the most promising lasing material observed by Alison Ford[7] in her investigation and given the narrow aperture of the active region in the cartwheel cells used, this was deemed the most important factor in obtaining a clear measure of the laser output. The components of the mixture used were: 93.12% FFO8OCB, 4.85% BDH1281 and 2.03% DCM laser dye. The mixture was found to enter the chiral nematic phase from the isotropic at 137˚C.

The mixture was capillary filled into a cartwheel cell and was first tested in the infra-red electro-optic rig to confirm the presence of a flexoelectro-optic deformation. The resulting electro-optic response is shown in Figure 3.1. From the figure it can be seen that a director deformation does indeed occur in the dye doped samples in a similar fashion to the other bimesogenic mixtures examined previously. The response of the cell is of reasonable magnitude, giving $I/I_0 = 0.25$, and fast response; $T_{10\text{-}90} = T_{90\text{-}10} = 120\mu s$. A large degree of asymmetry of the response to field polarity is observed, probably due to pre-tilt in the cell surface alignment. The transmission dip at the field polarity change point indicates a substantial degree of flexoelectric coupling in the response. This response indicated the cell was functional and ready for insertion into the lasing experiment.

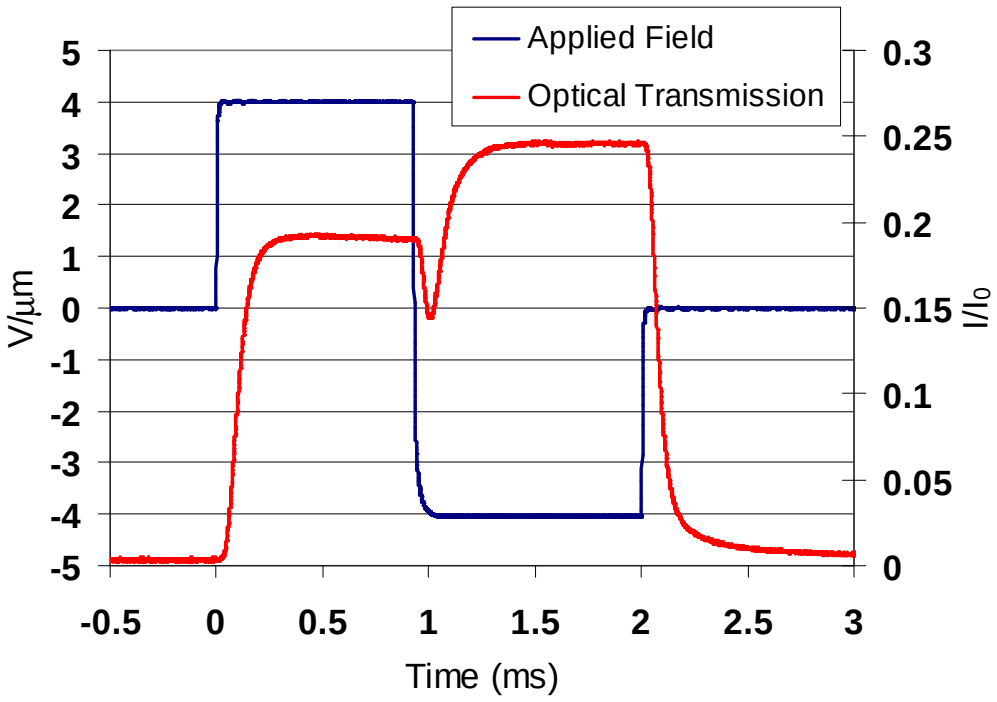

Figure 3.1: *The electro-optical response at 1550nm of the dyed chiral FFO8OCB cell to a +/-4 V/µm, 2ms duration bipolar square pulse at T_C-10˚C.*

The experimental set-up for the laser tuning experiment was as outlined in Chapter 3.2.3, and all experiments were carried out in collaboration with Alison Ford. As indicated previously, this liquid crystal mixture had produced very high efficiency lasing in tests in plain glass cells without any applied field. The narrow aperture of the cartwheel cell introduced considerable difficulty in allowing enough laser light to be generated to allow detection at the spectrometer (the 50µm aperture of the cartwheel cell is half the diameter of the pump beam waist), but these difficulties were overcome by realigning the optics for maximum collection of the laser light, and increasing the pump pulse power. Achieving a suitably uniform texture in these cells for lasing also proved extremely difficult, but repeated efforts eventually yielded a suitably monodomain sample. Lasing output was then observed from the cartwheel cell as it was cooled, with the onset at approximately T = 130˚C. The spectrometer output as observed is shown in Figure 3.2.

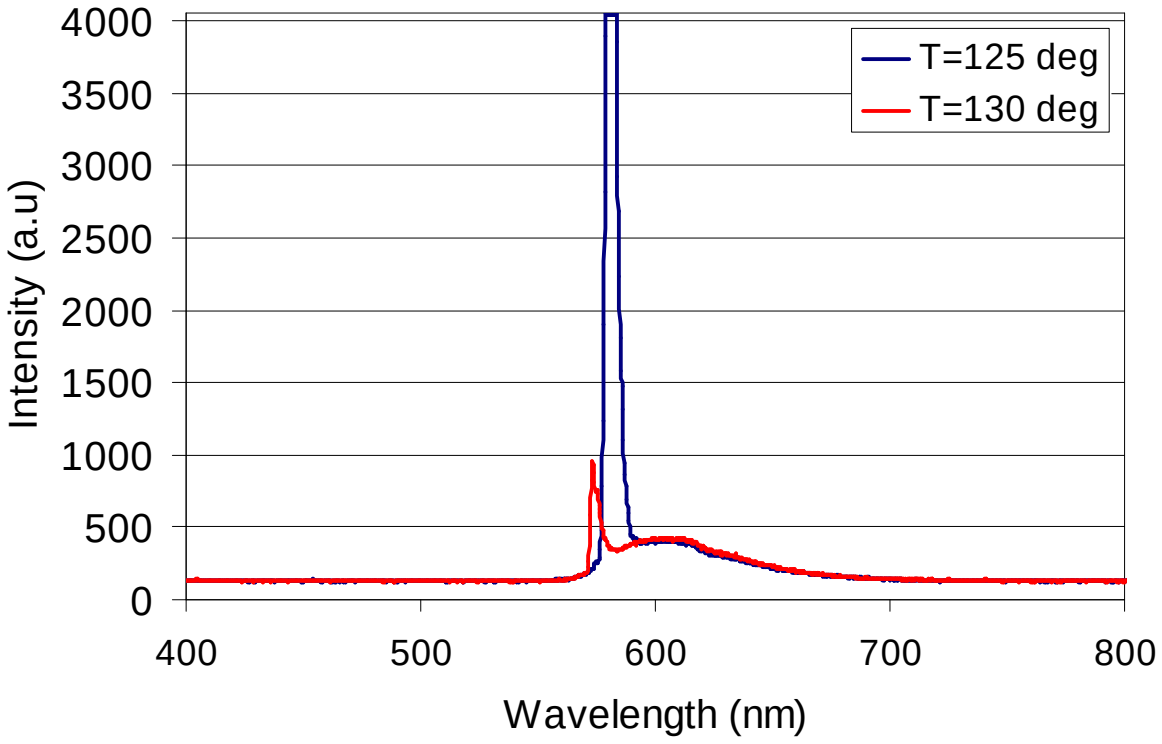

Figure 3.2: *Laser emission from the dyed chiral FFO8OCB cell at 125˚C and 130˚C.*

As can be seen in the figure, the laser output grows out of the detectable DCM fluorescence peak as the cell is cooled. This is expected, as the laser output from is dependent on the order parameter of the material.[8] The laser line is positioned at the edge of the photonic band edge gap, and therefore changes with temperature as the pitch changes. This adds to the increased laser output effect in this sample with decreasing temperature, as this both increases the order parameter of the sample and moves the photonic band-edge closer to the fluorescence peak.

With a clear lasing output from the cell present, the cell was held at a constant temperature of 120˚C to prevent temperature based pitch changes. Bipolar electric pulses were then applied to the cell to coincide with the pump pulse. As the field strength was increased, a slight but definite red-shift was observed in the laser output. The output spectra for a range of applied field strengths are shown in Figure 3.3.

It can be seen from the figure that when the horizontal axis is expanded sufficiently to show clearly the field-induced wavelength shift, the individual laser lines are not sharp. This is due to the fact that a clear monodomain Grandjean texture is harder to achieve in the cartwheel cells than in the Lucid cells usually used for lasing tests. This was not a problem for the infra-red electro-optic

measurements of Chapters 4 and 5, as the infra-red laser spot size incident on the cell was approximately 10μm in diameter, so a small area of clear texture could be found and used. The larger beam waist of the pump laser beam in this set-up, however, results in the excitation of several micro-domains and multi-mode lasing occurs.

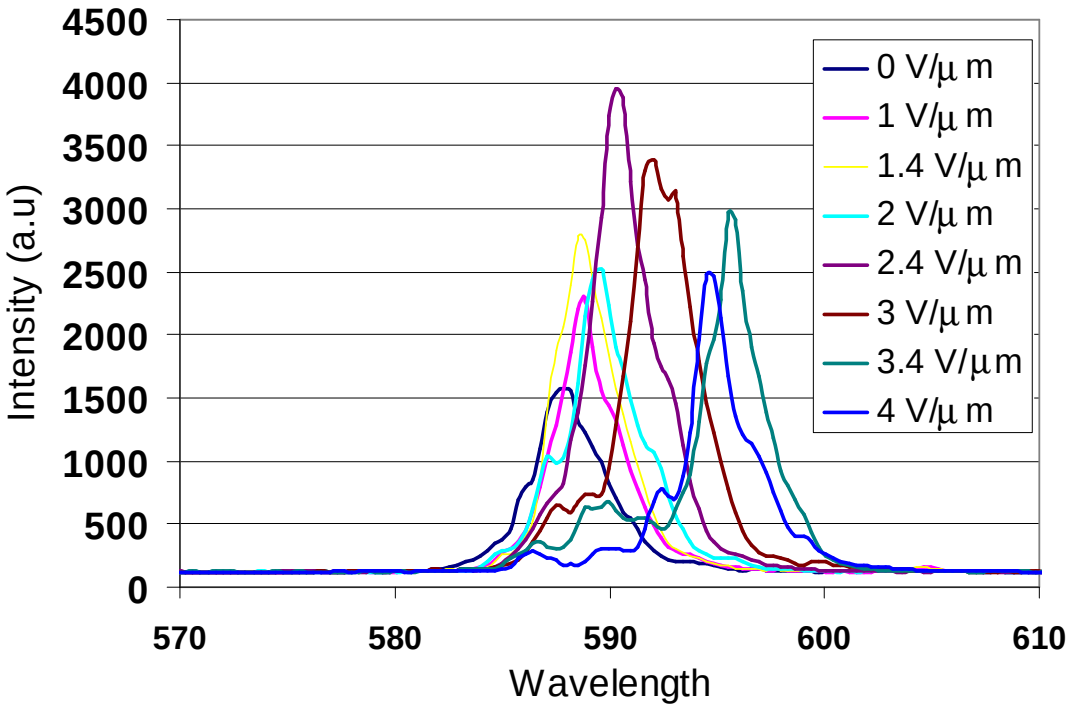

Figure 3.3: *Laser output spectra from the dyed chiral FFO8OCB cell at a range of applied field strengths at T = 120˚C.*

The peaks are still narrow enough for the tuning effect to be observed however. The wavelength at the peak of each spectrum is plotted against the applied field under which that output was observed, the trend is observed being shown in Figure 3.4.

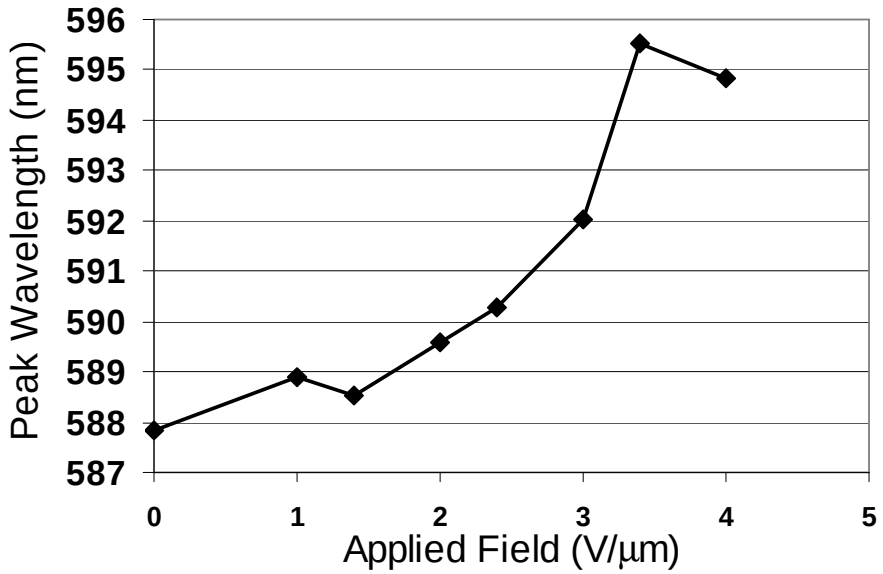

Figure 3.4: *Laser output wavelength against applied field in the FFO8OCB cell.*

A clear red-shift is observed, but also the magnitude of the laser output can be seen to decrease at higher applied fields, leading to an eventual drop in wavelength at the highest applied field of 4 V/μm. However, before this point is reached, as maximum shift in the output wavelength of approximately 8nm is observed. This shift is the result of the d.c. portion of an applied bipolar pulse, having been applied to the sample for 220μs before the pump laser pulse is incident on the sample. The tuning can therefore be said to have been implemented within this timescale. Due to the non-polymerised nature of the sample, only pulsed addressing was possible, so the relative contributions to the tuning effect from dielectric and flexoelectric coupling cannot be separated. While the plot in Figure 3.1 indicates roughly equal contribution from both effects to the birefringence, it cannot be stated how these might individually effect the pitch over such a short timescale.

This was the largest tuning range observed in this sample, but the experiment was also performed at the higher temperature of 130˚C, with a higher pump pulse input energy to compensate for the lower lasing efficiency, and a similar red-shift was observed. This is illustrated in Figure 3.5.

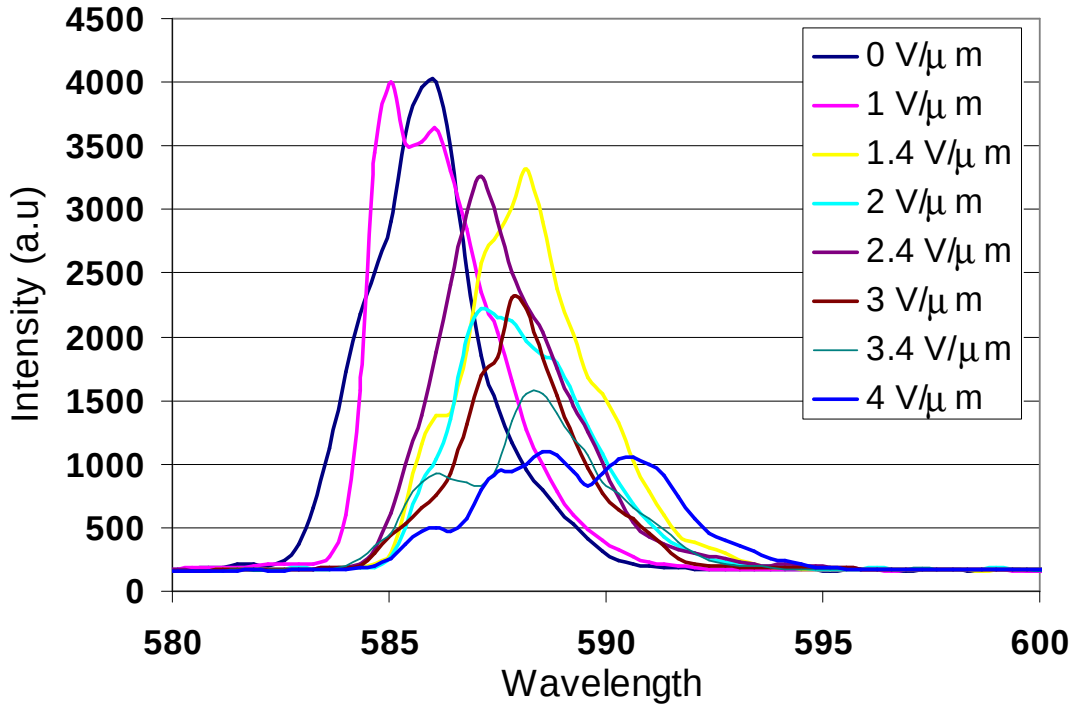

Figure 3.5: *Laser output spectra from the dyed chiral FFO8OCB cell at a range of applied field strengths at T = 130˚C.*

At this raised temperature, the induced shift in output wavelength was reduced to approximately 6nm, and the degradation of the laser line at higher fields can be seen to be more severe.

As the tuning range for this method was smaller than expected and the uncertainty in the induced shift was increased by the excessive width of the laser lines, it was decided to attempt to observe the effect in a different type of cell in which the electrodes were only patterned on the surface rather than occupying the bulk of the cell. This should allow monodomain samples to be obtained producing sharper laser lines of 0.4nm full-width-at-half-maximum as observed in the "lucid cells",[7] making the induced shifts clearer. For this reason, the 100μm electrode gap patterned electrode cells were fabricated, as shown in Chapter 3.3.1.3.

As the quality of lasing is increased in these cells with monodomain Grandjean textures, and the tuning in the previous material was unexpectedly small, a material with a larger flexoelectro-optic tilt angle was chosen to test in these cells. This was due to it being determined that the magnitude of the response to the applied field was now more important than the ease of obtaining lasing action. For this reason a dyed chiral mixture based on the bimesogen FFO11OCB was composed. Due to the increased electrode spacing in these cells, the maximum field strength that could be

applied was 3.4 V/µm. The cell was placed in the lasing apparatus and pulsed with the applied field. No tuning effect was immediately visible, but on averaging the output from 100 pulses, a very small shift of approximately 1nm was observed. This averaged output is shown in Figure 3.6.

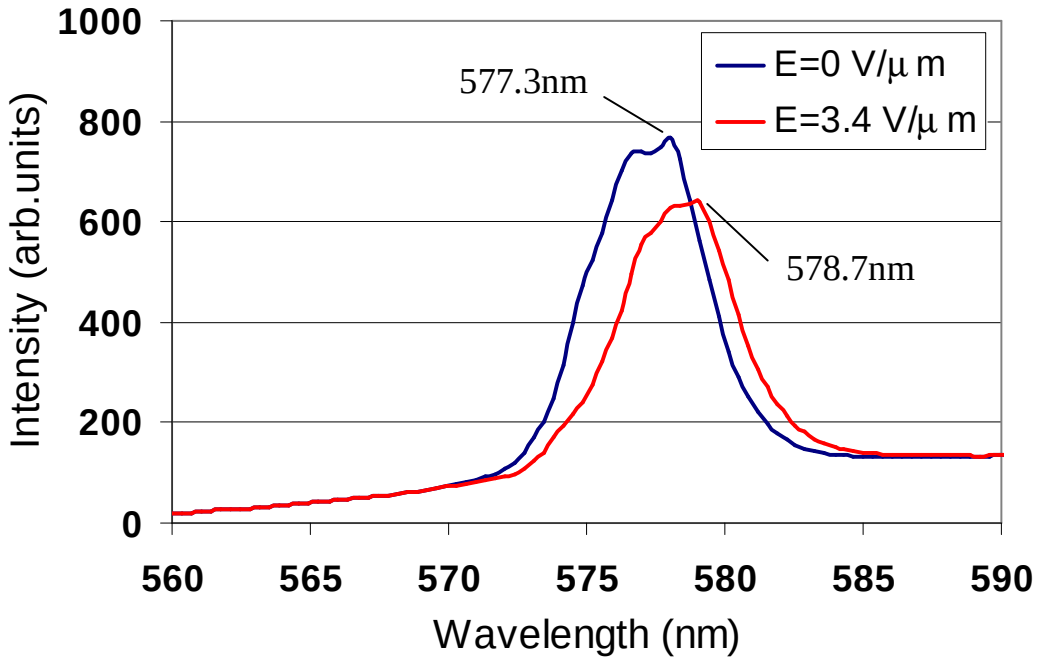

Figure 3.6: *Averaged lasing output spectra for 100 pulses from the dyed chiral FFO11OCB cell with and without an applied field.*

This field induced wavelength shift was again smaller than expected, but repeated collections of the 100 pulse average yielded the same 1nm shift. It was thought that perhaps this was because the material was not responding to the applied field in the 220µs available before sampling by the pump pulse, although the infra-red measurements in Chapter 5.4.1 suggest that the response times are within this timescale. In case this was the situation, an a.c. field was applied to the cell to allow a constant dielectric coupling to occur with the flexoelectric response in addition to this. Unfortunately, as with the non-polymerised cartwheel cells of Chapter 4, this caused flow of the liquid crystal and ruined the Grandjean texture. This degradation is recorded in the photomicrographs of Figure 3.7.

Figure 3.7: *Photomicrographs of the Grandjean texture in the dyed chiral FFO11OCB cell before application of a 133V R.M.S, 10kHZ square wave in the plane of the cell(left), immediately after application (centre), and several seconds after application(right).*

The above figure shows that immediately as the field is applied, the edges of the electrodes on the surface become visible, and within a few seconds the flow has ruined the texture in the active region.

For this reason it was decided to fabricate a polymer stabilised sample and observe for any wavelength shift under a.c. waveforms. It was found that the DCM laser dye was bleached by the UV light required to crosslink the reactive mesogen, so a mixture was made instead using the pyromethane dye PM597. These were able to be cross-linked due to the dye's narrowed absorption peak relative to DCM, and lasing was achieved in this new mixture also. The texture of the polymer sample was indeed rugged to the applied field, but no wavelength shift was observed. This is probably due to pinning of the pitch by the polymer, as observed in Chapter 6. Non polymer stabilised dyed chiral mixtures of both 7OCB, which exhibited the largest induced birefringence in the Grandjean texture in Chapter 5, and FFO8OCB, in which the original 8nm shift was observed in the cartwheel cell, were also made. However, no detectable shift was observed in the patterned electrode cell in either. These mixtures were also tried in 50μm electrode spacing patterned electrode cells, made by Tim Wilkinson of the department of Engineering at the University of Cambridge, in order to increase the maximum applied field, but again no shift was detected.

It was thought that perhaps no director deformation was taking place in these cells as opposed to the cartwheel cells, so the 7OCB and FFO11OCB patterned electrode cell samples were placed in the infra-red experiment, and an induced birefringence was observed in each which closely matched the nature of the response of the material in the cartwheel cell, eliminating this possibility. This leaves the possibility that it is the excessive spot size of the pump laser beam, as incident on the sample, which is causing lasing from regions outside those affected by the applied field. This

output could be swamping the field tuned output from the active region preventing an observable effect in these cells. This could not have been the case in the cartwheel cells as the bulk electrodes blocked any pump light which was incident outside the active region. Unfortunately, obtaining a clear enough texture over a large enough region in the cartwheel cells for lasing proved too unreliable, and fabrication of a patterned electrode cell with an aligned shield to shadow areas outside the active region would have involved too great a lead-time to be included in this work.

7.14. CONCLUSIONS

It was predicted that the large flexoelectro-optic tilt of the bimesogenic mixtures, as observed in the ULH texture in previous studies and in the Grandjean texture in Chapter 5 would have some effect on the pitch of the material undergoing the deformation. It was decided to use the spectral position of the photonic band edge laser line in dyed chiral samples as a high resolution marker of the edge of the selective reflection band in Grandjean textured samples, in order to observe the effect of the flexoelectro-optic deformation on that band edge, and by association, the pitch of the material. In this manner, it was hoped to determine the effect of a large flexoelectro-optic deformation on the pitch of a material, compare it to the effect of dielectric helix unwinding on the pitch, and demonstrate fast electrical tuning of the PBE laser output from dyed chiral nematic samples.

A field dependent wavelength shift of up to 8nm, induced by up to 3.5 V/μm applied fields, was observed in the laser output from a sample based on the non-symmetric bimesogen FFO8OCB in a cartwheel cell as used in Chapters 4 and 5. This effect was smaller than anticipated, but nonetheless provides the first observation of fast electrical tuning of the PBE laser output from a chiral nematic liquid crystal. The effect was repeated at a shifted temperature and observed again to a slightly lesser extent. The effect could not be repeated with different samples in other cartwheel cells due to difficulties obtaining a sufficiently monodomain sample to achieve good lasing. For this reason, it was attempted to observe the effect in patterned ITO electrode cells in which the lack of bulk electrode in the body of the cell allows mechanical rubbing of a planar alignment layer and reliable achievement of a clear Grandjean texture. However, the effect was much reduced in these cells, and only observed in a mixture based on the non-symmetric

bimesogen FFO11OCB. In this instance, the output from 100 pump-pulses had to be averaged in order to make visible a 1nm wavelength shift induced by an applied field of 3.4 V/μm.

It is believed the combination of the reduced maximum applied field caused by the increase in electrode spacing in these cells, and the spot size of the pump beam incident on the sample exceeding the width of the active region lead to this reduce effect. However, attempts to increase the applied field by fabrication of reduced electrode spacing patterned ITO cells, and masking of the region of the cell outside the active area yielded no improvement. Polymer stabilised samples which were also tested yielded no field induced wavelength shift, so differentiation between the contributions from flexoelectric and dielectric coupling to the effect were not possible due to the ability to apply only isolated electric pulses to the non polymer-stabilised samples which exhibited an effect.

In conclusion, although the magnitude of the observed effect and the difficulty in repeating the effect in subsequent samples are disappointing, it is believed that the results presented in this Chapter do provide demonstration of a very novel effect. The potential for further work in solidifying this evidence and improving the magnitude of the effect is also substantial; unfortunately this was just beyond the scope of this work.

7.15. REFERENCES

[1]H. J. Coles, B. Musgrave, M. J. Coles and J. Willmott, *Journal of Materials Chemistry*, **11**, (11), 2709, (2001).

[2]H. J. Coles, M. J. Clarke, S. M. Morris, B. J. Broughton and A. E. Blatch, *Journal of Applied Physics*, **99**, 034104, (2006).

[3]P. De Gennes and J. Prost, *The Physics of Liquid Crystals*, Oxford: Clarendon Press, (1993).

[4]M. Kawachi and O. Kogure, *Japanese Journal of Applied Physics*, **16**, (9), 1673-8, (1977).

[5]S. M. Morris, A. D. Ford, M. N. Pivnenko and H. J. Coles, *J. Appl. Phys.*, **97**, (2), art. no.-023103, (2005).

[6]M. J. Clarke, PhD Thesis, University of Southampton, (2004).

[7]A. D. Ford, PhD Thesis, University of Cambridge, (2005), in preparation.

[8]S. M. Morris, A. D. Ford, M. N. Pivnenko and H. J. Coles, *P. Soc. Photo-Opt. Ins.*, **5289**, 236-45, (2004).

[9]S. M. Morris, A. D. Ford, B. J. Broughton, M. N. Pivnenko, and H. J. Coles, *P. Soc. Photo-Opt. Ins.*, **5741**, 118-28, (2005).

Chapter Eight

CONCLUSIONS

8.1. SUMMARY AND REMARKS

The work presented in this thesis was carried out with the objective of assessing the potential of the flexoelectro-optic effect in chiral nematic liquid crystals for application in fibre-optical communications devices. The flexoelectro-optic effect is principally of interest because, unusually among liquid crystal electro-optic effects, it combines the fast, sub-millisecond response times of ferroelectric devices with the analogue electric optic axis deformation of nematic liquid crystals. This interest has been substantially increased by the development of bimesogenic liquid crystal materials which, through their characteristic possession of both high flexoelectric coefficients and low dielectric anisotropy, allow very high optic axis tilt angles to be achieved in uniform lying helix (ULH) aligned chiral nematic samples. The effect therefore allows the production of fixed retardation waveplates, which are electrically rotatable through large angles (+/- 85˚ achieved to date), with fast response. Despite these advantages, the flexoelectro-optic effect has so far remained unexplored from a telecoms standpoint. This work aimed to address this situation as follows:

An outline of the theory of the optics liquid crystals and their behaviour under the application of electric fields, relevant to the experiments later described, is given in Chapter Two. Particular attention is given to the optics of chiral nematic liquid crystals and the electro-optic effects resulting from both the dielectric and flexoelectric coupling of the liquid crystal director structure to the applied field. These provide the basis of the effects detailed in the later experimental Chapters. A brief overview of lasing at the edge of the photonic band gap intrinsic to chiral nematic liquid crystals is also given. Additionally, theoretical calculations are made as to the birefringence induced by the flexoelectro-optic effect in Grandjean textured samples, the first observations of which are later documented.

The experimental methods and equipment used throughout this work are introduced in Chapter Three. The subsequent experimental chapters utilise three primary experiments; each in turn investigating the infra-red electro-optics of Grandjean textured chiral nematic liquid crystals, the visible electro-optics of ULH aligned chiral nematics and tuning of the output wavelength of chiral nematic photonic band edge lasers by in-plane electric fields. These are detailed alongside the polarizing microscopy and electro-optic cell construction techniques fundamental to liquid crystal based experimentation.

A novel device type is introduced in Chapter Four, in which the conventional geometry for the flexoelectro-optic effect (ULH aligned liquid crystal and electric field applied between the cell walls) is rotated, having the chiral nematic liquid crystal aligned in the Grandjean texture, or standing helix geometry, and the electric field applied in the plane of the cell via bulk metallic electrodes.

The cell is optically neutral at zero applied field, due to having its macroscopic optic axis lie parallel to the direction of light propagation through the cell and having insignificant polarisation rotation at optical communication wavelengths (1550nm). This is due to the helical pitch of the material being substantially shorter than the illuminating wavelength. Application of an electric field in the plane of the cell deflects the optic axis of the material giving it some component in the polarisation plane of the light and therefore inducing a birefringence. This device concept was developed because the magnitude of induced birefringence has analogue field dependence, and the direction of the resultant optic axis is dependent on the direction of the applied field. This makes it suitable for use as an endlessly rotatable variable waveplate. Such a device would have applications in polarisation mode dispersion compensation in fibre-optical communications systems. The first observations of the Grandjean flexoelectro-optic effect are detailed in this Chapter, and were found to be in good agreement with the predictions made in Chapter Two.

A number of chiral nematic materials were investigated in the device, the largest induced birefringence observed being that in the 7OCB sample, in a cell approximately 40μm thick, which was effectively a half waveplate at 1550nm at 3 V/μm. This birefringence was not attributable solely to flexoelectric coupling, but was thought to be predominantly due to dielectric helix unwinding. Nevertheless, the birefringence was found to develop upon application of the field, and disappear upon removal over a timescale of 200-300 μs. The uppermost problem discovered with the effect was the inability of the samples to withstand continuous applied a.c. field without break-up of the liquid crystal texture into a scattering state. The results could therefore only be obtained via the application of isolated electrical pulses.

The results presented in Chapter Five build on those of the previous Chapter by examining the Grandjean Flexoelectro-optic effect in polymer stabilised chiral nematic samples. In these cells, a small percentage of reactive mesogenic monomer is dissolved in the chiral nematic material which, when the desired Grandjean texture is obtained in the cell, is exposed to UV light causing the

monomer to cross-link and provide a stabilising polymer network within the bulk of the liquid crystal. This was found to be extremely successful in enhancing the ruggedness of the texture and eliminating flow to allow application of a.c. fields without degradation of the liquid crystal alignment.

According to the theory, the flexoelectric and dielectric coupling mechanisms have differing frequency dependence for the birefringence they induce, therefore variation of the applied frequency should allow a method of distinguishing the portions of the electro-optical response resulting from the two effects. This was indeed observed to be the case, and in this way, the chiral nematic material used in the cells was developed and tested to maximise the flexoelectric portion of the response.

Several chiral nematic mixtures were tested, based on the monomesogen 7OCB and bimesogenic materials, culminating in the mixture of roughly equal parts of the symmetric bimesogens FFO9OFFB, FFO11OFF, FFE9EFF and FFE11EFF with 4.3% (w/w) reactive mesogen and 1.8% chiral dopant (for elaboration on the acronyms used, please see Chapter 5). This mixture showed no dielectric helix unwinding contribution to the field-induced birefringence, and exhibited the highest flexoelectrically induced birefringence of the bimesogenic materials: $\Delta n = 0.012$ at 6.8V/µm and 1550nm.

The highest overall induced birefringence, of both flexoelectric and dielectric origin, of the materials studied was still 7OCB which showed $\Delta n = 0.037$ for the same field. The addition of the polymer network appeared to have little effect on the response time of the effect, all the mixtures again showing sub-millisecond switching at the higher end of their respective chiral nematic temperature ranges. Therefore this effect shows considerable promise for use as a fast response, continuously variable phase retarder for operation at telecommunications wavelengths.

Each of the mixtures studied in the Grandjean texture was also polymer stabilised in the ULH geometry and tested for its flexoelectro-optic properties in this configuration. In this way, the correlation between flexoelectro-optic tilt angle in the ULH and magnitude of the flexoelectrically induced birefringence in the Grandjean textures is shown to be good and the response times of the electro-optic switches in the two configurations for each material are shown to be comparable. This lends further confidence to the proposed mechanism of the effect.

The effect that the stabilising polymer network has on the flexoelectric properties in the ULH texture was further investigated in Chapter Six. This was important, as the previous Chapter had shown that the polymer network is crucial to the useful operation of the Grandjean flexoelectro-optic device, and the effect the polymer may be having on the electro-optic performance of the materials used was unknown. Also, although the literature reveals that the ULH texture had been polymer stabilised before, no investigation had been performed into the quantitative effect of the concentration of the reactive mesogen used on the electro-optic properties of this type of device.

It was found that the addition of the polymer network reduced the optic axis tilt angles for a given field, and also reduced the response times of the switch, relative to undoped samples of the same mixture. These effects were found to be relatively insignificant in samples doped with 3% (weight/weight) of reactive mesogen, the tilt angle and response times being reduced to just 88% and 96% respectively, of their values without the polymer network. This showed there was no cause for concern over possible detrimental effect the polymer may be having in the Grandjean device. However, the impact of the polymer was greater when the concentration was increased to 6%(w/w) of reactive mesogen in the mixture. This reduced the tilt angles and response times to 48% and 63% of their initial values respectively. 10%(w/w) of reactive mesogen resulted in microphase separation of the polymer from the liquid crystal host, and consequently a ULH geometry could not be obtained in the sample.

In addition to the effect on the electro-optic response, the presence of the polymer network was also found to produce increased temperature independence in the reactive mesogen doped samples. This was shown to be principally due to the polymer network locking the helical pitch of the chiral material to its value at the time of curing, preventing its usual variation with temperature and consequent impact on the material electro-optics. Further measurements showed that this fixing of the pitch produced greater temperature independence in the tilt angle of the material than in the response time, in agreement with theory. This creates the situation whereby the tilt angle exhibited by a polymerised sample is mainly dependent on the temperature of polymerisation, while the response time is largely dependent on the temperature of operation. These two device parameters with previously opposing temperature performance characteristics can now be optimised simultaneously for the first time.

A new potential application of the effect developed in Chapters Four and Five is investigated in Chapter Seven. The possibility that the flexoelectro-optic deformation in large tilt angle materials

would also produce some change in the helical pitch length of the material, and therefore provide a means of electrically affecting the pitch, is explored. This is done by using the output wavelength of a chiral nematic photonic band edge (PBE) laser as a highly accurate probe of the edge of the chiral nematic photonic band gap. Dye doped, Grandjean textured chiral nematic samples were subjected to a pump pulse from a frequency doubled Nd:Yag laser coinciding with an electric field pulse applied in the plane of the cell. The change in the output wavelength of the laser light produced by the liquid crystal as a function of the applied field was monitored, and the electric field was found to generate a red-shift of up to 8nm at 3.5 V/μm. This effect was smaller than anticipated, but nonetheless provides the first observation of fast electrical tuning of the PBE laser output from a chiral nematic liquid crystal. The effect was also repeated at a shifted temperature and observed again to a slightly lesser extent. Repeated observation of the effect in other materials in other cells proved extremely difficult however, due to several problems. These included the difficulty of obtaining a clear monodomain texture in the tightly confined cells with bulk metallic electrodes, and the difficulty of getting sufficient light throughput from these same cells, with only a 50 μm electrode gap, to be detected by the spectrometer.

This led to the development of patterned electrode cells to apply in-plane fields solely from transparent electrodes on the cell surfaces, allowing easy alignment of the liquid crystal within. A very small effect (1nm redshift) was observed in these cells, but it was thought that the incidence of the pump beam on areas of the cell not subjected to the applied field was obscuring the effect. However, attempts to increase the applied field by fabrication of reduced electrode spacing patterned ITO cells, and masking of the region of the cell outside the active area yielded no improvement. Despite the disappointing magnitude of the observed effect and the difficulty in repeating the effect in subsequent samples, it is still believed that the results obtained do nonetheless provide demonstration of a very novel effect.

The work presented here as a whole therefore, provides demonstration and development of a novel electro-optic device based on a new geometry for the flexoelectro-optic effect. This device is found to be a promising candidate for future photonic telecommunications components due to its significant magnitude, fast response, and analogue electric field control of the optic axis tilt angle and azimuth. The polymer stabilisation of the device is shown to offer improved ruggedness with little detriment to electro-optic performance, and liquid crystal material development allows control over the device characteristics. Polymer stabilisation of flexoelectro-optic materials in general is shown to give added control and improvement of device characteristics, and finally, in

initial tests, the new device type is shown to offer an electrical tuning mechanism for liquid crystal lasers.

8.2. FUTURE WORK

The novelty of the work undertaken here means that a substantial portion of this thesis is given to providing proofs of concept and documenting initial findings, limiting the developments that could be made thereon. A consequence of this is that, as a result of the findings shown in the thesis, many questions are posed, providing plenty of potential for future work. These are some of the questions raised and potential avenues of further exploration:

The principal application that was in mind during the development of the Grandjean textured flexoelectro-optic device was as a faster version of dielectrically coupled, nematic, endlessly rotatable waveplates for polarisation mode dispersion (PMD) compensation in optical fibre systems. For this to be possible, the optic axis of the device has to rotate in the plane of the cell. The cartwheel cells used here in the development of the effect are designed with the capability to endlessly rotate the electric field in the active region in order to provide this functionality, but unfortunately the examination of the device under these conditions was just beyond the scope of this work. The results so far achieved indicate that the effect fulfils all the requirements for this to be a possibility, and that the materials used would indeed outperform the present devices. However, the time that would be required for the development of the necessary electronics was prohibitive, due to the high voltages needed and the d.c. nature of the effect, meaning experimental verification was beyond the timescale available to the project.

A theoretical examination of the device under these conditions was carried out by Andrew Davidson in Oxford, as part of the COMIT collaboration, and although in the initial findings it was not clear that the flexoelectric device would offer an increased maximum rotational velocity of the optic axis, it appeared that the surface anchoring effect that limited the predicted performance could be overcome. The obvious first step in continuing the work started here then would be to obtain the required electronics and measure the maximum rotational velocity of the device. A positive result here would confirm the device as a genuine candidate for telecoms components.

The effect may also have potential in display devices, and this possibility also warrants investigation. This would require the manipulation of visible light, rather than the infra-red wavelengths in which the concept was proven, but this should be no major impediment. The use of high twisting power chiral dopants allows control of the pitch of the chiral nematic material used, and this could be adjusted for the red, green and blue areas of the display. As long as it could be ensured that the material pitch was sufficiently shorter than the wavelength of illumination to render optical activity insignificant, the cell would provide extinction at zero voltage and allow passage of light under an applied field. In this way, the fast switching times and greyscale capability of the flexoelectro-optic effect and the excellent optical clarity of the Grandjean texture could be utilised to provide a very high contrast, fast response display. This would be a valuable enhancement of current twisted nematic displays which suffer from motion blur in rapidly changing scenes. The first step in evaluating this possibility would be to produce Grandjean textured, in-plane field cells with the appropriate pitch lengths, and prove their capabilities for rapid manipulation of red, green and blue light.

The results of Chapter Six also raise the possibility of novel display types, this time with ULH aligned liquid crystals. The rapid light control capabilities of the ULH flexoelectro-optic effect are well known, but the tendency of the texture to be awkward to obtain, to degrade to the Grandjean over time, and to provide very limited contrast due to the patchiness of the texture has limited the applicability of the effect. The polymer stabilisation and surface texture stabilisation schemes proposed by the Chalmers group solve the first two of these problems in low-tilt devices, but the contrast issue remains, and only in this work have polymer stabilised large tilt angle materials been proven effective. Additionally, the contrast issue is not a problem in phase devices, in which the overall retardation is the key factor and small scale texture defects as seen in ULH devices would simply be averaged out.

An application in which the stabilised ULH flexoelectro-optic effect has excellent potential therefore is phase hologram for optical routing and beam steering photonics applications. Here again, the flexoelectro-optic device's ability to respond in the microsecond timescale while also being an analogue effect with greyscale capability is very advantageous. This provides the possibility of a phase hologram which is re-configurable as fast as a ferroelectric device but, not being limited to binary operation like an SSFLC, has equivalent diffraction efficiency to a nematic device. The tendency for these devices to be implemented on LCoS chips is also beneficial, as the

careful temperature and optical path length control provided by these devices is important for reliable performance in a flexoelectro-optic device.

Finally, the initial observations of electrical wavelength tuning in chiral nematic PBE lasers certainly warrant further investigation. Specialised cells need to be constructed for the effect to be made more reliable and the results presented here reproduced. This should allow for a better understanding of the mechanism to be developed. With this achieved however, it ought to be possible to improve the range of tuning and produce a very interesting device.

PUBLICATIONS AND PRESENTATIONS

JOURNAL PAPERS

"Optimised Flexolectric Response in a Chiral Liquid Crystal Phase Device", B. J. Broughton, M. J. Clarke, A. E. Blatch and H. J. Coles, *Journal of Applied Physics*, **98**, (3), 034109, (2005).

"The Effect of Polymer Concentration on Stabilized Large Tilt-angle Flexoelectro-optic Switching", B.J. Broughton, M.J. Clarke, S.M. Morris, A.E. Blatch, and H.J. Coles, *Journal of Applied Physics*, **99**, 023511, (2006).

"Strong flexoelectric behavior in chiral bimesogenic liquid crystals" H. J. Coles, M. J. Clarke, S. M. Morris, B. J. Broughton and A. E. Blatch, *Journal of Applied Physics*, **99**, 034104, (2005).

CONFERENCE PROCEEDINGS

"Liquid crystal based continuous phase retarder: from optically neutral to a quarter waveplate in 200 microseconds", B.J. Broughton, M.J. Clarke, R.A. Betts, T. Bricheno and H.J. Coles, *Proceedings of SPIE*, **5741**, 190-196, (2005).

"Liquid crystal lasers: coherent and incoherent micro-sources", S.M. Morris, A.D. Ford, B.J. Broughton, M.N. Pivnenko and H.J. Coles, *Proceedings of SPIE*, **5741**, 118-127 (2005).

PATENTS

International Patent Application Number PCT/GB2005/002630, filed on 4 July 2005, entitled "Liquid Crystal Device"**,** claiming priority from UK Patent Application GB0414882.1 filed on 2 July 2005. Inventors: Harold James Coles, Marcus James Coles, Stephen Mathew Morris, and Benjamin John Broughton.

International Patent Application Number PCT/GB2005/002622, filed on 4 July 2004, entitled "Liquid Crystal Device"**,** claiming priority from UK Patent Application GB0414888.8 filed on 2 July 2005. Inventors: Harold James Coles, Marcus James Coles, Stephen Matthew Morris, Alison Diane Ford, and Benjamin John Broughton

ORAL PRESENTATIONS

"Flexoelectric Phase Device", B.J. Broughton, M.J. Clarke and H.J. Coles, *British Liquid Crystal Society Annual Conference*, 23/03/2005.

"Liquid Crystals and their use in Telecommunications Devices", B.J. Broughton and H. J. Coles, *COMIT Faraday Partnership Annual Workshop*, 06/07/2003.

"Flexoelectric Phase Device", B.J. Broughton, M.J. Clarke and H.J. Coles, *COMIT Faraday Partnership Annual Workshop*, 06/01/2005.

"The Polymer Stabilized Flexoelectro-optic Effect", B.J. Broughton, M.J. Clarke and H.J. Coles, *COMIT Faraday Partnership Telecoms Project Meeting*, 26/07/2005.

POSTER PRESENTATIONS

"Flexoelectrically induced Birefringence in a Grandjean textured Chiral Nematic" *ILCC 2004*, Ljubljana, Slovenia.

"Liquid Crystal based continuous Phase Retarder" B.J. Broughton, M.J. Clarke and H.J. Coles, *Photonics West 2005*, San Jose, USA.